

POWER ENGINEERING

GAYNULLINA L.R., TUTUBALINA V.P. Dibutylsulfide oxidation research the concentrated hydrogen peroxide solution by means of thermograms	3
TAIMAROV M.A., ILYIN V.K., OSIPOV A.L. , DOLGOVA A.N., AKHMEROV A.V. Heat pumps complex for recycling of secondary energy resources of petrochemical plants.....	7
SAIFULLIN E.R., LARIONOV V.M., VANKOV YU.V. Numerical modeling of stabilization of the heat output of a steam boiler in the combustion of associated petroleum gas.....	15
FARAKHOV T.M., LAPTEV A.G. Determination of local heat transfer coefficients at the entrance region of streamlined bodies.....	22
STEPANOV V.S., STEPANOVA T.B., STARIKOVA N.V. Evaluation the energy potential of compressed air for determining efficiency of air-accumulating electric	27
ALI Y.S.S., CHICHIROVA N.D. Electric power system of Yemen, its structure and characteristics.....	38
MAKSIMOV V.I. , SALOUM A. The water heat pump operation under frost conditions on the evaporator surface.....	44
VLADIMIROV O.V., IVSHIN I.V., NIZAMIEV M.F., TSVETKOV A.N., USMANOV I.K., GIBADULLIN R.R. Stand for after repair tests of asynchronous motors with voltage up to 1000 V. . .	52
MALAFEEV A.V., IULDASHEVA A.I. Selection of options for the reconstruction of the power supply system based on the fuzzy sets theory and the criteria of decision-making theory	59
BARTOLOMEY P.I., SEMENENKO S.I.State estimation method development for scada and synchronized phasor measurements within power system.....	68
NGUYEN D.T., FAM D.N., MINGALEEVA G.R. Assessment of indicators of efficiency of the steam-turbine mini-thermal power plants burning coal.....	79
FEDOTOV A.I., ABDULLAZYANOV R.E., MUDARISOV R.M. Synchronous motors stability estimation methodologies under three-phase faults in power supply grids.....	90
SHABUROV E.L. , DEREVIANKO O.V., FEDYUKHIN A.V., SMYATSKAYA YU.A., POLITAEVA N.A. Determination of thermal capacity of processed sorbents from residual biomass of <i>Chlorella Sorokiniana</i> and duckweed <i>Lemna Minor</i>	100

ELECTRICAL ENGINEERING

SAVENKO A.E., SAVENKO S.E., SAVENKO P.S. Study of the reasons and parameters of common-mode fluctuations of power in autonomous electrical complexes.....	107
---	-----

PHYSICS

KARTASHOV E.M., SOLOVIEV I.A. The stochastic formulation of the Stephan's roblem in hyperbolic representation.....	116
--	-----

ЭНЕРГЕТИКА

ГАЙНУЛЛИНА Л.Р., ТУТУБАЛИНА В.П. Исследование окисления дибутилсульфида концентрированным раствором пероксида водорода при помощи термограмм.	3
ТАЙМАРОВ М.А., ИЛЬИН В.К., ОСИПОВ А.Л., ДОЛГОВА А.Н., АХМЕРОВ А.В. Теплонасосный комплекс для утилизации вторичных энергоресурсов нефтехимических заводов.	7
САЙФУЛЛИН Э.Р., ЛАРИОНОВ В.М., ВАНЬКОВ Ю.В. Численное моделирование стабилизации теплопроизводительности парового котла при сжигании попутного нефтяного газа.	15
ФАРАХОВ Т.М., ЛАПТЕВ А.Г. Определение локальных коэффициентов теплоотдачи на начальном участке обтекаемых тел.	22
СТЕПАНОВ В.С., СТЕПАНОВА Т.Б., СТАРИКОВА Н.В. Определение энергетического потенциала сжатого воздуха для оценки эффективности работы воздушно-аккумулирующей электростанции.	27
АЛИ Я.С.С., ЧИЧИРОВА Н.Д. Электроэнергетическая система Йемена, ее состав и характеристики.	38
САЛУМ А.А., МАКСИМОВ В.И. Работа водяного теплового насоса в условиях образования льда на поверхности трубки испарителя.	44
НИЗАМИЕВ М.Ф., ВЛАДИМИРОВ О.В., ИВШИН И.В., ЦВЕТКОВ А.Н., УСМАНОВ И.К., ГИБАДУЛЛИН Р.Р. Стенд для послеремонтных испытаний асинхронных двигателей напряжением до 1000 В.	52
МАЛАФЕЕВ А.В., ЮЛДАШЕВА А.И. Выбор вариантов реконструкции системы электроснабжения на основе теории нечетких множеств и критериев теории принятия решений.	59
БАРТОЛОМЕЙ П.И., СЕМЕНКО С.И. Развитие метода оценивания состояния для интеграции СВИ и измерений SCADA в ЭЭС.	68
НГУЕН Д.Т., ФАМ Д.Н., МИНГАЛЕЕВА Г.Р. Оценка показателей эффективности парогурбинных мини-ТЭС, работающих на угле.	79
ФЕДОТОВ А.И., АБДУЛЛАЗНОВ Р.Э., МУДАРИСОВ Р.М. Методики оценки устойчивости синхронных двигателей при трехфазных коротких замыканиях в системе внешнего электроснабжения.	90
ШАБУРОВ Е.Л., ДЕРЕВЯНКО О.В., ФЕДЮХИН А.В., СМЯТСКАЯ Ю.А., ПОЛИТАЕВА Н.А. Определение теплотворной способности отработанных сорбентов из остаточной биомассы <i>Chlorella sorokiniana</i> и ряски <i>Lemna minor</i>	100

ЭЛЕКТРОТЕХНИКА

САВЕНКО А.Е., САВЕНКО С.Е., САВЕНКО П.С. Исследование причин и параметров синфазных колебаний мощности в автономных электротехнических комплексах.	107
---	-----

ФИЗИКА

СОЛОВЬЕВ И.А., КАРТАШОВ Э.М. Стохастическая постановка задачи Стефана в гиперболическом представлении.	116
---	-----

THERMOGRAPHIC STUDY OF DIBUTYL SULFIDE OXIDATION BY CONCENTRATED HYDROGEN PEROXIDE SOLUTION

L.R. Gaynullina, V.P. Tutubalina

Kazan State Power Engineering University, Kazan, Russia

gainullina7819@mail.ru

Abstract: We used the thermographic method to study reaction of oxidation of dibutyl sulfide in *n*-octane concentrated by 95,6 % solution of hydrogen peroxide in a mixing reactor with propeller mixer.

It was established that dibutyl sulfide oxidation by hydrogen peroxide in an equimolar ratio of 1:1 at a temperature of 80 °C proceeds to formation of dibutyl sulfoxide, and at a ratio of 1:2 and at a temperature of 100 °C it proceeds to formation of dibutyl sulfone.

The increase in amount of hydrogen peroxide and rise of temperature leads to formation of sour products: the sulfonium and sulfonic acids.

Gas-liquid chromatography was used to prove that during oxidation of dibutyl sulfide by hydrogen peroxide it does not destruct.

Keywords: transformer oil, dibutyl sulfide, oxidation, hydrogen peroxide, thermogram.

For citation: Gaynullina L.R., Tutubalina V.P. Dibutylsulfide oxidation research the concentrated hydrogen peroxide solution by means of thermograms. *Proceedings of the higher educational institutions. ENERGY SECTOR PROBLEMS.* 2019; 21(3-4):3-6. (In Russ). doi:10.30724/1998-9903-2019-21-3-4-3-6.

Introduction

At present, the chemistry of bivalent sulfur compounds faced the appearance of new substances with unique properties. It is known that organic sulfur compounds are widely used as inhibitors of oxidative conversion of hydrocarbons of oil fractions ($T_{\text{boil}}=300-400^{\circ}\text{C}$) and transformer oils, improving their physical-chemical and operational characteristics [1, 2].

The researchers attention is attracted to organic sulfoxides and sulfones, which are formed during thermal and oxidative transformations of organic sulfur compounds [3-8].

Sulfides and oxidized organic sulfur compounds inhibit the oxidation of oil hydrocarbons, increasing their thermal stability, due to their ability to destroy hydroperoxides, which stimulate the auto-oxidation of hydrocarbons in the chain-oxidative process [1].

Experimental part

This research work is devoted to study the nature of interaction between individual sulfide (dibutyl sulfide) with hydrogen peroxide. To understand the mechanism of reaction of oxidative transformation of dibutyl sulfide, it is necessary to have reliable information about the products formed during the oxidation of dibutyl sulfide by hydrogen peroxide. In order to determine the reaction products and the influence of temperature on the course of the reaction, we used chromatographic analysis and thermographic studies. The concentration of dibutyl sulfide in

terms of total sulfur was 0,5 % and remained constant in all experiments in order to obtain comparable experimental data. It is known [1], that this concentration of sulphides is optimal.

The reaction of dibutyl sulfide oxidation by hydrogen peroxide was carried out in *n*-octane medium, taken in amount of 100 cm³, in the thermostate mixing device equipped with a propeller stirrer. In all experiments, the number of revolutions of mechanical mixer was 800 rpm, which is optimal for obtaining sulfoxides and sulfones.

Hydrogen peroxide of 95,6 % concentration was used as the oxidizing agent. The amount of hydrogen peroxide in the reaction of oxidation of dibutyl sulfide varied with a ratio of dibutyl sulfide: hydrogen peroxide in the range of 1:1,1:2 and higher.

It is known [9] that when the ratio of dibutyl sulfide: hydrogen peroxide is 1:1, sulfoxides are formed, and at a ratio of 1:2 sulfones are formed.

Preparation of model mixtures of *n*-octane-dibutyl sulfide and sampling from them were carried out in accordance with the Russian State Standard GOST R 52714-2007.

The concentration of total sulfur in model mixtures was found according to the Russian State Standard GOST R 51859-2002. The concentration of sulfide and sulfoxide sulfur was evaluated according to the method described in [10].

The concentration and composition of products formed during the oxidative transformation of dibutyl sulfide under the action of hydrogen peroxide were investigated using the Crystallux 4000 M chromatograph equipped with a thermal conductivity detector and having a sensitivity of 1500 MV·cm³/mg. The gas chromatography column has a form of helix made from stainless steel, its inner diameter is 3 mm, its length is 2,5 m. Molecular NaX sieves with particle sizes of 0,2–0,4 mm were used as a sorbent. Silica gel KSM No. 5 was used as a desiccant, the particle sizes of which were 0,4–0,8 mm (GOST 3956-76). As a carrier gas we used helium (TU 51-689-75), medical or technical oxygen (GOST 5583-78). The reducer for oxygen supply was DKP-1-65 (TU 26-05-463-76). The relative error in determining the concentration of reaction products did not exceed 0,5 %.

In order to identify the sequence of dibutyl sulfide transformation, when interacting with hydrogen peroxide, thermograms of reactions were recorded using the TQ 170 thermograph in the temperature range of 30–130 °C with a measurement error of ±1,0 °C. The obtained thermograms are shown in the figure.

Results and discussion

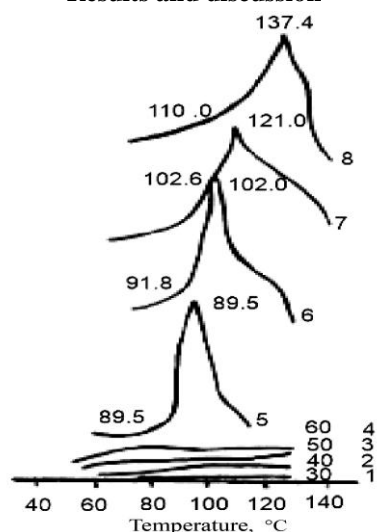


Fig. Thermograms of interaction of dibutyl sulfide with hydrogen peroxide at temperatures: 1, 2, 3, 4 – respectively 30, 40, 50 and 60 °C; 5 – 80 °C; 6 – 100 °C; 7 – 120 °C; 8 – 130 °C

The experimental data presented in the figure shows that oxidation of dibutyl sulfide by hydrogen peroxide practically does not proceed at temperatures of 30, 40, 50 and 60 °C. Oxidation reactions proceed very slowly without formation of a thermal effect, as evidenced by the curves 1, 2, 3 and 4.

Intensive interaction of dibutyl sulfide with hydrogen peroxide begins at a temperature of 80 °C. In the figure, this is expressed by curve 5, which can be characterized by a narrow and high exo-effect. The resulting exo-effect is characterized by a 9,5 °C rise in temperature.

When concentration of hydrogen peroxide in dibutyl sulfide oxidation reaction is increased to a dibutyl sulfide: hydrogen peroxide ratio of 1:2, a slight shift of the exo-effect to high temperatures is observed (curve 2). In this case, hydrogen peroxide is completely consumed for oxidation of dibutyl sulfide to the corresponding sulfone. At

the same time, the exo-effect of the reaction is 12,5 °C (curve 5).

Analysis of the resulting products of oxidation of dibutyl sulfide by a concentrated solution of hydrogen peroxide showed that when the ratio dibutyl sulfide: hydrogen peroxide is 1:1, the oxidation proceeds with the predominant formation of sulfoxide for temperatures up to 89,5 °C.

The output of sulfoxide is 98,7 %. At higher temperature and ratio of dibutyl sulfide: hydrogen peroxide, equal to 1:2, the formation of dibutyl sulfone is observed with a yield of 97,9 % (curve 6).

With an increase in the reaction temperature and the amount of hydrogen peroxide supplied, dibutyl sulfide is oxidized by hydrogen peroxide to form sulfinic and sulfonic acids and the exo-effect shifts to higher temperatures (curves 7 and 8).

The obtained experimental data show that oxidation of dibutyl sulfide by hydrogen peroxide proceeds with formation of sulfoxides and sulfones only in the temperature range of 80–100 °C and for dibutyl sulfide: hydrogen peroxide ratio of 1:1 and 1:2. The temperature rising up to 120 and 130 °C and increasing the amount of hydrogen peroxide is accompanied by formation of acidic products, as evidenced by low pH values of the reaction mass: 5 and 6, respectively. The exo-effect of the reaction increases, respectively, by 19 and 16,4 °C.

Therefore, the oxidation of dibutyl sulfide by hydrogen peroxide can be represented as the following scheme:



In accordance with the proposed scheme, the oxidation of dibutyl sulfide by concentrated solution of hydrogen peroxide can proceed with formation of acidic compounds at high temperatures and increased amounts of hydrogen peroxide.

According to the thermogram shown in the figure, oxidation of dibutyl sulfide by hydrogen peroxide proceeds without destruction of its molecule. By varying the temperature and the amount of hydrogen peroxide, the dibutyl sulfide oxidation reaction can be purposefully turned towards formation of sulfoxides and sulfones.

Analysis of the reaction mixtures by gas liquid chromatography showed that the main product of the dibutyl sulfide oxidation reaction by hydrogen peroxide is water. No decomposition of dibutyl sulfide was detected, since no evolution of gases, including hydrogen sulfide, was observed.

Thus, oxidation of dibutyl sulfide by concentrated 95,6 % hydrogen peroxide solution purposefully proceeds with formation of dibutyl sulfoxide and dibutyl sulfone for dibutyl sulfide: hydrogen peroxide ratios, respectively, equal to 1:1 and 1:2, and temperatures of 80 and 100°C.

Conclusions

1. It was shown that an increase in the amount of hydrogen peroxide fed to the reaction system over the dibutyl sulfide-hydrogen peroxide ratio of 1:2 results in a shift of exo-effect towards high temperatures, and formation of acidic products.
2. Gas-liquid chromatography was used to prove that during dibutyl sulfide oxidation by hydrogen peroxide dibutyl sulfide is not destroyed and the main products of reaction are sulfoxides, sulfones and water.

References

1. Harlampidi HE, Gaynullina LR, Tutubalina VP. Individual'nye sermistye soedineniya – ingibitory okisleniya uglevodorodov transformatornogo masla. *Herald of Tekhnological University*. 2016; 19(7):5–7. (In Russ).
2. Gaynullina LR, Tutubalina VP, Harlampidi HE. Seroorganicheskie soedineniya maslyanoy frakcii arlanskoj nefti. *Herald of Tekhnological University*. 2017; 20(10):67–

Литература

1. Харлампиدي Х.Э., Гайнуллина Л.Р., Тутубалина В.П. Индивидуальные сернистые соединения – ингибиторы окисления углеводородов трансформаторного масла // Вестник технологического университета. 2016. Т.19, №7. С. 5–7.
2. Гайнуллина Л.Р., Тутубалина В.П., Харлампиدي Х.Э. Сераорганические соединения

69. (In Russ).

3. Bruzzoniti MC, De Carlo RM, Sarzanini C, Maina R, Tumiatti V. Stability and Reactivity of Sulfur Compounds against Copper in Insulating Mineral Oil: Definition of a Corrosiveness Ranking. *Industrial & Engineering Chemistry Research*. 2014; 53(21):8675–8684. DOI: 10.1021/ie4032814.

4. Mazgarov AM, Kornetova OM. *Sernistyie soedineniya uglevodородного syr'ya*. Kazan: Kazan State University; 2015. (In Russ).

5. Singh D, Chopra A, Mahendra PK, Kagdiyal V, Saxena D. Sulfur compounds in the fuel range fractions from different crude oils. *Petroleum Science and Technology*. 2016; 34(14):1248–1254. DOI: 10.1080/10916466.2016.1196218.

6. Arystanbekova SA, Lapina MS, Volynskii AB. Determination of individual sulfur-containing compounds in liquid hydrocarbon raw materials and their processing products by gas chromatography. *Journal of Analytical Chemistry*. 2017; 72(5):473–489.

7. Krivtsov EB., Golovko AK. Kinetika okisleniu sernistykh soedinenii dizel'noi frakcii nefti ozono-kislorodnoi smes'yu. *Bulletin of the Tomsk Polytechnic University*. 2012; 321(3):157–161. (In Russ).

8. Zarifyanova MZ, Vafina SD, Valiullina RR, Aristov IV, Konstantinova AV, Harlampidi HE. Kinetika okisleniya sulfidov dizel'noj frakcii v prisutstvii ledyanoy uksusnoj kisloty. *Herald of Technological University*. 2012; 15(9):196–198. (In Russ).

9. Karaulova EN. *Chemistry of Petroleum Sulfides*. Moscow: Nauka; 1970. (In Russ).

10. Galpern GD (Ed.) *Metody analiza organicheskikh soedinenij nefti, ih smesej i proizvodnyh*. Moscow: Nauka; 1969. (In Russ).

масляной фракции арланской нефти // Вестник технологического университета. 2017. Т. 20, №10. С.67–69.

3. Bruzzoniti M.C., De Carlo R.M., Sarzanini C., Maina R., Tumiatti V. Stability and Reactivity of Sulfur Compounds against Copper in Insulating Mineral Oil: Definition of a Corrosiveness Ranking // *Ind. Eng. Chem. Res.* 2014. 53 (21). Pp. 8675–8684. DOI: 10.1021/ie4032814.

4. Мазгаров А.М. Сернистые соединения углеводородного сырья / А.М. Мазгаров, О.М. Корнетова. Казань: Казан. ун-т, 2015. 36 с.

5. Singh D., Chopra A., Mahendra P. K., Kagdiyal V., Saxena D. Sulfur compounds in the fuel range fractions from different crude oils // *Petroleum Science and Technology*. V. 34. 2016. pp. 1248–1254.

6. Arystanbekova S.A., Lapina M.S., Volynskii A.B. Determination of individual sulfur-containing compounds in liquid hydrocarbon raw materials and their processing products by gas chromatography // *Journal of Analytical Chemistry*. May 2017, Vo. 72, Issue 5. pp. 473–489.

7. Кривцов Е.Б., Головки А.К. Кинетика окисления сернистых соединений дизельной фракции нефти озono-кислородной смесью // *Известия Томского политехнического университета*. 2012. Т. 321, No 3. С.157–161.

8. Зарифянова М.З., Вафина С.Д., Валиуллина Р.Р., Аристов И.В., Константинова А.В., Харлампиدي Х.Э. Кинетика окисления сульфидов дизельной фракции в присутствии ледяной уксусной кислоты // *Вестник технологического университета*. 2012. Т.15, №9. С.196–198.

9. Караулова Е.Н. *Химия сульфидов нефти*. М.: АН СССР, 1970. 136 с.

10. Методы анализа органических соединений нефти, их смесей и производных / Под ред. Г.Д. Гальперна. М.: Наука, 1969. 210 с.

Authors of the publication

Leysan R. Gaynullina – PhD in Engineering sciences, Associate Professor of the Department of Power Supply of Enterprises and Energy Resource-Saving Technologies of Kazan State Power Engineering University. E-mail: gainullina7819@mail.ru.

Valeria P. Tutubalina – Grand PhD in Engineering sciences, Professor, Chief Researcher, Kazan State Power Engineering University.

Received

February, 18 2019



HEAT PUMPS COMPLEX FOR RECYCLING OF SECONDARY ENERGY RESOURCES OF PETROCHEMICAL PLANTS

M.A. Taimarov¹, V.K. Ilyin¹, A.L. Osipov¹, A.N. Dolgova^{1,2}, A.V. Akhmerov¹

¹Kazan State Power Engineering University, Kazan, Russia

²Rostov State Transport University, Rostov-on-Don, Russia

Abstract: The created heat pump complex allows one to simultaneously utilize different types of secondary energy resources of petrochemical industries. For the developed heat pump complex the main potential for the resources used is the heat of flammable waste gases and heat of circulating water. The final received energy resources are heat of heating water of 150 °C temperature and electricity for internal and external consumption.

Keywords: heat pump complex, secondary energy resource, heat pump, energy potential, heat.

For citation: Taimarov M.A., Ilyin V.K., Osipov A.L., Dolgova A.N., Akhmerov A.V. Heat pumps complex for recycling of secondary energy resources of petrochemical plants. *Proceedings of the higher educational institutions. ENERGY SECTOR PROBLEMS*. 2019;21(3-4):7-14. (In Russ). doi:10.30724/1998-9903-2019-21-3-4-7-14.

Statement of the problem

Many secondary energy resources in forms of thermal discharges of sewage treatment plants, circulating water of cooling towers, warm satellite waters, irretrievable condensate etc are formed during deep processing of petrochemical raw materials. Significant share of secondary energy resources is formed in the form of hydrocarbon and fuel gases, methane-hydrogen fractions, resins, subdimeric water, "yellow" oil and coke residue after delayed coking units [1–5].

Non-used combustible waste in the form of "yellow" oil amounted to 600 tons/year, in the form of liquid combustible sorbent A-2 amounted to 2 tons/hour, in the form of heat of waste water with a temperature of 27°C at the sewage treatment plant amounted to 50000 m³/hour at PJSC "Nizhnekamskneftekhim" in 2016 [6–7].

According to the data from PJSC "Kazanorgsintez", thermal secondary resources volumes in 2016 are the following: in the form of circulating water with a temperature of 25°C in cooling towers is 5000 m³/hour, in the form of combustible waste of pyrolysis resin is 400 ton/year, in the form of waste combustible gases is 150 m³/hour in 2016.

At PJSC "Nizhnekamskneftekhim" and PJSC "Kazanorgsintez" performance indicator of waste gas burning on flares and candles is 5 % of the total volume of the gaseous hydrocarbon raw material used in the technology in 2017.

The delayed coker unit commissioned at JSC "TANECO" in 2017 will have a raw material capacity of 2 million tons per year. Along with main commercial products such as acid gas, unstable gasoline, light and heavy gas oil, it produces a secondary fuel product: petroleum coke in the amount of 700 thousand tons/year [8–10].

The presented analysis shows that the secondary energy resources of oil refinery include fuel component in the form of liquid, gaseous, solid combustible waste and heat component in the form of heat of circulating water of cooling towers and heat of waste water of sewage treatment plants.

Therefore, the development of technology and units for complex use of secondary energy resources is the main focus of research on the energy saving potential of oil refinery enterprises.

This article discusses the use of gas turbine and heat pump units to utilize secondary energy resources of oil refinery plants.

Evaluation of power and operating parameters of a heat pump unit for disposal of secondary combustible and secondary thermal energy resources

Thermal energy characteristics of secondary energy resources of oil refinery plants are given in Table 1.

Table 1

Thermal energy characteristics of secondary energy resources of oil refinery plants

Secondary energy resources	Heat of combustion Q_h^r		Enthalpy, kJ/kg	Average energy potential of the resource, MW
	kJ/kg	kJ/m ³		
Circulating water in cooling towers at 25 °C	-	-	105	15
Wastewater from sewage treatment plants at 27 °C	-	-	114	30
Non-returnable condensate at 90 °C	-	-	377	10
Reverse heat-satellite water at 95 °C	-	-	399	20
Exhaust combustible factory gases	-	27255	-	227
Fuel gas	-	33369	-	220
Heavy pyrolysis resin with spent pyrobenzene and "yellow" oil	39300	-	-	10
Liquid combustible sorbent A-2	41636	-	-	23
Methane-hydrogen fraction	-	28526	-	200
Petroleum coke	30180	-	-	200
Reverse heat-satellite water at 70 °C	-	-	294	14,7
Condensate from polycarbonate production at 130 °C	-	-	547	11

Table 1 shows that secondary energy sources of petrochemical plants with a fuel component in the form of combustible gases have the greatest potential.

Nowadays, at petrochemical industries, fuel and waste secondary combustible gases are burned in huge quantities in flares and in process candles [8–9] besides their usage for the factory technological consumption.

The discharged emergency and waste gases in the amount of 230 tons per hour are burned in flare No. 768 from 2009 at the block E-500 of the 3rd stage of the high pressure heater plant of PJSC “Kazanorgsintez”. The disadvantages of this technical solution are:

1. Pollution of the atmosphere and the environment.
2. Failure to save potential energy to reduce the cost of production.

Heavy flooded pyrolysis resins and combustible liquid sorbent are burned in boilers mixed with fuel gas.

At the SKI PJSC "Nizhnekamskneftekhim" there is a unit recycling liquid secondary combustible waste in the form of A-2 sorbent in the amount of 0,8 tons/hour, which are mixed with fuel gas in the amount of 12,000 m³/hour in two steam boilers KVG-3GM with the generation of steam energy parameters in the amount of 120 tons/hour and the supply of this steam to the turbine connected to the generator.

At the plant SKI PJSC "Nizhnekamskneftekhim" the second unit of the same type for disposal of liquid waste was launched with two boilers at 75 tons of steam per hour [8].

The disadvantage of this solution is low operational reliability of combustion of liquid waste in boilers with obtaining of water steam of energy parameters and subsequent supply of this steam to the steam turbine connected with electric generator..

At the SKI PJSC "Nizhnekamskneftekhim" due to high heat of combustion of secondary combustible waste in the form of A-2 sorbent, the superheater tubes in boilers KVG-3GM are systematically destroyed. The composition of sorbent is not constant due to changes in the content of heavy resins and water and the heat of combustion varies from 16,000 kJ/kg to 40,000 kJ/kg. At low heat of combustion of liquid combustible waste, additional supply of natural gas to the furnace is necessary to generate the required amount of energy steam for the operation of the steam turbine.

The number of secondary combustible energy resources in the form of methane-hydrogen fraction obtained in PJSC "Taif-NK" is expected to be 381,4 million m³ in 2019, and 382,5 million m³ in 2020.

Since with growth of production capacity of petrochemical plants the need for electricity increases, so many TPS are planning to switch to mixed fuel in power boilers: natural gas in a mixture with a methane-hydrogen fraction to reduce the cost of electricity generation. The disadvantage of this technical solution is limitation of the burned amount of methane-hydrogen fraction in the fuel fraction of 12 % mixed with natural gas.

Petroleum coke is supposed to be burned in a mixture with natural gas. In the future, by 2030, Nizhnekamsk CHP-2 will use as fuel the following substances: gas – 65 %, petroleum coke – 33 %, fuel oil – 2 % [9]. The disadvantage of this solution is the need to prepare petroleum coke for chamber flaring in energy boilers and the presence of high-calorific gas fuel that is burnt together with petroleum coke.

The use of energy potential of 1,5 MW in the form of heat from the circulating water at the high pressure heater of LDPE Production Plant PJSC "Kazanorgsintez" was implemented in 2007 using the absorption refrigerating machine ABHM-1500P, i.e. single-stage thermal bromine lithium pump with steam heating. The disadvantages of this technical solution is low power of utilized heat and the need for heating steam in the amount of 4,31 tons/hour with a temperature of 115°C. The result of this technical solution is the production of cold of +7°C, used in the technology.

Design of absorption refrigerating machine (ARS) Thermax [10,11] with a capacity of 5,35 MW and with a conversion ratio of 1,4, working on burning gas or liquid fuel, producing cold water of +2°C in summer and hot water of +60 °C in winter is known. Its disadvantage is low temperature of hot water.

The steam-compression heat pump NT-3000 [12-15] produced by CJSC "Energiya" with power of utilized water heat of 2,8 MW, temperature of +30°C and consumed electric power of 0,63 MW produces heated water of +55°C and cold water of +7°C with conversion factor of 4,45. The disadvantage is the need for electricity and low temperature of heated water.

Since 2005, the gas turbine power plant GTE-15 with an electrical capacity of 15 MW and with an efficiency of 30 % in a cogeneration cycle, using the methane-hydrogen fraction with a hydrogen content up to 26 % (vol.) has been operated at the Mozyr Oil Refinery [16]. The GTE-15 uses a ZKR-204 booster screw compressor, compressing the methane-hydrogen fraction from a pressure of 0,9 MPa to 2 MPa. The disadvantage of this scheme is the impossibility of using low-grade thermal energy of recycled and waste water.

As it can be seen from the analysis presented above, the available technical solutions for the use of secondary energy resources are not comprehensive and universal in terms of the final result, suitable for practical use with a high energy saving indicator.

The proposed scheme for the integrated use of secondary energy resources of petrochemical industries is shown in Figure 1. The energy balance of the universal module of heat pump complex for utilization of secondary energy resources of petrochemical plants, calculated taking into account the results from [12–20], is given in Table 2.

The universal module of heat pump complex for utilization of secondary energy resources of petrochemical plants (Fig. 1) consists of three blocks: gas-turbine unit 1 based on GTE-2,5 with an electric power of 2,5 MW with a steam heat recovery boiler, a steam-compression heat pump

unit based on two heat pumps NT-3000 with a unit capacity of up to 2,8 MW, absorption heat pump unit of two Thermax ARS with a unit capacity of up to 5,35 MW.

The power of the resource Q_e obtained in the evaporator of the heat pump NT-3000 is determined by the formula, MW

$$Q_e = G(i_{w2} - i_{w1}), \quad (1)$$

where G is flow rate of circulating water, kg/s; i_{w2} , i_{w1} is enthalpy of circulating water at the outlet and inlet of the evaporator (kJ / kg), respectively.

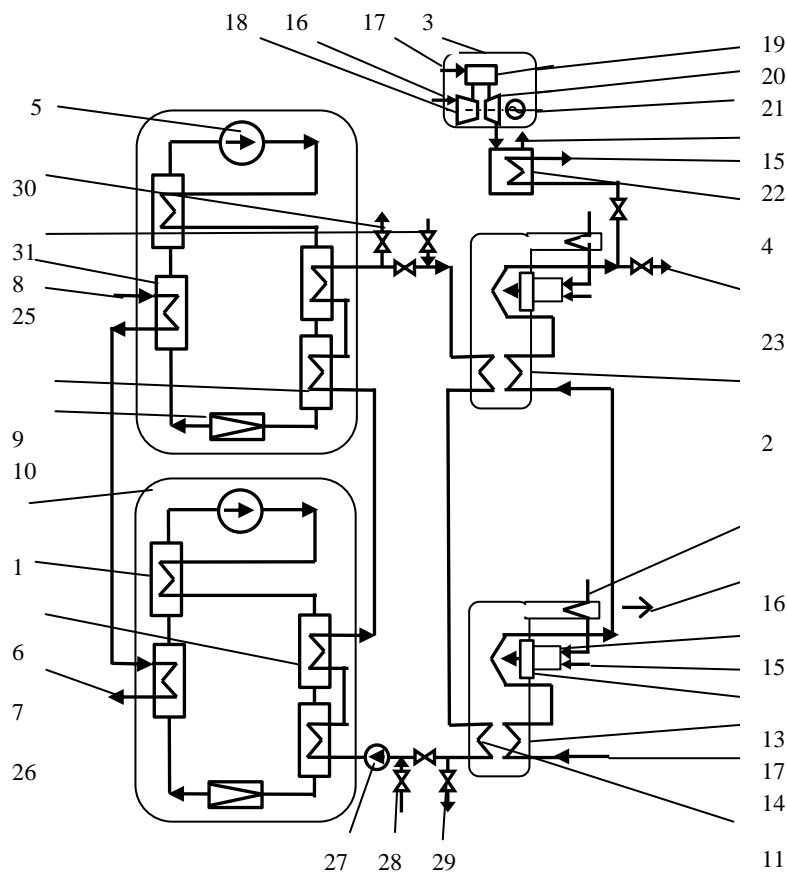


Fig. 1. Scheme of the universal module of heat pump complex for utilization of secondary energy resources of petrochemical plants: 1 – steam compression heat pump; 2 – absorption bromine-lithium heat pump; 3 – gas turbine unit; 4 – water recovery boiler; 5 – electrically driven compressor; 6 – regenerative heat exchanger; 7 – condenser; 8 – evaporator; 9 – subcooler; 10 – throttle; 11 – absorber; 12 – evaporating heat exchanger; 13 – generator; 14 – condenser; 15 – combustion products; 16 – air intake; 17 – fuel; 18 – compressor; 19 – combustion chamber; 20 – gas turbine; 21 – electric generator; 22 – superheated heating water of 150 °C; 23 – heating water of 130 °C; 24 – circulating water of 70 °C; 25 – circulating water of 25 °C; 26 – circulating water of 5 °C; 27 – circulation pump; 28 – water being cooled of 40 °C; 29 – cooled water of 10 °C; 30 – heated water of 70°C; 31 – circulating water of 30°C

Table 2

Energy balance of the universal module of the heat pump complex for utilization of secondary energy resources of oil refinery plants

Come in		Come out	
Energy resource	Value	Energy resource	Value
Gas Turbine Unit			
Heat of combustible fuel gas, MW	10	Electric power for two steam compression heat pumps, MW	1,26
Heat supplied with water at 130 °C for heating, MW	7,0	Electricity to consumers, MW	1,24
		Heat output with water heated to 150 °C, MW	13,9
		Heat loss with outgoing gases, MW	0,6
Total energy received, MW	17,0	Total energy consumed, MW	17,0
Unit of two steam compression heat pumps			
Electric power for two steam compression heat pumps, MW	1,26	Energy resource given to circulating water for heating up to 70 °C, MW	7,0
Heat of circulating water at 25 °C, MW	5,74		
Total energy received, MW	7,0	Total energy consumed, MW	7,0
Unit of two absorption heat pumps			
Heat of combustion of waste gas in the heat pump generator, MW	5	Heat given to water when it is heated to 130 °C, MW	7,0
Energy resource brought with circulating water with a temperature of 70 °C, MW	2,3	Heat loss with outgoing gases, MW	0,3
Total energy received, MW	7,3	Total energy consumed, MW	7,3
Total come in, MW	31,3	Total come out, MW	31,3

The power spent in steam compression heat pump to transfer heat from the circulating water to the heated water, MW:

$$N_s = Q_e \cdot \eta / \varphi_s \quad (2)$$

where $\eta=0,8$ is coefficient taking into account the degree of perfection of thermodynamic cycle of steam-compression heat pump [1–5]; $\varphi_s=4,45$ is the energy conversion factor for the steam compression heat pump NT-3000.

For absorption heat pump, the power consumed for burning secondary fuel Q_f (MW) is calculated as:

$$Q_f = Q_a / \varphi_a, \quad (3)$$

where Q_a is power received by the consumer from absorption heat pump, MW; $\varphi_a=1,4$ is conversion coefficient for the absorption heat pump Thermax [10,11].

Discussion of results

The results presented in table. 2 show that for operation of a universal module consisting of GTE-2,5, two NT-3000 and two ARM Thermax, the main share of secondary energy source belongs to waste and fuel gases in the amount of 15 MW. The heat capacity of circulating water of 25°C consumed for operation of heat pump complex is 5,74 MW. The module of the heat pump complex has a thermal power according to the secondary energy resources used at the input $Q_{in}=15,74$ MW. The final product of operation of heat pump complex is heat $Q_{out}=13,9$ MW in the form of water heated to 150°C and electricity in the form of 2,5 MW power of.

Energy efficiency of energy resources usage in the heat pump complex module $\eta_{e.u.} = Q_{out} \cdot 100 / Q_{in} = 88,3\%$.

Compared with the known existing and discussed above technical solutions, the proposed module of the heat pump complex is universal both in terms of the potential of the secondary energy resources used in it and in their types. The complex operation does not require external supply of electricity.

The conventional structural formula of the module: 1 Gas Turbine Unit + 1 boiler + 2 steam compression heat pumps + 2 absorption heat pumps Thermax allows, according to the nomenclature and type of equipment available in the industry, to create units and, on their basis, heat pump modules for utilization of secondary resources in oil refinery with a wide range of used capacities.

Conclusion

1. The created heat pump complex allows simultaneously utilizing various types of secondary energy resources of oil refinery plants.

2. The main potential for the resources used for the developed heat pump complex is the heat of combustible waste gases and heat of recycled water, and the final energy resources obtained are heat of heating water with a temperature of 150°C and electricity for internal and external consumption.

References

1. Taimarov MA., Efremov DA., Stepanova TO. Povyshenie effektivnosti ispol'zovaniya vtorichnyh teplovyh energoresursov v PJSC Kazanorgsintez. *Herald of Kazan Technological University*. 2015; 18(22):75-78. (In Russ).
2. Taimarov MA. *Napravleniya razvitiya energosberezheniya v energetike*. Kazan: KSPEU; 2003. (In Russ).
3. Taimarov MA. *Osnovy fiziko-himicheskikh processov proizvodstva teplovoj energii*. Kazan: KSPEU; 2003. (In Russ).
4. Grigorov VG., Neiman VK., Surakov SD. *Utilizaciya nizkopotencial'nyh teplovyh vtorichnyh energoresursov na himicheskikh predpriyatiyah*. Moscow: Himiya; 1987. (In Russ).
5. Kalkin IM. Perspektivy razvitiya teplovyh nasosov. *Kholodil'naya Tekhnika*. 1994; 1:4-8. (In Russ).
6. Slesarenko VV, Knyazev VV, Slesarenko IV. Perspektivy primeneniya teplovykh nasosov pri utilizatsii teploty gorodskikh stokov. *Energosberezheniye i vodopodgotovka*. 2012;3(77): 28–33.
7. Anikina ID, Sergeev VV, Amosov NT, Luchko MG. Ispol'zovaniye teplovykh nasosov v tekhnologicheskikh skhemakh generatsii teplovoj energii TETs. *Alternativnaya energetika i ekologiya*. 2016; 3–4 (191–192): S. 39–49.
8. Informacionnoe agentstvo. *REGNUM*. Available at: <https://www.regnum.ru/news/26965.html> Accessed: 16 Dec 2017. (In Russ).
9. Delovaya elektron'naya gazeta Tatarstana. *Biznes online*. Available at: <https://www.regnum.ru/news/26965.html>. Accessed: 04 Feb 2018. (In Russ).
10. Alexikov IY. Opyt primeneniya

Литература

1. Таймаров М.А., Ефремов Д.А., Степанова Т.О. Повышение эффективности использования вторичных тепловых энергоресурсов в ОАО "Казаньоргсинтез" // Вестник Казанского технологического университета. 2015. Т.18, № 22. С. 75-78.
2. Таймаров М.А. Направления развития энергосбережения в энергетике. Казань: КГЭУ, 2003. 67 с.
3. Таймаров М.А. Основы физико-химических процессов производства тепловой энергии. Казань: КГЭУ, 2003. 120 с.
4. Григоров В.Г., Нейман В.К., Сураков С.Д. Утилизация низкопотенциальных тепловых вторичных энергоресурсов на химических предприятиях. М: Химия, 1987. 240 с.
5. Калкин И.М. Перспективы развития тепловых насосов // Холодильная техника. 1994. №1. С. 4-8.
6. Слесаренко В.В., Князев В.В., Слесаренко И.В. Перспективы применения тепловых насосов при утилизации теплоты городских стоков // Энергосбережение и водоподготовка. 2012. №3 (77): С. 28–33.
7. Аникина И.Д., Сергеев В.В., Амосов Н.Т., Лучко М.Г. Использование тепловых насосов в технологических схемах генерации тепловой энергии ТЭЦ // Альтернативная энергетика и экология. 2016. №3–4 (191–192): С. 39–49.
8. Информационное агентство REGNUM. Доступно по: <https://www.regnum.ru/news/26965.html>. Ссылка активна на 16 декабря 2017.
9. Деловая электронная газета Татарстана «Бизнес online». Доступно по: <https://www.business-gazeta.ru/news/315798>. Ссылка активна на: 04.02.2018.

absorbcionnogo holodil'nogo oborudovaniya dlya povysheniya energoeffektivnosti pri modernizacii neftepererabatyvayushchih i neftekhimicheskikh predpriyatij. *Himicheskaya Tekhnika*. 2016; 2:18-20. (In Russ).

11. Kovetsky VM, Kovetsky MM, Lavrik VM. Effektivnoe ispol'zovanie vnutrennih toplivnyh istochnikov neftepererabatyvayushchih zavodov. *Industrial heat engineering*. 2010; 32(5):72-78. (In Russ).

12. Sokolov AD, Muzychuk SY, Muzychuk RI. Waste heat and its influence on the energy efficiency of the Russian economy: Territorial and industrial dimensions. *Economic Analysis: Theory and Practice*. 2016; 15(6):42-54.

13. Slesarenko VV, Knyazev VV, Slesarenko IV. Perspektivy primeneniya teplovyh nasosov pri utilizacii teploty gorodskih stokov. *Energoberezhenie i vodopodgotovka*. 2012; 3(77):28-33.

14. Anikina ID, Sergeev VV, Amosov NT, Luchko MG. Heat pumps application in flow-sheet of heat generation at thermal power plants. *Alternative Energy and Ecology (ISJAE)*. 2016;(3-4):39-49. (In Russ.) <https://doi.org/10.15518/isjaee.2016.03-04.003>.

15. Bondarenko AS, Callash VL, Litvin AA. Eksploatatsiya sudovyh gazoturbinnih dvigatelej na gazojle i vodorodsoderzhashchem gaze, poluchaemyh pri pererabotke nefti. *Nauchnye trudy*. V.61., Iss.48. Kiev: National Library of Ukraine of Vernadsky, 2006. pp. 218-219. (In Ukraine).

16. Pedersen SE. Teplonasosnaya stantsiya moshchnost'yu 18 MVt, utiliziruyushchaya nizkopotencial'noe sbrosnoe teplo stochnyh vod v Norvegii. *Teplovye nasosy*. 2011; 1:36-37. (In Russ.).

17. Gorshkov VG, Pazdnikov AG, Mukhin DG., et al. Promyshlennyj opyt i perspektivy ispol'zovaniya otechestvennyh absorbcionnyh bromistolitievyyh holodil'nyh mashin i teplovyh nasosov novogo pokoleniya. *Kholodil'naya Tekhnika*. 2007; 8:23-31. (In Russ).

18. Daniel Brdar R, Robert M Jones. GE IGCC Technology and Experience with Advanced Gas Turbines. *GE Power Systems*. Available at: <http://www.netl.doe.gov/technologies/coalpower/turbines/refshelf/igcc-h2-sygas>.

19. Nakamura DN. Global ethylene capacity increases slightly in 2006. *Oil and Gas Journal*. 2007; 105(27):45-48.

20. Hisajlma D, Kawamura H, Oouchi T. Determination of Thermal Properties of Dilute LiBr-Water Solutions. *International Journal of Thermophysics*. 1997; 18(2):397-406.

10. Алексиков И.Ю. Опыт применения абсорбиционного холодильного оборудования для повышения энергоэффективности при модернизации нефтеперерабатывающих и нефтехимических предприятий // Химическая техника. 2016. №2. С. 18-20.

11. Ковецкий В.М., Ковецкая М.М., Лаврик В.М. Эффективное использование внутренних топливных источников нефтеперерабатывающих заводов // Промышленная теплотехника. 2010. Т.32, №5. С. 72–78.

12. Соколов А.Д., Муzychuk С.Ю., Муzychuk Р.И. Тепловые отходы и их влияние на энергоэффективность российской экономики: территориальный и отраслевой аспекты // Экономический анализ: теория и практика. 2016. №6. С. 42-54.

13. Слесаренко В.В., Князев В.В., Слесаренко И.В. Перспективы применения тепловых насосов при утилизации теплоты городских стоков // Энергосбережение и водоподготовка. 2012. №3 (77). С. 28-33.

14. Аникина И.Д., Сергеев В.В., Амосов Н.Т., Лучко М.Г. Использование тепловых насосов в технологических схемах генерации тепловой энергии тэц. Альтернативная энергетика и экология (ISJAE). 2016;(3-4):39-49. <https://doi.org/10.15518/isjaee.2016.03-04.003>.

15. Бондаренко А.С., Каллаш В.Л., Литвин А.А. Эксплуатация судовых газотурбинных двигателей на газойле и водородсодержащем газе, получаемых при переработке нефти // Наукові праці. 2006. Том 61, випуск 48. С. 218-219.

16. Pedersen S.E. Теплонасосная станция мощностью 18 МВт, утилизирующая низкпотенциальное сбросное тепло сточных вод в Норвегии // Тепловые насосы. 2011. №1. С. 36–37.

17. Горшков В.Г., Паздников А.Г., Мухин Д.Г., и др. Промышленный опыт и перспективы использования отечественных абсорбиционных бромистолитиевых холодильных машин и тепловых насосов нового поколения // Холодильная техника. 2007. №8. С. 23-31.

18. Daniel Brdar R., Robert M. Jones. GE IGCC Technology and Experience with Advanced Gas Turbines // GE Power Systems. Доступно по: <http://www.netl.doe.gov/technologies/coalpower/turbines/refshelf/igcc-h2-sygas>.

19. Nakamura D. N. Global ethylene capacity increases slightly in 2006 // Oil and Gas Journal. 2007. V. 105, № 27. P.45-48.

20. Hisajlma D., Kawamura H., Oouchi T. Determination of Thermal Properties of Dilute LiBr-Water Solutions // International Journal of Thermophysics. 1997. Vol. 18, No. 2. P. 397-406.

Authors of the publication

Mikhail A. Taimarov – Professor of the Department «Energy supply of manufactures and energy resources saving technology» Kazan State Power Engineering University; doct. sci. (techn.); E-mail: taimarovma@yandex.ru.

Vladimir K. Ilin – Professor of the Department of the Department «Energy supply of manufactures and energy resources saving technology», Pro-vice-chancellor for academic affairs of Kazan State Power Engineering University; doct. sci. (techn.); E-mail: ilinwk@rambler.ru.

Ayrat L. Osipov – Associate Professor of the Department «Energy supply of manufactures and energy resources saving technology» Kazan State Power Engineering University; cand. sci. (techn.); E-mail: nord7077@yandex.ru.

Anastasia N. Dolgova –Associate Professor of the Department «Energy supply of manufactures and energy resources saving technology» Kazan State Power Engineering University; Associate Professor of the Department «Energy supply of manufactures and energy resources saving technology»; Rostov State Transport University; cand. sci. (techn.); E-mail: dolgova.an@list.ru.

Artem V. Akhmerov –Associate Professor of the Department «Energy supply of manufactures and energy resources saving technology» Kazan State Power Engineering University; cand. sci. (chem.); E-mail: akhm@mail.ru.

Received

October, 30 2018



NUMERICAL MODELING OF STABILIZATION OF THE HEAT OUTPUT OF A STEAM BOILER DURING COMBUSTION OF ASSOCIATED PETROLEUM GAS

E.R. Saifullin¹, V.M. Larionov¹, Yu.V. Vankov²

¹Kazan Federal University, Kazan, Russia

²Kazan State Power Engineering University, Kazan, Russia

ORCID: <http://orcid.org/0000-0003-0823-9051>, mr.emilsr@gmail.com

Abstract: *The composition of gaseous fuel can vary widely, depending on the source, time and stage of development of a particular field. Changes in composition lead to a change in thermophysical characteristics of fuel, which affects the stability of operation of boiler units. This article presents the results of numerical simulation of stabilization of heat output and the completeness of combustion of associated petroleum gas (APG) in the event of prolonged, continuous change in its composition. The simulation was carried out using the previously developed algorithm for optimizing the combustion process of the hydrocarbon fuel (HCF) of variable composition. The simulation results showed that with a slow continuous change in fuel low heating value with a relative rate of change of 1 % during the time of thermal inertia, the stabilization of operation of the boiler according to the proposed algorithm allows maintaining the steam temperature at the outlet within 10 % of the required one.*

Keywords: *heat power engineering, industrial boiler, combustion optimization, variable fuel composition, heat engineering, associated petroleum gas*

Acknowledgments: *The work is performed according to the Russian Government Program of Competitive Growth of Kazan Federal University*

For citation: Saifullin E.R., Larionov V.M., Vankov Yu.V. Numerical modeling of stabilization of the heat output of a steam boiler in the combustion of associated petroleum gas. *Proceedings of the higher educational institutions. ENERGY SECTOR PROBLEMS*. 2019; 21(3-4):15-21. (In Russ). doi:10.30724/1998-9903-2019-21-3-4-15-21

Introduction

According to the Decree of the President of the Russian Federation No. 899 dated 07.07.2011, priority direction of science, technology, and engineering development is “Energy Efficiency, Energy Saving, Nuclear Energy”, and one of the critical technologies of the Russian Federation development is “Energy Efficient Production Technologies and Energy Conversion Using Organic Fuels” [1]. Also in the Energy Strategy of Russia for the period until 2030, priority areas for energy development are the reduction of specific fuel costs in the production and consumption of energy resources through the use of energy-saving technologies and equipment [2]. One of the ways to reduce the consumption of traditional energy is the use of alternative fuels, such as biogas, synthesis gas and industrial gaseous waste. For the Russian Federation, the use of associated petroleum gas (APG) is more relevant.

In 2009, the Government of the Russian Federation adopted Resolution No. 7 of January 8 “On Measures to Promote the Reduction of Atmospheric Air Pollution by Products of Associated Petroleum Gas Burning in Flares” which laid down the requirement to increase the

level of rational use of associated gas to 95 % [4]. The United States also notes the importance of the rational use of hydrocarbon wastes, so the US Environmental Protection Agency, since 2008, considers any gas generated at a refinery to be used as fuel [5]. At present, the following methods of rational utilization of APG are used [10–14]:

1. Processing at a gas processing plant.
2. Injection into the reservoir (cycling process, "gas lift").
3. Processing of APG using GTL technology (gas to liquid) or liquefaction in LPG (liquefied petroleum gas).
4. Injection to seasonal underground storage.
5. The use of APG as an alternative fuel for generation of electric and thermal energy in power plants.

Unlike traditional fuels, the component content of associated petroleum gas can vary widely depending on the source, time and stage of field development. In the oil reservoir, associated petroleum gas is dissolved in oil or is located above the oil in a "gas cap". The composition of gases in the "gas cap" can be very different from the composition of gases dissolved in oil. The composition of gases depends on conditions of sampling, its pressure in the well, proportion of free gas in a sample from the reservoir and proportion of gas released from the oil during its rise in the borehole. In this regard, the content and composition of heavy hydrocarbons in gases selected in the same area show significant fluctuations.

A characteristic feature of APG composition is the presence in them not only methane (CH₄), ethane (C₂H₆), propane (C₃H₈), butane (C₄H₁₀), but also vapor of heavier hydrocarbons. APG has a high calorific value, which varies from 37673 to 62788 kJ/m³ due to the instability of its composition [3].

These changes lead to thermal effect instability of the combustion process, which can lead to negative consequences [4, 5]. There is a probability of blowout (flame going deep into the furnace space), flashback (flame propagation inside the burner), combustion instability (pressure pulsations), self-ignition (ignition of the gas-air mixture in the mixture-forming space), local surface overheating.

The available methods for optimizing a boiler operation, based on controlling the composition of flue gases, calculating the thermal efficiency, and measuring the combustion temperature, are not perfect. The common disadvantages of these methods are high labor intensity, constructive complexity of execution and, most importantly, the inability to quickly respond to random changes in the composition of the combusted fuel. This situation is a consequence of the insufficient knowledge of the thermodynamic characteristics of the hydrocarbon fuels combustion process during periods of changes in its composition, the lack of scientifically based methods for stabilizing the thermal effect of combustion and the heat flux transferred to the coolant. All of the above indicates the relevance of this topic.

The aim of this work was to numerically simulate the stabilization of heat output and the complete combustion of purified associated petroleum gas according to the algorithm developed earlier in the event of a long continuous change in its composition.

Methods

The authors had previously developed a quasistationary model of stabilizing the heat release rate during combustion of a mixture of methane hydrocarbon fuels with air, ensuring complete combustion of fuel in the event of short-term and long-term changes in its calorific value [6–9], and allowing one to stabilize the heat release of the boiler when burning the methane hydrocarbon fuels variable composition with ensuring its complete combustion. According to the algorithm, when the outlet temperature of the heat carrier decreases, caused by a decrease in the fuel calorific value, it is necessary to begin a gradual increase in the fuel flow rate without changing the air flow rate until the heat carrier temperature becomes initial. In case of a constant temperature, the burning mode is specified by a one-time reduction in fuel consumption. A sharp decrease in temperature indicates the optimal combustion mode, and,

according to the algorithm, it is necessary to return to the previous value of fuel flow rate and back to the optimum mode. The constancy of the temperature after a single reduction in the fuel flow rate indicates that an increase in specific heat of combustion has begun, which compensates fuel underburning because the air flow rate has not changed. Therefore, it is necessary to continue a further reduction in fuel flow rate until the temperature starts to decrease. After that, it is necessary to return the previous value of fuel flow rate which corresponds to the initial constant temperature.

Numerical simulation was carried out according to the developed algorithm using the standard method of thermal calculation of boilers [12].

Calculation conditions

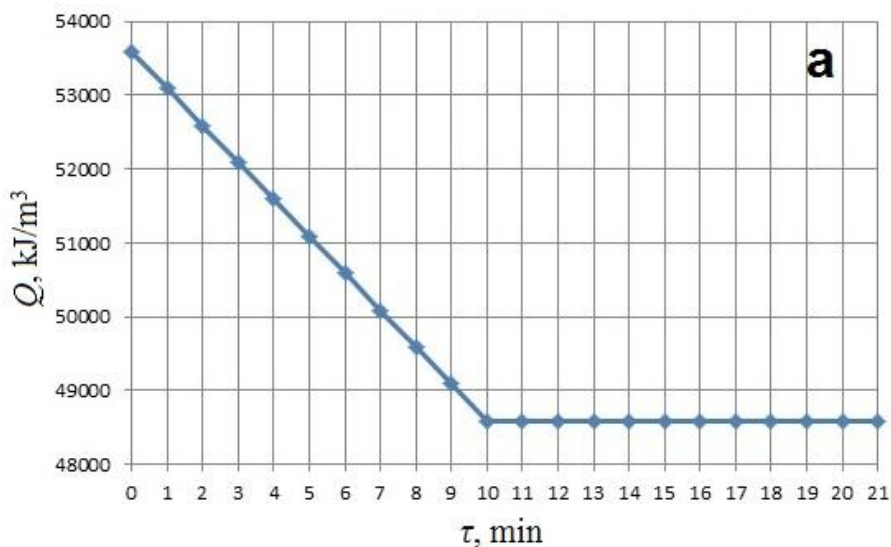
For the calculation we selected steam boiler DE 10-14. The parameters of the boiler operation are shown in the table.

Table

Parameters of the boiler operation

№	Parameter	Value
1.	Boiler steam output D , kg/h	6097
2.	Saturated-steam temperature t_s , °C	172,1
3.	Saturated-steam enthalpy H_s , kJ/kg	2770
4.	Entering water temperature t_w , °C	100
5.	Entering water enthalpy H_w , kJ/kg	508
6.	Exhaust gases temperature ϑ , °C	125
7.	Air temperature at the boiler inlet t_{ina} , °C	27
8.	Thermal inertia time τ_{ij} , min	1

As an example of a hydrocarbon fuel of variable composition, purified associated petroleum gas (i.e., only the hydrocarbon composition of the gas was taken into account) was taken. Two cases were considered: a prolonged decrease and increase in the fuel calorific value (Fig. 1).



a)

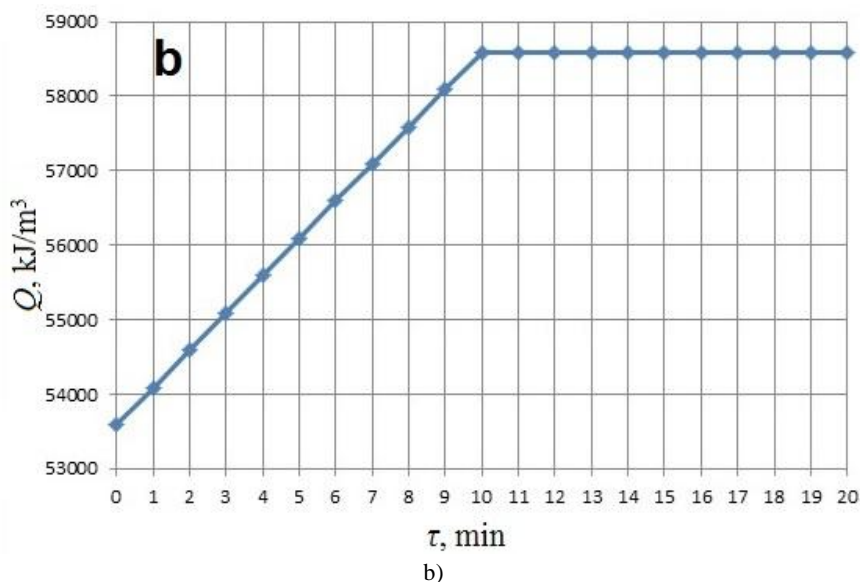
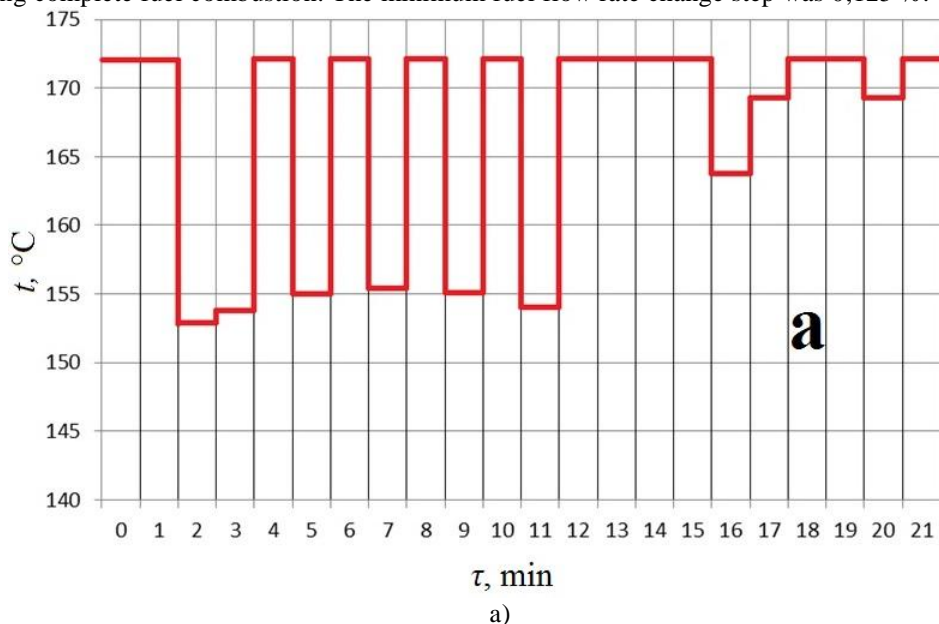


Fig. 1. Prolonged decrease (a) and increase (b) of the fuel calorific value over time

The rate of fuel calorific value change is $\lambda_q=500 \text{ kJ}/\text{min}\cdot\text{m}^3$, initial fuel flow rate $G_f=276,5 \text{ m}^3/\text{h}$, gross efficiency $\eta=0,931$. The analysis was performed in a quasistationary approximation. This means that in the time interval equal to the time of the boiler's thermal inertia, the enthalpy of steam remains constant. At the end of the time interval, the enthalpy quickly takes on the value corresponding to fuel calorific value, which was at the beginning of the interval, so $H_s(\tau)$ is considered a function of $Q_n^r(\tau-\tau_{ii})$.

Results

Numerical simulation showed that regulation of the boiler operation according to the proposed algorithm allows maintaining the steam temperature within 10 % of the initial one (Fig. 2, a, Fig. 3, a) as a result of appropriate control of fuel flow rate (Fig. 2, b, Fig. 3, b) ensuring complete fuel combustion. The minimum fuel flow rate change step was 0,125 %.



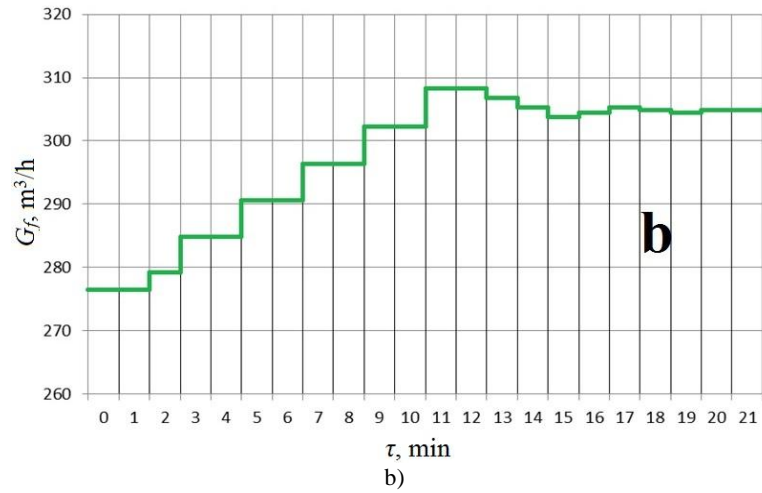


Fig. 2. The change in outlet steam temperature t (a) and the optimal fuel flow rate G_f (b) over time in the case of a prolonged decrease in fuel calorific value

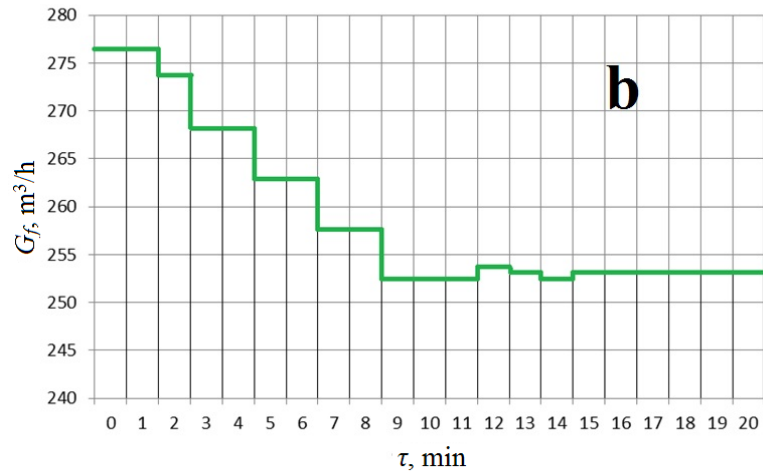
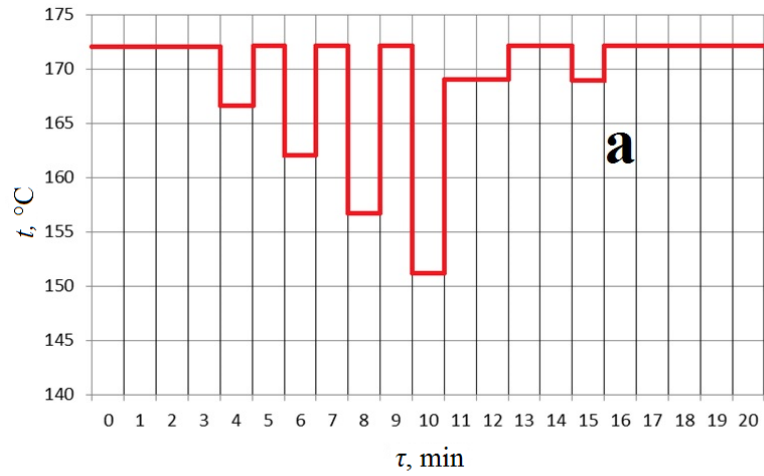


Fig. 3. The change in outlet steam temperature t (a) and the optimal fuel flow rate G_f (b) over time in the case of a prolonged increase in fuel calorific value

Conclusion

Numerical simulation has shown that with continuous random decrease (or increase) of APG specific calorific value, caused by fluctuations in its composition, the heat output of the steam boiler DE 10-14 with the complete combustion of fuel is stabilized by discrete increases (or decreases) steam temperature in a given control range of 10 %.

References

1. Decree of the President of the Russian Federation "On the approval of priority directions for the development of science, technology and technology in the Russian Federation and the list of critical technologies of the Russian Federation" of July 7, 2011 No. 899. *Collected Legislation of the Russian Federation*.

2. Act of the Government of the Russian Federation "The Energy Strategy of Russia for the period until 2030" of November 13, 2009 No. 1715-p. *Meeting of the Legislation of the Russian Federation*.

3. Gur'yanov AI, Evdokimov OA, Piralishvili ShA., et al. Analysis of the Gas Turbine Engine Combustion Chamber Conversion to Associated Petroleum Gas and Oil. *Russian Aeronautics*. 2015; 58:205–209. (In Russ).

4. On measures to stimulate the reduction of atmospheric air pollution by the products of associated gas flaring in flares: Government Decree No. 7 of January 8, 2009.

5. U.S. Environmental Protection Agency, Standards of Performance for Petroleum Refineries, 40 CFR 60, Subpart J, Section 60.101(d), U.S. Government Printing Office, Washington, DC, Electronic Code of Federal Regulations, current as of June 12, 2008.

6. Kayadelen HK. Effect of natural gas components on its flame temperature, equilibrium combustion products and thermodynamic properties. *Journal of Natural Gas Science and Engineering*. 2017; 45:456–473.

7. Sayad P. Operational stability of lean premixed combustion in gas turbines. An experimental study on gaseous alternative fuels, Doctoral Dissertation (2016), Lund University.

8. Saifullin ER., Vankov YuV. Optimization of burning process of hydrocarbon fuels with varying specific heat of combustion. *IOP Conference Series: Materials Science and Engineering*, 2015; 86:012006. DOI: 10.1088/1757-899X/86/1/012006.

9. Saifullin ER., Larionov VM., Busarov AV., et al. Thermal effect of hydrocarbon fuels combustion after a sudden change in the specific calorific value. *Journal of Physics: Conference Series*. 2016; 669(1):012043. DOI: 10.1088/1742-6596/669/1/012043.

10. Saifullin ER., Larionov VM., Busarov AV., et

Литература

1. Указ Президента Российской Федерации "Об утверждении приоритетных направлений развития науки, технологий и техники в Российской Федерации и перечня критических технологий Российской Федерации" от 7 июля 2011 г № 899 // Собрание законодательства Российской Федерации.

2. Акт правительства Российской Федерации "Энергетическая стратегия России на период до 2030 года" от 13 ноября 2009 г. № 1715-р // Собрание законодательства Российской Федерации.

3. Gur'yanov A.I., Evdokimov O.A., Piralishvili Sh.A., et al. Analysis of the Gas Turbine Engine Combustion Chamber Conversion to Associated Petroleum Gas and Oil // *Russian Aeronautics (Iz.VUZ)*. 2015. №58. С. 205-209.

4. О мерах по стимулированию сокращения загрязнения атмосферного воздуха продуктами сжигания попутного нефтяного газа на факельных установках: Постановление Правительства РФ №7 от 8 января 2009 года.

5. U.S. Environmental Protection Agency, Standards of Performance for Petroleum Refineries, 40 CFR 60, Subpart J, Section 60.101(d), U.S. Government Printing Office, Washington, DC, Electronic Code of Federal Regulations, current as of June 12, 2008.

6. Kayadelen H.K. Effect of natural gas components on its flame temperature, equilibrium combustion products and thermodynamic properties, *Journal of Natural Gas Science and Engineering*, 45 (2017) 456-473.

7. Sayad P. Operational stability of lean premixed combustion in gas turbines. An experimental study on gaseous alternative fuels, Doctoral Dissertation (2016), Lund University.

8. Saifullin E.R., Vankov Yu.V. Optimization of burning process of hydrocarbon fuels with varying specific heat of combustion // *IOP Conference Series: Materials Science and Engineering*. V. 86. 2015. № 012006.

9. Saifullin E.R., Larionov V.M., Busarov A.V., et al. Thermal effect of hydrocarbon fuels combustion after a sudden change in the specific calorific value // *Journal of Physics: Conference Series*. V. 669. 2016. № 012043.

10. Saifullin E.R., Larionov V.M., Busarov A.V., et al. Optimization of hydrocarbon fuels combustion variable composition in thermal power plants // *Journal*

all. Optimization of hydrocarbon fuels combustion variable composition in thermal power plants. *Journal of Physics: Conference Series*. 2016; 669(1):012037. DOI: 10.1088/1742-6596/669/1/012037.

11. Saifullin ER, Nazarychev SA, Malahov AO., et al. The heat effect of combustion process depending on fuel composition fluctuations. *Journal of Physics: Conference Series*. 2017; 789(1):012045. DOI: 10.1088/1742-6596/789/1/012045.

12. Larionov VM, Saifullin ER, Nazarychev SA., et al. Algorithm for optimizing the process of burning associated petroleum gas in thermal power plants, taking into account the variability of its composition. Proceedings of the higher educational institutions. ENERGY SECTOR PROBLEMS, 2017. № 19. pp. 3-9.

13. Larionov VM, Vankov YuV, Sayfullin ER, et al. Sposob avtomaticheskoy optimizacii processa szhiganiya topliva peremennogo sostava [Method of fuel with variable composition combustion process automatic optimization]. Patent RUS №2647940. 21.03.2018. Byul. №9. Available at: https://yandex.ru/patents/doc/RU2647940C1_20180321. Accessed: 22 Apr 2019. (In Russ).

14. Teplovoj raschet kotel'nyh agregatov (normativnyj metod) [Thermal calculation of boiler units (normative method)]. Saint- Petersburg: NPO CKTI, 1998. (In Russ).

of Physics: Conference Series. V. 669. 2016. № 012037.

11. Saifullin ER, Nazarychev SA, Malahov AO., et al. The heat effect of combustion process depending on fuel composition fluctuations // *Journal of Physics: Conference Series*. V. 789. 2017. № 012045.

12. Larionov VM, Saifullin ER, Nazarychev SA., et al. Algorithm for optimizing the process of burning associated petroleum gas in thermal power plants, taking into account the variability of its composition // Proceedings of the higher educational institutions. ENERGY SECTOR PROBLEMS. 2017. № 19. pp. 3-9.

13. Ларионов В.М., Ваньков Ю.В., Сайфуллин Э.Р., и др. Способ автоматической оптимизации процесса сжигания топлива переменного состава. Патент РФ на изобретение №2647940. 21.03.2018. Бюл. №9. Доступно по: https://yandex.ru/patents/doc/RU2647940C1_20180321. Ссылка активна на 22 апреля 2019.

14. Тепловой расчет котельных агрегатов (нормативный метод). Изд-е 3-е, перераб. и доп. СПб: НПО ЦКТИ, 1998. 256 с.

Authors of the publication

Emil R. Saifullin – Ph.D. student at Kazan Federal University.

Viktor M. Larionov – Doctor of Technical Sciences, Professor at Kazan Federal University.

Yuriy V. Vankov – Doctor of Technical Sciences, Professor at Kazan State Power Engineering University.

Received

January, 16 2019



DETERMINATION OF LOCAL HEAT TRANSFER COEFFICIENTS AT THE ENTRANCE REGION OF STREAMLINED BODIES

T.M. Farakhov¹, A.G. Laptev²

¹ Engineering-Promotional Center “Inzhekhim”, Kazan, Russia

² Kazan State Power Engineering University, Kazan, Russia

vt_kgeu@mail.ru

Abstract: Prandtl's two-layer model of the turbulent boundary layer is considered and the expression obtained through the use of the model is applied to calculate the heat transfer coefficient, calculations for which agree well with experimental data on mean values of the coefficients for various bodies. Determination of parameters of this expression is shown for the case of calculating local heat transfer coefficients in the entrance regions of the channels. The main parameters are dynamic velocity, dimensionless thickness of the boundary layer and dimensionless thickness of the viscous sublayer. Based on the power-law and logarithmic velocity profiles, expressions are obtained for calculating the dimensionless parameters of the turbulent boundary layer. A satisfactory agreement of the results of calculations of local heat transfer coefficients for the flow over a flat plate and the pipe flow is shown. The presented approach represents a theoretical basis for modeling the local heat transfer for bodies of more complex shapes, if the friction coefficients are known.

Keywords: local heat transfer, boundary layer, turbulence, entry region.

Acknowledgments: The work was performed within the framework of the basic part of the state task in the field of scientific activity (No.13.6384.2017/BCH).

For citation: Farakhov T.M., Laptev A.G. Determination of local heat transfer coefficients at the entrance region of streamlined bodies. *Proceedings of the higher educational institutions. ENERGY SECTOR PROBLEMS*. 2019; 21(3-4):22-26. (In Russ). doi:10.30724/1998-9903-2019-21-3-4-22-26.

Introduction

Solving the problems of mathematical modeling and improving the efficiency of heat transfer processes represent an important task, which is relevant for practically all industries as well as for power engineering [1–4]. Several monographs and textbooks have been published in recent years in this field [5–7].

In the course of solution of the problems of mathematical modeling of heat transfer processes, in addition to the average heat transfer coefficients in the flow around various bodies of relatively small spills (for example, at the entrance regions of short channels), the calculation of local heat transfer coefficients must be performed. The hydrodynamic stabilization of the boundary layer in the channels takes place at the entrance region, the length of which ranges from 20 to 50 pipe diameters, depending on the Reynolds number.

The purpose of the present work is to present examples of calculations of local heat transfer coefficients for flows over a flat plate and in a pipe based on the application of Prandtl's boundary layer model.

Prandtl's two-layer model of the turbulent boundary layer is the simplest model from the standpoint of its mathematical description; however, it gives results for the transfer coefficients, which are only slightly different from the results obtained via the more complex models (Karman, Deissler, Levich, Hanratty, Owen, Van Driest and others).

Based on application of Prandtl's model, an expression for the heat transfer coefficient was obtained in the form [8, 9]:

$$\alpha = \frac{\rho c_p u_*}{\text{Pr}^m \left[R_1 + \frac{1}{\chi} \ln(R_\delta / R_1) \right]}, \quad (1)$$

where α is heat transfer coefficient, $\text{W/m}^2 \cdot \text{K}$; Pr is Prandtl number; u_* is dynamic velocity, m/s; R_1 is dimensionless thickness of the viscous sublayer (for fully-developed flat plate flow $R_1 = 11,6$); $R_\delta = u_* \delta / \nu$ is dimensionless thickness of the boundary layer; δ is thickness of the boundary layer, m; ν is kinematic viscosity, m^2/s ; $\chi = 0,4$ is turbulence constant; ρ is density of the medium, kg/m^3 ; c_p is specific heat capacity of the medium, $\text{J/kg} \cdot \text{K}$.

Expression (1) gives satisfactory results of calculations for average heat transfer coefficients under various flow conditions in the channels [8, 9].

The use of expression (1) for calculating local heat transfer coefficients is discussed below.

Local heat transfer from a plate

At first, let us consider an example of flow over a flat plate in the turbulent stationary mode. For this case, we need to determine the main parameters in expression (1) depending on the distance of the free-stream flow in the longitudinal direction of the plate. Then for the flat plate flow ($m=0,57$), we can write

$$\alpha_x = \frac{\rho c_p u_{*x}}{\text{Pr}^{0,57} \left[R_{1x} + \frac{1}{\chi} \ln(R_{\delta x} / R_{1x}) \right]} \quad (2)$$

Dynamic velocity is expressed through the local friction factor of the plate C_{fx} :

$$u_{*x} = u_\infty \sqrt{C_{fx} / 2}, \quad (3)$$

where u_∞ is external-flow velocity, m/s.

For the flat plate flow at $\text{Re}_x = u_\infty x / \nu$ in the range from 10^5 to 10^6 , $C_{fx} = 0,058 / \text{Re}_x^{0,2}$, where Re_x is Reynolds number; x is longitudinal coordinate, m.

An expression for the local value of thickness of the turbulent boundary layer on the plate, as is known, has the form

$$\delta = \frac{0,37x}{\text{Re}_x^{0,2}}. \quad (4)$$

Then an expression for the value of $R_{\delta x}$ can be obtained from (3) and (4) in the form:

$$R_{\delta x} = 0,37 \text{Re}_x^{0,8} \sqrt{C_{fx} / 2}. \quad (5)$$

Dimensionless thickness of the viscous sublayer R_{1x} can be expressed as a function of the coordinate, which can be found from the power-law velocity profile on the plate:

$$\frac{u}{u_*} = C(n) \left(\frac{yu_*}{\nu} \right)^{1/n} = C(n) (y^+)^{1/n}, \quad (6)$$

where for $40 < y^+ < 700$, $C(n) = 8,74$; $n = 7$.

In the viscous sublayer, the velocity profile is described by the linear function:

$$\frac{u}{u_*} = \frac{u_* y}{\nu}. \quad (7)$$

At the boundary of the viscous sublayer, functions (6) and (7) give the identical value

$$R_1 = \frac{u_* \delta_1}{\nu} = C(n) \left(\frac{u_* \delta_1}{\nu} \right)^{1/n}. \quad (8)$$

The value $C(n)$ can be determined from the velocity profile (6); at $y = \delta$ and $u = u_\infty$, we have

$$\frac{u_\infty}{u_*} = C(n) R_\delta^{-1/n}. \quad (9)$$

Then

$$C(n) = \frac{u_\infty}{u_*} R_\delta^{-1/n}. \quad (10)$$

As a result, from (8)–(10) we obtain for $n=7$ a local value, where $u_{*x} = u_\infty \sqrt{C_{fx}/2}$ (3); thus, we have

$$R_{1x} = \left(\frac{2}{C_{fx}} \right)^{7/12} R_{\delta x}^{-1/6}. \quad (11)$$

Calculations reveal that the value obtained via (11) practically does not change and is equal to $R_{1x} = 12,4$, which is close to the value $R_1 = 11,6$ provided by the boundary layer theory. It is likely that a small discrepancy is due to an error of the approximation of the velocity profile by a power-law function. Therefore, we can adopt $R_{1x} = R_1 = 11,6$.

A velocity profile in the turbulent region of the boundary layer is also described by a logarithmic function having the form

$$\frac{u}{u_*} = 2,5 \ln \frac{u_* y}{\nu} + 5,5. \quad (12)$$

At the boundary of the viscous sublayer, the linear velocity profile and the logarithmic one take the same value, i.e. at $y = \delta_1$: $u_1 / u_* = R_1$ and

$$R_1 = 2,5 \ln R_1 + 5,5. \quad (13)$$

This expression leads to the constant value $R_1 = 11,63$.

The local heat transfer coefficient on the plate is calculated via the known criterial expression [1]

$$\text{Nu}_x = 0,03 \text{Re}_x^{0,8} \text{Pr}^{0,43}, \quad (14)$$

where $\text{Nu}_x = \alpha_x x / \lambda$ is local Nusselt number; λ is thermal conductivity of the medium, W/m K.

Expression (2) can be written in a dimensionless form with u_{*x} determined from (3)

$$\text{Nu}_x = \frac{\text{Re}_x \sqrt{C_{fx}/2} \text{Pr}^{0,43}}{11,6 + 2,5 \ln(R_{\delta x} / 11,6)}. \quad (15)$$

From calculations via (14) and (15) at $\text{Re}_x = 2 \cdot 10^5$ in line with expression (14), we have $\text{Nu}_x = 513,6$, and line with (15), we have $\text{Nu}_x = 502,5$ (at $\text{Pr} = 1$).

The deviation is around 3%. At $\text{Re}_x = 10^6$, accordingly we obtain $\text{Nu}_x = 1861$ and $\text{Nu}_x = 1882$, and the deviation is around 2%.

Thus, adequacy of expression (15) for Nu_x with parameters (5) and $R_1 = 11,6$ is proved for modeling of local heat transfer on the plate under turbulent flow conditions.

Heat transfer at the entrance region of the pipe

At turbulent motion of a single-phase flow in a pipe, length of the hydrodynamic stabilization region $l_{CT} < 50d$, where d is pipe diameter [1, 10]. At the entrance region, the flow velocity on the channel axis changes from an average inlet value u_{av} to a value u_{max} present beyond the hydrodynamic stabilization region. Taking into account that the thickness of the turbulent boundary layer (4) depends on the longitudinal coordinate x as $\delta \sim x^{4/5}$, the flow velocity on the axis can be approximately determined from the expression

$$u_{max(x)} = u_{av} + u_m(x) (x / l_{CT})^{4/5}, \quad (x \leq l_{CT}), \quad (16)$$

where at $x=0$ we have $u_{max} = u_{av}$ (entrance to the pipe); at $x = l_{CT}$, $u_{max} = u_{av} + u_m$, where $u_m = 4u_*$; at $0 < x < l_{CT}$, $u_m = 4u_*(x)$ is velocity on the axis, m/s.

In the literature, there is no function for the friction coefficient for the entrance region of the pipe; therefore, for the first approximation at $x < l_{CT}$, we make use of the expression for the flat plate flow $C_{f,x}$ and the dynamic velocity in formula (3).

The value of $R_{\delta,x}$ is calculated via formula (5), where the Reynolds number is calculated through the velocity from (16), similarly to calculation of $C_{f,x}$.

In addition, from the logarithmic profile (12), one can obtain a local value of $R_{\delta,x}$ for the entrance region of the pipe. For $u = u_\infty$ and $y = \delta$, we have

$$R_{\delta,x} = \exp \left[0,4 \left(\frac{u_{av} + 4u_{*x}}{u_{*x}} \right) - 5,5 \right]. \quad (17)$$

Length of the hydrodynamic stabilization region in a circular pipe can be approximately estimated from expression (4) at $\delta \approx R$ and $u_\infty \approx 1,15u_{cp}$. We obtain

$$l_{CT} = \left(\frac{R}{0,37} \right)^{5/4} \left(\frac{1,15u_{av}}{v} \right)^{1/4}, \quad (18)$$

where R is pipe radius, m.

The calculation shows that the ratio of the local heat transfer coefficient α_x (2) to the average one α at $x/d = 1,0$ becomes $\alpha_x / \alpha = 1,35$ ($Re_d = 5 \cdot 10^4$). In monographs [1, 7, 10], the value $\alpha_x / \alpha = 1,34$ was given. The calculations of α_x / α are in satisfactory agreement with the known corrections, which take into account the entrance region in the pipe at different Reynolds numbers and, accordingly, length of the entrance region (18).

Conclusions

The use of an expression for heat transfer coefficient obtained earlier by the authors via Prandtl's model is considered for the case of local heat transfer at the entrance regions of the channels. The local boundary layer parameters for flows over a flat plate and in a pipe are determined. An agreement of the results of calculations for local heat transfer coefficients versus known results is shown. The presented approach is a theoretical basis for modeling local heat transfer for bodies having different geometries of streamlined surfaces.

References

1. Khrustalev B.M., Timoshpol'skij V.I., et al.;
Nesenchuk A.P., editor. *Тепло и массообмен*. Pt.1. Minsk:

Литература

1. Хрусталеv Б.М., Несенчук А.П.,
Тимошпольский В.И., и др. *Тепло и массообмен*. Ч.1.;

Belarusian National Technical University Press; 2007. (In Russ).

2. Molchanov AM, Bykov LV., Yanyshv DS. Three-Parameter Model of Turbulence for High-Velocity Flows. *Journal of Engineering Physics and Thermophysics*. 2018; 91(4):720-727. DOI: 10.1007/s10891-018-1789-9.

3. Minakov AV, Guzei DV, Meshkov KN., et al. Experimental study of turbulent forced convection of nanofluid in channels with cylindrical and spherical hollows. *International Journal of Heat and Mass Transfer*. 2017; 115:915-925. DOI: 10.1016/j.ijheatmasstransfer.2017.07.117.

4. Leont'ev AL, Kuzma-Kichta YA, Popov IA. Heat and mass transfer and hydrodynamics in swirling flows (review). *Thermal Engineering*. 2017; 64(2):111-126. DOI: 10.1134/S0040601517020069.

5. Kudinov IV., Kudinov VA, Eremin AV., et al. *Matematicheskoe modelirovanie gidrodinamiki i teploobmena v dvizhushchihsya zhidkostyah*. Saint-Petersburg: Lan Publishing House, 2015. (In Russ).

6. Marinyuk B. Rascheti teploobmena v apparatah i sistemah nizkotemperaturnoj tekhniki. Moscow: Mashinostroenie, 2015. (In Russ).

7. Rudskoy AI. Matematicheskoe modelirovanie gidrodinamiki teploobmena v dvizhushchihsya zhidkostyah. Saint-Petersburg: Lan Publishing House, 2015. (In Russ).

8. Laptev AG, Basharov MM, Farakhov TM. Teplo- i massootdacha v vozmushchennyh turbulentnyh pogranychnyh sloyah. *Trudy Akademenergo*. 2016; 1: 53-71. (In Russ).

9. Laptev AG, Basharov MM. Mathematical Model and Calculation of Heat Transfer Coefficients of Rough Turbulent-Flow-Carrying Channels. *Journal of Engineering Physics and Thermophysics*. 2015; 88(3):656-662. DOI: 10.1007/s10891-015-1237-z.

10. Mikheev MA, Mikheev IM. *Osnovy teploperedachi*. Moscow: Energiya, 1977. (In Russ).

под ред. А.П. Несенчука. Минск: БНТУ, 2007. 606 с.

2. Молчанов А.М., Быков Л.В., Янышев Д.С. Трехпараметрическая модель турбулентности для высокоскоростных течений // Инженерно-физический журнал. 2018. Т. 91, №4. С. 720–727.

3. Minakov A.V., Guzei D.V., Meshkov K.N., Popov I.A. Experimental study of turbulent forced convection of nanofluid in channels with cylindrical and spherical hollows // *International Journal of Heat and Mass Transfer*. 2017. Т. 115. С. 915–925.

4. Leont'ev A.L., Kuzma-Kichta Y.A., Popov I.A. Heat and mass transfer and hydrodynamics in swirling flows (review) // *Thermal Engineering*. 2017. Т. 64, № 2. С. 111–126.

5. Куудинов И.В., Куудинов В.А., Еремин А.В., и др. Математическое моделирование гидродинамики и теплообмена в движущихся жидкостях. СПб.: Лань, 2015. 208 с.

6. Маринюк Б. Расчеты теплообмена в аппаратах и системах низкотемпературной техники. М.: Машиностроение, 2015. 272 с.

7. Рудской А.И. Математическое моделирование гидродинамики теплообмена в движущихся жидкостях. СПб.: Лань, 2015. 208 с.

8. Лаптев А.Г., Башаров М.М., Фарахов Т.М. Тепло- и массоотдача в возмущенных турбулентных пограничных слоях // *Труды Академэнерго*. 2016. №1. С. 53–71.

9. Лаптев А.Г., Башаров М.М. Математическая модель и расчет коэффициентов теплоотдачи в шероховатых каналах при турбулентном режиме // *Инженерно-физический журнал*. 2015. Т. 88, №3. С. 656–662.

10. Михеев М.А., Михеев И.М. *Основы теплопередачи*. М.: «Энергия», 1977. 344 с.

Authors of the publication

Timur M. Farakhov – Ph.D., Principal Engineer, Engineering-Promotional Center “Inzhexhim”.

Anatoly G. Laptev – D.Sc., Professor and Chairman of Department “Technology of Water and Fuel”, Kazan State Power Engineering University.

Received

October, 16 2018



ASSESSMENT OF COMPRESSED AIR ENERGY POTENTIAL FOR DETERMINING EFFICIENCY OF AN AIR STORAGE POWER PLANT

V. Stepanov, T. Stepanova, N. Starikova

Irkutsk National Research Technical University, Irkutsk, Russia

ORCID*: <http://orcid.org/0000-0002-2649-5318>, Natalia-starikova@yandex.ru

Abstract: The article is devoted to thermodynamic analysis of the processes occurring in energy storages of compressed atmospheric air. As a tool for study of compression-expansion processes, we propose a method of compiling and analyzing of exergy balance. As a result, the main characteristics can be assessed, namely, potential of compressed air and efficiency of all elements of the circuit and air storage power plant (ASPP) as a whole. The study procedure is shown on the example of an adiabatic ASPP. The dependences of the final temperature, specific exergy and compression work per 1 ths. m^3 of atmospheric air on the degree of its compression were calculated. Due to external factors ASPP of this type cannot have high thermodynamic efficiency. However, it has a number of economic advantages, and is well compatible with renewable energy sources, for example, with wind power plants. To increase the efficiency of the process, it is necessary to convert the ASPP type to non-adiabatic one, which will require changes in circuit and operation modes of its elements. At the same time, compression in the compressor should be carried out with the highest possible heat removal, and the expansion process in open-type gas turbine units should be carried out with heat supply.

Keywords: energy storages, air storage power plant, thermodynamics analysis, exergy method.

Acknowledgments: The work was done as a personal initiative.

For citation: Stepanov V.S., Stepanova T.B., Starikova N.V. Evaluation the energy potential of compressed air for determining efficiency of air-accumulating electric. *Proceedings of the higher educational institutions. ENERGY SECTOR PROBLEMS*. 2019; 21 (3-4):27-37. (In Russ). doi:10.30724/1998-9903-2019-21-3-4-27-37.

Introduction

In recent years, many countries have significantly increased their interest in renewable energy sources (RES), the use of which does not violate the natural energy balance of our planet. Renewable energy sources include reserves that are replenished naturally and are practically inexhaustible in the foreseeable future. First of all, these include solar radiation, wind energy, river energy, etc. [1–3].

However, almost all sources of renewable energy have a probabilistic mode of energy output during a day, season, time period, which is a distinctive feature of all natural processes. Moreover, schedule of such power generation does not match with requirements of power system in terms of covering the load to consumers, and even is often opposed to it. In other words, these sources do not have the constancy of the output power, are not subject to regulation, and cannot adjust to the power system's power consumption mode. In other words, the use of RES is associated with a number of difficulties, due to the probabilistic nature of generation and, therefore, the complexity of integrating them into the operating mode of traditional power systems.

Currently, a new concept is actively being promoted - the construction of future smart energy systems, called the Smart Grid. This concept is aimed at achievement the following

important goals: widespread use of modern means of control and management, including Internet technologies, integration of renewable energy sources into the power supply system, as well as various kinds of energy storage devices in order to increase the reliability and efficiency of power generation and its quality.

It is known that energy storage can be carried out in the form of potential energy of an agent (energy carrier), for example: water, by using it at water storage power plant (WSPP), or compressed gas (air), feeding it into compressionless gas turbines installed at the air storage power plants (ASPP) of various types.

Energy of compressed air can be accumulated by pumping it with a high-pressure compressor into specially designed tanks or underground natural and artificial containers. When required, compressed air from the storage is fed to the corresponding element of the ASPP.

There are two types of compressed air storages which differ by location of the storage. The first one is called the *ground storage system*, and the other is *underground storage system*. Each of them has its own specific requirements and scope. Currently, it is economically feasible to use underground tanks of compressed air as part of air-storage power plants with a capacity of 100 kW and more, and ground storage facilities can operate as part of small power plants with a capacity of 10 to 100 kW.

Natural gas pipelines, for whatever reason turned out to be idle can be used as ground storages of compressed air. Specially constructed tanks for storing compressed air can be used as part of a small capacity ASPP.

Underground compressed air storages are more economical, for which it is advisable to use natural voids in the earth's crust, salt caves, spent natural gas deposits, etc.

Energy storages of compressed air (ESCA) allow one to save large quantities (volumes) of energy for a long time at a relatively low cost. Therefore, their widespread use in the smart grid of the future (Smart Grid) has very good prospects in view of further improving the energy efficiency of the storages themselves.

Improving the processes of compression and expansion of air to increase the efficiency of ESCA is possible only when one understands the complex processes that occur in compressors, and the nature of changes in air parameters and energy transformations in other ASPP elements [1].

Thermodynamic principles of air compression and expansion [4, 5]

To describe the nature of change in air parameters in this process, the thermodynamic function of polytropes $pV^n = \text{idem}$ with different values of its exponent n is used.

All the variety of processes of compression and expansion of air can be divided into two types. The processes carried out without exchange of heat of a compressible/expanding agent with environment, that is for $dq=0$ and $dS=0$, are called *adiabatic* or *isentropic*. The polytropic index of such processes is $n=k$, where k is adiabatic index equal to the ratio between the isobaric and isochoric heat capacities of air, $k = \frac{C_p}{C_v}$. All other processes occurring with heat exchange are called non-adiabatic or diabatic.

The processes of air compression can be carried out with heat removal from the compressible agent, the polytropic index for them is $n < k$. Moreover, if the process of gas compression takes place with complete heat removal, i.e. the process proceeds at a constant initial temperature $T_1 = \text{idem}$, then it is called *isothermal*. The polytropic index of such processes is $n=1$.

In general case, for non-adiabatic air compression processes carried out with heat removal, the polytropic index is $n < k$, and it is $n > k$ when heat is supplied. The polytropic indices for non-adiabatic expansion processes when heat is applied are $n < k$, and $n > k$ when heat is removed.

Fig. 1 shows the relationship between the agent state parameters in an ideal compressor and the polytropic index, describing various processes of air compression. The diagram shows the

$$V^k = V_1 \frac{p_1^{1/k}}{p^{1/k}}. \quad (2)$$

As a result of substitution and integration, we obtain an expression for determining the work of adiabatic air compression:

$$l = e_{\text{TM}} = \frac{k}{k-1} p_1 V_1 \left[\left(\frac{p_2}{p_1} \right)^{\frac{k-1}{k}} - 1 \right]. \quad (3)$$

Thus, in systems of storage and use, compressed air is constantly subjected to processes of compression and expansion. However, the specialists have some doubts in regard to use of the terms of energy or exergy while answering the following questions: What kind of energy transformations occur with air? How its energy potential changes? And how one can evaluate this potential? This article uses the concepts of exergy and exergy balance [6–9].

The equation of energy and exergy balances of reversible processes of compression and expansion for a unit mass of any gas is:

$$l = h_2 - h_1 + q \quad (4)$$

and

$$l = e_2 - e_1 + e_q = e_2 - e_1 + q \cdot \tau_e. \quad (5)$$

Here $\tau_e = \frac{T - T_0}{T}$ is heat efficiency coefficient, where T is an arbitrary temperature; T_0 is ambient temperature.

Processes can be carried out at different ratios of temperatures T and T_0 . Of interest is the case of compression at $T = T_0$, when $e_q = 0$. In this case $l = e_2 - e_1$, that is, the work of isothermal compression (expansion) at ambient temperature is equal to the difference between gas exergy in the initial and final states.

From equation (4) it follows that the change in gas energy (in a continuous process, gas energy is measured by enthalpy) is equal to the difference between the spent work l and the heat removed q :

$$h_2 - h_1 = l - q. \quad (6)$$

For an ideal gas, this value is zero, because its exergy does not depend on pressure, and the heat released during the compression process is exactly equal to the spent work.

In general case, for a real gas $q \neq l$, and the difference $h_2 - h_1$ is determined by the magnitude and sign of the isothermal Joule-Thomson effect of the gas under consideration Δh_T at a given temperature, i.e.

$$\Delta h_T = h_1 - h_2. \quad (7)$$

The magnitude and sign of the Joule – Thomson effect is determined by the ratio between the gas work and the work of external pressure forces, as well as the properties of the gas itself, in particular the size of its molecules and their interaction.

For gases such as air, oxygen, and nitrogen at T_0 and pressures up to 30 MPa, Δh_T are greater than zero (positive Joule – Thomson effect) and, therefore, the energy of such compressed gases is less than for uncompressed ones ($h_2 < h_1$).

For other gases (helium, neon, hydrogen) at T_0 $\Delta h_T < 0$ (negative Joule – Thomson effect), and the energy of compressed gas is several percent more than that of the expanded one. However, this difference is very small compared with the amount of work spent for gas compression.

Thus, the energy of compressed gas is slightly different from the energy of uncompressed gas, and in most cases is less than it.

In cases when isothermal compression occurs at $T \neq T_0$ the value e_q in equation (4) is not zero.

The energy balance of the compression process in general can be written as:

$$l = q - \Delta h_T. \quad (8)$$

And the exergy balance has the following form

$$l = e_2 - e_1 + e_q = \Delta e + q \cdot \tau_e. \quad (9)$$

By substituting q from (8) into (9) and using the expression for τ_e , we obtain:

$$l = \Delta e \frac{T}{T_0} + \Delta h_T \left(\frac{T}{T_0} - 1 \right) = (\Delta e + \Delta h_T) \frac{T}{T_0} - \Delta h_T \quad (10)$$

and

$$q = (\Delta e + \Delta h_T) \frac{T}{T_0}. \quad (11)$$

For an ideal gas, the value of the isothermal Joule-Thomson effect $\Delta h_T = 0$. In this case, expressions (10) and (11) are reduced to the following formula:

$$l = q = \Delta e \frac{T}{T_0}. \quad (12)$$

In order to estimate the energy potential of compressed air at its various pressures, we performed calculations of thermomechanical exergy of 1000 m³ of atmospheric air for the corresponding pressures. In the calculations it was assumed that exergy of air is equal to the work of its adiabatic compression in an ideal compressor, which was calculated using expression (3).

The results of calculations for pressure ranges from 3 to 90 atm are given in Table. 1. The resulting dependence can be used to solve a number of specific tasks, for example: to optimize the composition of virtual power plants using the energy of compressed air storages or when choosing the composition of generating sources of autonomous power systems and optimizing their operating modes, taking into account the uneven load curve of the considered system.

In addition, the thermomechanical exergy of compressed air allow us to determine the energy potential of air entering the storage facility at known pressures p_1 and p_2 . For a known volume V , it can be found as the difference in exergies at corresponding pressures, i.e.

$$\Pi_f = (e_2 - e_1) \cdot V. \quad (13)$$

Obviously, the potential of the same air volume coming from the storage to the gas turbine will be the same. For example, if the pressure in the storage has changed from 80 to 90 atm. while the compressor delivers 100 ths. m³ of air, then the energy potential of this air volume will be

$$\Pi_f = (257,80 - 245,98) 100 = 1182 \text{ kW} \cdot \text{h}.$$

Since the energy potential of compressed air is compression work, then, knowing this value, it is possible to determine the amount of electrical energy spent on the compressor drive when it compresses air of a given volume. This value can be found using the expression:

$$W_{el}^c = \frac{\Pi_f}{\eta_c \cdot \eta_{ed}}, \quad (14)$$

where η_c is efficiency of compressor; η_{ed} is efficiency of electric drive.

Similarly, one can determine the amount of electrical energy that can be obtained using the gas turbine unit:

$$W_{el}^c = \Pi_f \cdot \eta_{GT} \cdot \eta_{eg},$$

where η_{GT} is efficiency of gas turbine unit; η_{eg} is efficiency of electric generator.

The obtained values of the thermomechanical exergy of air can be used to estimate the energy potential of compressed air of storages used in various circuits and in different operating modes of ASPP.

ASPP schematics and hardware

As was noted above, heat is generated during the compression phase, i.e. the compressed air is heated. The higher is the degree of increase in air pressure β , the higher its final temperature T_{fin} is:

$$T_{fin} = T_0 \left[\beta^{\frac{n-1}{n}} \right]. \tag{15}$$

Two typical ASPP schemes are distinguished depending on the use of heat generated during air compression: adiabatic and non-adiabatic. Further we consider the features of building an adiabatic ASPP, the scheme of which is shown in Fig. 2

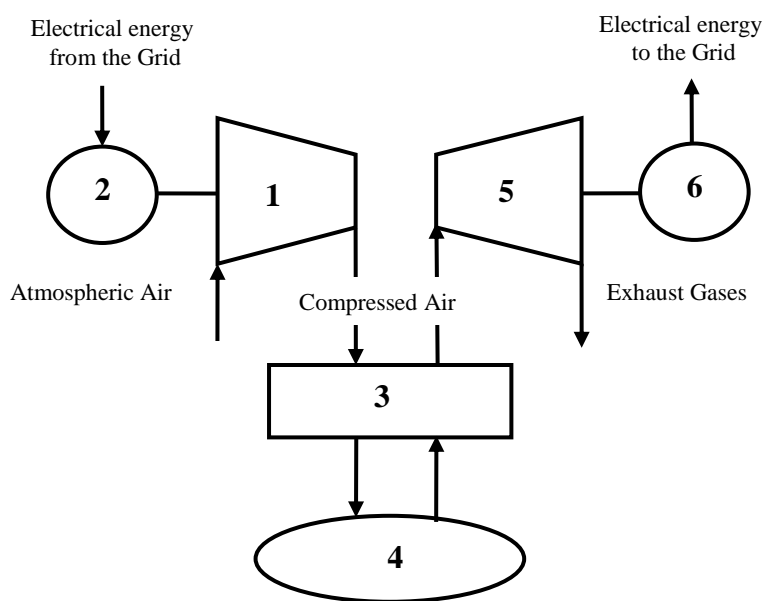


Fig. 2. Schematic diagram of the adiabatic ASPP: 1 – Compressor; 2 – Electric drive; 3 – Heat accumulator – heat exchanger; 4 – Compressed air storage; 5 – Uncompressed gas turbine (UGT); 6 – Electric generator

The ASPP includes: a compressed air storage unit, a compressor driven by an electric motor, an uncompressed gas turbine and an electric generator located on the same shaft as the turbine. The ASPP operation principle is as follows. The air compressed in the compressor, is adiabatically heated to the appropriate temperature, depending on the degree of increase in pressure β . As β increases, the temperature of the compressed air leaving the compressor increases, which, in turn, leads to an increase in the work expended on the compressor drive. To obtain the dependence of the final temperature on the degree of air compression, calculations were made using formula (15).

Consequently, the increase in T_{fin} leads to an increase in compression work, which was determined by formula (12). The results of these calculations are given in Table 1.

Table 1

Relationship between final temperature, specific exergy and compression work of 1 ths. m³ of atmospheric air and the degree of its pressure increase

$\beta = \frac{P_{fin}}{P_0}$	Final temperature of the compressed air T_{fin}	Thermomechanical exergy e_{TM}		Work for compression l_{com}	
		kJ	kW·h	kJ	kW·h
3	401,24	130,44	36,21	178,50	49,58
5	464,23	206,44	57,22	327,00	90,83
10	565,97	330,88	91,90	639,25	177,58
20	689,43	478,29	132,86	1126,36	312,88
30	774,11	580,45	161,24	1533,54	425,92
40	840,62	660,69	183,52	1896,00	526,80
50	895,91	727,50	202,08	2224,70	617,97
60	943,81	785,12	218,09	2529,63	702,69
70	986,31	836,38	232,39	2814,42	781,70
80	1024,66	882,69	245,13	3085,0	856,94
90	1060,32	925,11	256,98	3349,82	930,30

The obtained results allow one to determine the energy potential of compressed air, and therefore make it possible to compose the exergy balance of the corresponding circuit elements and the ASPP as a whole and determine their efficiency.

In the considered scheme, in order to increase the efficiency of a compressed air energy storage device, it is usually envisaged to utilize its heat after compression using a heat exchanger-accumulator, through which compressed air passes before it enters the storage unit. Compressed air from the storage is supplied to the uncompressed turbine being previously pre-heated by the heat stored in heat exchanger. However, in this scheme, the heat of compressed air entering the turbine may have a relatively low temperature, much lower than T_C . Therefore, the efficiency of such ASPP will not be very high. This does not mean that the use of adiabatic ASPP never makes sense. As it can be seen from Fig. 2, such a scheme is simple in terms of a set of equipment (there is no compressor for a gas turbine), and therefore does not require large capital investments, i.e. it has economic advantages.

The experience of usage of gas utilization non-compressor turbines (GUNT) operating on blast-furnace gas overpressure at the metallurgical plants convincingly shows their technical and economic efficiency. Specific capital investments per 1 kW of installed capacity of a gas-expanding station (GES) with GUNT are 35 % less, and operating costs for generating 1 kW·h of electricity for it are 45 % less compared with that for CHP [9, 10].

So, according to the facts presented in the theoretical section of the paper, in order to increase the energy efficiency of adiabatic ASPP, it is necessary to fundamentally change its scheme. Compression in compressor should be carried out with the maximum possible removal of heat (bringing the process closer to isothermal), and the expansion process in turbine should be carried out with heat supply (bringing the process closer to the adiabatic one).

A schematic diagram of such a non-adiabatic ASPP is shown in Fig. 3.

The scheme shows that compressor is equipped with coolers to remove the heat released during air compression. To increase the efficiency of using compressed air energy, it is directed not into the uncompressed gas turbine, but into the scheme of a conventional open-type gas turbine unit (GTU). Such GTU consists of a fuel combustion chamber (gaseous or liquid), the combustion products of which are sent to a gas turbine (GT). GT shaft is connected to shaft of compressor and electric generator. For fuel combustion, compressed air is supplied to the combustion chamber

from its own compressor. In general case, a gas turbine unit can be of any scheme and operate in autonomous mode, in particular, in cogeneration mode.

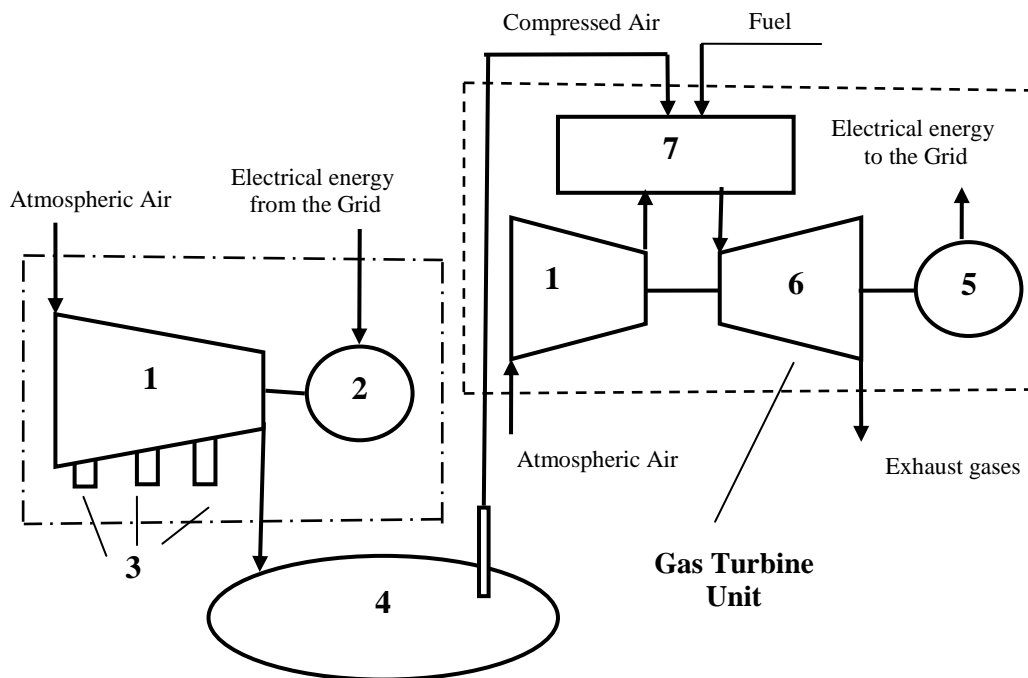


Fig. 3. Schematic diagram of a non-adiabatic ASPP in combination with GTU:
 1 – Compressor; 2 – Electric motor; 3 – Coolers; 4 – Compressed air storage;
 5 – Generator; 6 – Turbine; 7 – Combustion chamber

When considering GTU combination with a compressed air energy storage unit, compressed air from the storage is fed into the fuel combustion chamber, replacing the air and work on its compression in its own compressor of the gas turbine station. As a result, the output of GTU significantly increases. The efficiency of such a combination of ASPP + GTU can be increased by using the heat of gases coming out of the turbine (about 600–700 °C). This heat can be used to heat the compressed air before it is fed into the combustion chamber, which will reduce the amount of burned fuel and, consequently, reduce the negative impact of the object on the environment.

There is another way of using this heat by organizing production of by-products, i.e. hot water or steam at GTU (cogeneration mode). It also leads to an increase in energy efficiency of the complex and a reduction in harmful emissions to the environment.

The non-adiabatic (diabatic) ASPP with a capacity of 290 MW has been operating according to the scheme (shown in Fig. 3) in Germany since 1978. It has the following characteristics: the phase of air pumping into the storage facility lasts 8 hours; to compress 300 ths. m³ of air from 46 to 72 atm, a compressor with a 60 MW electric motor is used. During the discharge phase, the unit provides the system with a capacity of 290 MW for 2 hours. At the same time, for each output of 1 kWh of electricity, it additionally consumes 0,8 kWh of electricity and 1,6 kWh of natural gas energy.

The authors tried to evaluate the complex efficiency using its known characteristics, which, however are insufficient to compile its full energy balance, developed using the 1st and 2nd principles of thermodynamics [6, 8]. The amount of accumulated exergy (potential) of compressed

air was determined by the method presented above. As it can be seen from Table. 2, the achieved efficiency of the complex was $\eta_{compl} = 29,6\%$.

Table 2

The main energy characteristics of the complex combining non-adiabatic ASPP and gas turbine installation (real scheme)

Consumes	Generates
1. Compressor drive *(ED) $W_c = \frac{N_d}{\eta_d \eta_c} t_z = \frac{60}{0,93 \cdot 0,85} \cdot 8 = 607,6 \text{ MW} \cdot \text{h}$	1*. Electrical energy generation into the system $W_{gen} = P_m \cdot t_{dis} = 290 \cdot 2 = 580 \text{ MW} \cdot \text{h}$
2. Additional consumption of electrical energy $W_{add} = W_{gen} \cdot 0,8 = 580 \cdot 0,8 = 464 \text{ MW} \cdot \text{h}$	2*. The accumulated exergy (potential) of compressed air $\Pi_{comp} = (e_2 - e_1) \cdot V_a = (235 - 195) \cdot 300 = 12 \text{ MW} \cdot \text{h}$
3. Additional consumption of natural gas $W_{add \text{ gas3}} = W_{gen} \cdot 1,6 = 928 \text{ MW} \cdot \text{h}$	
Total: 1999,6 MW · h	$\eta_{compl} = \frac{592}{1999,6} = 0,296$

As noted above, the energy efficiency of the complex can be significantly increased if its structure is changed by replacing the compressor drive from electric motor with the drive from wind power plant (WPP), which will eliminate this item of electricity consumption from the network. In this case, the complex efficiency can achieve $\eta_{compl} = 42,5\%$ (Table 3).

As for the use of heat from GTU exhausted gases, there is no enough information to assess its impact on the complex efficiency. Using estimated calculation we determined the exergy of utilized gases heat, which amounted to $E_q = 23 \text{ MW} \cdot \text{h}$. This allows one to determine the

complex efficiency, which can be achieved: $\eta_{compl} = \frac{592 + 23}{1392} = \frac{615}{1392} = 0,442$.

Table 3

The main energy characteristics of the complex combining non-adiabatic ASPP, GTU and wind power plant to increase its efficiency

Consumes	Generates
1. Compressor drive *(ED)	1*. Electrical energy generation into the system $W_{gen} = P_m \cdot t_{dis} = 290 \cdot 2 = 580 \text{ MW} \cdot \text{h}$
2. Additional consumption of electrical energy gas $W_{add} = W_{gen} \cdot 0,8 = 580 \cdot 0,8 = 464 \text{ MW} \cdot \text{h}$	2*. The accumulated exergy (potential) of compressed air $\Pi_{comp} = (e_2 - e_1) \cdot V_a = (235 - 195) \cdot 300 = 12 \text{ MW} \cdot \text{h}$
3. Additional consumption of natural gas $W_{add \text{ gas}} = 928 \text{ MW} \cdot \text{h}$	
Total: 1392 MW · h	$\eta_{compl} = \frac{580 + 12}{1392} = \frac{592}{1392} = 0,425$

Conclusions

Compressed air energy storage devices are capable of storing a significant amount of potential energy that can be used in air-storage power plants. Depending on whether the heat of the compressible agent is discharged or not, ASPP is divided into two types - adiabatic and nonadiabatic. This article considers both types of ASPPs. The air in the compressor, storage and

other elements of the ASPP is in compression-expansion modes. This means that it is necessary to be able to determine the potential of compressed/expanded air required to compile the exergy balance of the corresponding elements of the scheme and the ASPP as a whole, without which it is impossible to evaluate their efficiencies.

The article proposes the method for determining the energy potential of compressed air, the procedure for drawing up the exergy balance and determining the efficiency of the corresponding circuit elements. Based on the analysis of the processes of air compression (expansion) in the adiabatic ASPP, it was concluded that such a scheme cannot have high efficiency from the standpoint of thermodynamics. However, this type of ASPP has a number of economic advantages: simplicity, low investment, due to the absence of a compressor, and a combustion chamber for a gas turbine. To increase the process efficiency, it is necessary to convert the ASPP type to non-adiabatic, which will require changing the scheme and operation mode of its elements. At the same time, compression in the compressor should be carried out with the highest possible heat removal, and the expansion process in open-type gas turbines should be carried out with heat supply.

Both types can successfully work in conjunction with a wind power plant, which is able to replace the compressor motor, thereby reducing power consumption from the grid.

References

1. Stychinskiy ZA, Voropay NI., editors. *Vozobnovlyayemye istochniki energii: teoreticheskiye osnovy, tekhnologii, tekhnicheskiye kharakteristiki, ekonomika* [Renewable energy sources: Theoretical bases, technologies, specifications. Economy]. Magdeburg: Otto-von-Guericke-Universitat Magdeburg; 2010. (in Russ.).
2. Litvak VV. Principles of regional energy saving (science-technical and production aspects). Tomsk: NTL, 2002 (in Russian).
3. Bezrukih PP. Using wind. Technologies. Economics. Ecology. Moscow: Coloss, 2008 (in Russian).
4. Brodyanskiy VM. Exergy method of thermodynamic analysis. Moscow: Energy, 1973. (in Russian).
5. Stepanov VS. Calculating thermo-mechanical exergy of gaseous fuels and potentials of energy saving in gas supply systems /VS. Stepanov, TB. Stepanova // *Industrial power engineering*. 2013. №11. P. 2–6. (in Russian).
6. Stepanov VS. Analysis of energy efficiency of industrial processes / VS. Stepanov. Heidelberg: Springer-Verlag, 1992.
7. Exergy calculations of technical systems / Red. AA. Dolinskiy, VM. Brodianskiy. Kiev: Naukova dumka, 1991. (in Russian).
8. Stepanov VS. Exergy analysis for systems of energy generation, transport and consumption / VS. Stepanov, TB. Stepanova, NV. Starikova. Irkutsk: IIRNITU, 2016. (in Russian).
9. Stepanov VS. Thermodynamics studies of metallurgical processes: energy balances, exergy analysis / VS. Stepanov, SV. Stepanov. Irkutsk: IrGTU, 2013. (in

Литература

1. Возобновляемые источники энергии: теоретические основы, технологии, технические характеристики, экономика / под ред. З.А. Стычинского, Н.И. Воропая. Магдебург–Иркутск: Отто-фон-Герике Университет Магдебург, 2010. 211 с.
2. Литвак В.В. Основы регионального энергосбережения (научно-технические и производственные аспекты). 2-е изд., испр. Томск: Изд-во НТЛ, 2007. 288 с.
3. Безруких П.П. Использование ветра. Техника. Экономика. Экология / П.П. Безруких . М.: Колосс, 2008.
4. Бродянский В.М. Эксергетический метод термодинамического анализа / В.М. Бродянский. М.: Энергия, 1973.
5. Степанов В.С. Определение термомеханической эксергии газообразного топлива и потенциала энергосбережения в системах газоснабжения / В.С. Степанов, Т.Б. Степанова // *Промышленная энергетика*. 2013. №11. С. 2–6.
6. Stepanov V.S. Analysis of energy efficiency of industrial processes / V.S. Stepanov. Heidelberg: Springer-Verlag, 1992. 186 p.
7. Эксергетические расчеты технических систем: справочное пособие / Под ред. А.А. Долинского, В. М. Бродянского. Киев: Наукова думка, 1991.
8. Степанов В.С. Эксергетический анализ систем генерирования, транспорта и потребления энергии / В.С. Степанов, Т.Б. Степанова, Н.В. Старикова. Иркутск: Изд-во ИРННТУ.
9. Степанов В.С. Термодинамические исследования металлургических процессов:

© *В.С. Степанов, Т.Б. Степанова, Н.В. Старикова*

Russian).

10. Stepanov VS. Potential and reserves of energy saving in industry / VS. Stepanov, TB. Stepanova. Novosibirsk: Nauka,1990. (in Russian).

энергетические балансы, эксергетический анализ / В.С. Степанов, С.В. Степанов. Иркутск: Изд-во ИрГТУ, 2006.

10. Степанов В.С. Потенциал и резервы энергосбережения в промышленности / В.С. Степанов, Т.Б. Степанова. Новосибирск: Наука, 1990.

Authors of the publication

Vladimir S. Stepanov – D.Sc., Professor, Department of power supply and electrical engineering, Irkutsk national research technical university.

Tatiana B. Stepanova – D.Sc., Professor, Department of power supply and electrical engineering, Irkutsk national research technical university.

Natalia V. Starikova – PhD in Engineering sciences, Associate Professor, Department of power supply and electrical engineering, Irkutsk national research technical university.

Received

October ,16 2018



ELECTRIC POWER SYSTEM OF YEMEN, ITS STRUCTURE AND CHARACTERISTICS

Y.S.S. Ali, N.D. Chichirova

Kazan State Power Engineering University, Kazan, Russia

Yazid20@yandex.ru

Abstract: *In this article we analyze the energy system of the Republic of Yemen, its structure and characteristics of transmission lines, power stations and substations. We also consider the prospects for development of power system in the country.*

Keywords: *Yemen, power system, power stations, high voltage line, electricity consumption.*

For citation: Ali Y.S.S., Chichirova N.D. Electric power system of Yemen, its structure and characteristics. *Proceedings of the higher educational institutions. ENERGY SECTOR PROBLEMS.* 2019; 21(3-4):38-43. (In Russ). doi:10.30724/1998-9903-2019-21-3-4-38-43.

Introduction

The Republic of Yemen is located on the Arabian Peninsula. The population of the country is about 25 million people, 70% of them are engaged in agriculture.

The main industrial potential of the country is historically concentrated in the coastal zone. The natural zoning of the country is responsible for the established centralized power supply zones, which are represented by two regions:

- Northern and central, where 17.5 mln. people live (makes up to 75% of the population);
- Southern, population in which is 7.5 mln. people.

In 1990, only 48% of the population used electricity from a centralized network. At the same time, per capita electricity consumption was only 300 kW·h per year. For comparison, the average value in the countries of South-West Asia was 1000 kW·h.

About 3 mln. people lives on elevated plateaus and in mountainous areas, where autonomous sources of electricity and relatively small sections of the distribution network are used. The eastern part of the country is smooth and mastered to a lesser extent than the western one.

In Yemen, for one person employed in power industry, there were 200 that were employed in other sectors of industry or in the service sector. In other countries of the South-East Asia the indicated characteristics is 2 times less. Developmental delay of power industry decelerates evolution of the Republic as a whole.

On May 22, 1990, two Republics were joined in one, which forced unification of their power systems.

Nowadays, Yemen's unified power grid is a complex of power plants and networks, united by a general regime and a single centralized operational management, which is developed according to the state plan. The transition to this form of organization of electric power industry creates the prerequisites and possibilities for the most rational use of energy resources and increasing the economy and reliability of power supply of the national economy and the country's population.

As the scale of the Yemen power system expands, the tasks of managing its modes become more and more responsible and complex. The special significance of these tasks is determined by

the role of electric power industry in ensuring the normal activity of all sectors of the national economy, in improving the functioning of social structures and living conditions of the population. The increasing difficulties of management are caused by the large length of electric networks of the electric power system (EPS), extremely uneven distribution of energy resources and productive forces over the territory of the country, and complexity of structure of generating capacities and schemes of the system of generating networks. All this requires the use of modern economic and mathematical methods and computer equipment for advanced and operational management. Considerable work has been carried out in the field of theory and practice of managing regimes by the Yemen power engineers. Achievements in this area are the result of purposeful joint activities of research, design and operational organizations. The research results and the experience gained in operation not only make it possible to successfully solve current management tasks, but also form the basis for solving more complex problems associated with completion of the Yemen EPS formation. So over the past 5 years, the coefficient of consumers' electrification has increased up to 70%, and construction of new HV lines made it possible to increase the network capacity by 40% and to increase the area of centralized power supply. Nevertheless, due to the lack of investments in power industry, its work is characterized by a number of unfavorable indicators, such as the tense balance of active power due to the lack of generating capacity, which necessitates consumer constraints; the use of relatively low nominal voltages for transmission of electricity over considerable distances (over 100-150 km at a voltage of 132 kV); low voltage levels at large load sites due to significant reactive power deficits; uneven development of the northern and southern parts of the power system; the presence of weak links between the northern and southern parts of the power system; lack of reliability of the main switchgear of power plants and substations; use of power equipment from various manufacturers, etc. All this determines the need to ensure more reliable operation of power system and its elements at the expense of more modern and complex technical solutions for the schemes of switching gears of stations, according to the scheme of the power system, control of its normal and emergency modes, and anti-emergency automation.

Electrical stations and their characteristics

The basis of the existing integrated system consists of 3 large thermal power plants (TPPs) and one gas turbine unit (GTU) located in the cities of Al-Hodeidah (two stations), Aden (one station) and Marib (GTU). The other stations run on diesel fuel.

Prior to unification of the Republic, the power system (PS) of southern Yemen had only one large TPP (5x25 MW) of the Soviet production. The other stations are diesel, of low power. In the northern power system of Yemen, there were two TPPs of Italian production of 5x33 and 4x40 MW.

The other generating capacity was composed of diesel stations. Peaks of load in various parts of Yemen did not coincide in time during the year, and it was necessary to have a significant rotating reserve in both parts of the PS.

On May 22, 1990, the two republics were joined into one, the Republic of Yemen, which forced unification of their energy systems. The unification of Yemen was accompanied by an increase in production. New factories opened, new hotels were built, etc. This caused the need to build new stations. The unification of Yemen also caused construction of new power transmission lines (PTLs), which connected the two power systems to ensure the flow of power between them. However, this did not solve the problem of power supply of the capital of the republic - Sana. And two diesel stations with a total capacity of 130 MW were built. Characteristics of generating sources of the Republic of Yemen are given in the Table.

Table

General characteristics of power plants in Yemen

Name of station	Type	Type of fuel	Generator capacity, MW	Amount of generators	Installed capacity of station, MW
Hiswa	TPP	Mazut	25	5	125
Ras-Katheeb	TPP	Mazut	33	5	165
Al-Makha	TPP	Mazut	40	4	160
Al-Manswra	Diesel	Diesel fuel	8	8	64
Sana	Diesel	Diesel fuel	40	2	80
Kor-Maksar	Diesel	Diesel fuel	2/4	4/6	32
Marib (Safir)	GTU	Gas	115	3	345

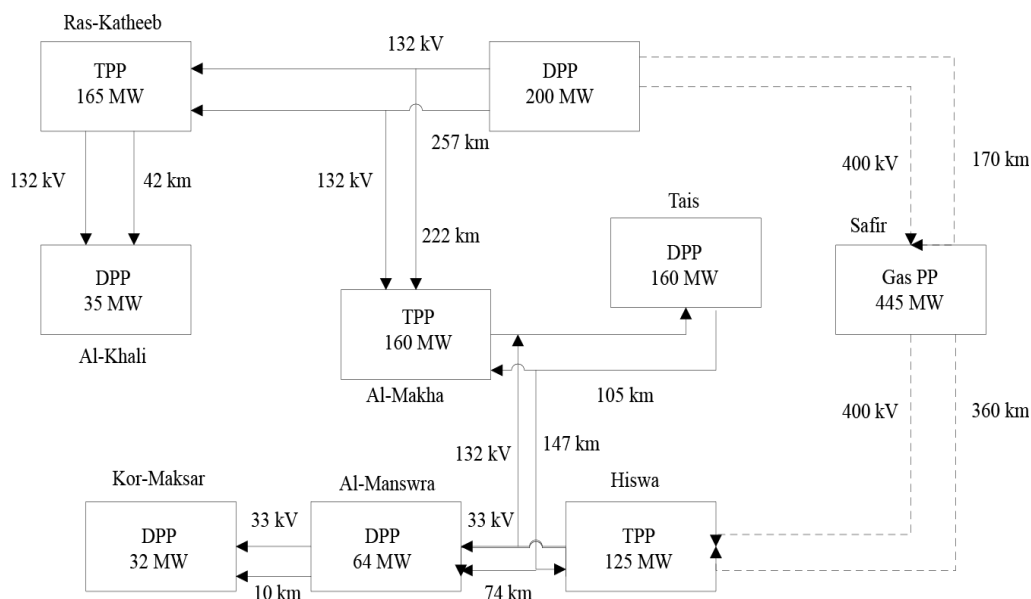


Fig. 1. Scheme of connections between power plants in Yemen.

Figure 1 presents a 400 kV double-circuit overhead line (OHL) (Safir - Sana and Safir - Hiswa) with a length of 170 km. To ensure operability, the power line is equipped with sequential and transverse control devices, which maintain the voltage at 400 kV ($\pm 5\%$). Autotransformers of 400/132 kV and transformers of 132/33 kV are installed at the substations. Diesel generators are provided to reserve their own needs at substations.

Electricity consumers and their characteristics

In 1992, the implementation of the global program for electrification of the agricultural regions of the country was launched in Yemen. The project developed by the national energy company (*Office National de L'Electric ale, Casablanca*) provides electrification of 40 ths. settlements throughout the country by 2025. The program provides supply of electricity to many localities which do not have their own sources and development of the existing power supply system.

The possible scenarios for the projected increase in electricity consumption in the energy system of Yemen (ESY) until 2025 are shown in Fig. 2

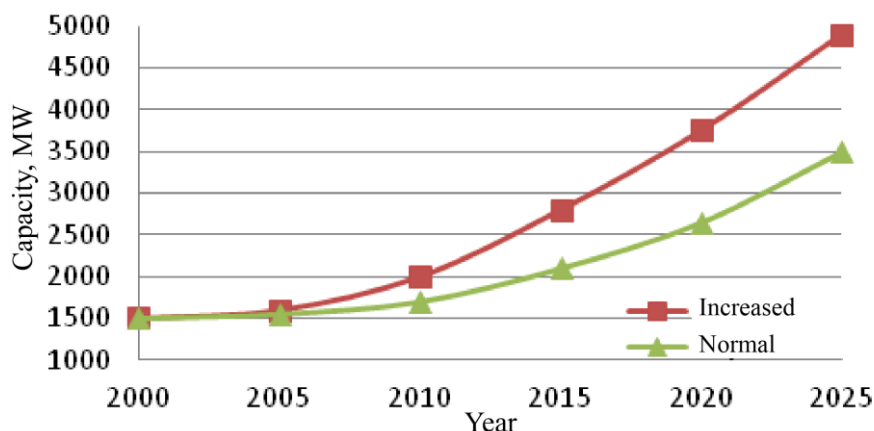


Fig. 2. Charts of the projected increase in power consumption in ESY.

The presented charts show that the power consumption in ESY will increase by 3–6 times by 2025.

This will ensure the growth of electricity consumption by the population, will provide an opportunity to solve a number of social problems and electrify agricultural production.

Prospects for development of electricity Yemen

Describing the evolution of electricity in Yemen, it can be noted that in 1990 only 48% of the population used electricity from a centralized network. The operation of the power system was characterized by a number of unfavorable indicators. The funds received for the payment of electricity do not provide repairs and recovery work, and investments for development of power industry are insignificant.

Along with a broad program of privatization of the electric power industry, the state retained its rights as the main regulatory body.

The main directions of reforming the country's electric power industry were as follows:

1. All issues related to operation and development of the generating complex are concentrated in individual state-owned companies.
2. Planning for the growth of demand for electricity is the responsibility of the established Committee on the Economy. Also it gathers data on generating power companies. It also provides them with raw materials for planning and subsequent development of the generating complex.
3. Monitoring of price indicators and preparation of materials for formation of financial policies.
4. Organization of the relevant department responsible for ensuring the quality of electricity in the power system and at consumers (voltage levels, frequency deviations, presence of harmonics, etc.).

All organizational and technical changes in electric power industry carried out in recent years in Yemen have yielded positive results. Thus, over the past 5 years, the coefficient of consumers' electrification rate has increased up to 70%, and construction of new OHL made it possible to ensure the growth of network capacity by 40% and increase the centralized power supply zone. At the same time, data on development of the electric power industry in the southern region indicates its significant lag behind the northern and central parts of the country. In order to meet the growing needs and, above all, the needs of mining industry in the southern region, it is necessary to increase the generating capacity, to build overhead lines and substations.

Conclusions

1. The basis of the existing unified power system is 4 large power plants located in the cities of Al-Hodeidah (two stations), Marib and Aden. A significant share of the installed capacity of the power system is autonomous operating diesel stations with a capacity of 2 to 8 MW.

2. Unification of two republics into one Republic of Yemen entailed the need to build new power lines, which connected the two power systems to ensure the flow of power between the power companies.

3. A specific feature of the Yemen's ES is predominance in the northern part of Yemen of the load in the form of heaters, used mainly in winter, as it is located in a mountainous region. In southern Yemen, the main share of load is made up of air conditioners and fans, mainly used in summer. Since the maxima of load in the north and south do not coincide in time, the power flows in the system are significant.

4. A feature of electrical equipment work and, above all, transformers, is high ambient temperature, which in the southern regions of the Republic can exceed 40 ° C.

5. The possibility of formation of significant power shortages in case of disconnection of communication lines in power system is obvious. The presence in the power system of a significant share of autonomously operating diesel stations, as well as the prospects for their inclusion in parallel operation with the power system of Yemen, requires the study of their frequency and power control systems. To conduct such studies, it is necessary to develop appropriate software, as well as to use modern methods for analyzing transient processes in various modes for various control systems and their tasks.

References

1. Zahure H, Aeish D. Calculation of the set modes of electrical systems the Republic Yemen taking into account frequency change. *Journal Future University*. Taiz University; 2013. (in Yemen).

2. Alshaghdari IT, Ahmed WC. Increase in overall performance of power supply systems. *Journal of the university researcher*. Ibb university; 2016. (in Yemen).

3. Al-Hetar EL, Al-Udnyi SD. Development of actions for reliability augmentation of the main schemes of power plants of the republic Yemen. *Journal of Science and Technology*. University of Science and Technology, Sana'a; 2015. (in Yemen).

4. *Energy-policy Framework Conditions for Electricity Markets and Renewable Energies*. 23 Country Analyses. Chapter Yemen; September 2016; Eschborn, Germany; 2016.

5. Al Wasube KF, Abdulkadir WB. A status and features of power industry of Yemen. *Journal Future University*. Taiz University; 2016. (in Yemen).

6. Al-Ashwal YA, Al-Mawgani LRC. Research of operation modes of an electrical power system of the republic Yemen. *Journal of Science and Technology*. University of Science and Technology, Sana'a; 2017: 12(42):292-299. (in Yemen).

7. Althothaily S.R., Alradaey Q.T. Automatic frequency unloading in separately to the working power supply system. *Increase in overall performance of power supply systems*, *Journal Future University*, Аден, 2014. (in Yemen).

8. Al Nozayly PS, Al Sabaehi MY. Relay protection and automatic equipment in power supply system of Yemen. *Journal of the university researcher*. Ibb university; 2018. pp. 221-230. (in Yemen).

Литература

1. Zahure H., Aeish D. Calculation of the set modes of electrical systems the Republic Yemen taking into account frequency change / *Journal Future University // Taiz University*, 2013. № 2. pp. 173-181.

2. Alshaghdari I. T., Ahmed W. C.. Increase in overall performance of power supply systems // *Journal of the university researcher / Ibb university*, 2016. № 5. pp 151-159.

3. Al- Hetar E. L., Al- Udnyi S. D. Development of actions for reliability augmentation of the main schemes of power plants of the republic Yemen // *Journal of Science and Technology / University of Science and Technology*, Sana'a, 2015. № 1. pp. 472-477.

4. *Energy-policy Framework Conditions for Electricity Markets and Renewable Energies // 23 Country Analyses / Chapter Yemen/ Eschborn*, September 2016. pp.486-497.

5. Al Wasube K.F., Abdulkadir W.B. A status and features of power industry of Yemen // *Journal Future University // Taiz University*, 2016. № 3. pp.134-142.

6. Al-Ashwal Y.A., Al-Mawgani L.R.C. Research of operation modes of an electrical power system of the republic Yemen // *Journal of Science and Technology / University of Science and Technology*, Sana'a, 2017. № 12(42). pp. 292-299.

7. Althothaily S.R., Alradaey Q.T. Automatic frequency unloading in separately to the working power supply system // *Increase in overall performance of power supply systems*, *Journal Future University*; Аден, 2014. № 10. pp. 681-690.

8. Al Nozayly P.S., Al Sabaehi M.Y. Relay protection and automatic equipment in power supply system of Yemen // *Journal of the university researcher / Ibb university*, 2018.

9. [Website]. Available at: www.asia-energy.com. Accessed: 15 Aug 2017.

10. Al-Ansi N.R., Wahid H., Wan S.H., et al. Status and perspectives of development of electrotechnologies in the republic Yemen. *Journal of the university researcher*. Damar university; 2015. pp. 451-459. (in Yemen).

№ 2, pp. 221-230.

9. [Электронный ресурс]. Доступно по: www.asia-energy.com. Ссылка активна на 15 августа 2017.

10. Al-Ansi N.R., Wahid H., Wan S.H., et al. Status and perspectives of development of electrotechnologies in the republic Yemen // *Journal of the university researcher* / Damar university, 2015. № 4. pp. 451-459.

Authors of the publication

Yazid S.S. Ali - department “Thermoelectric plants”, Kazan State Power Engineering University.

Natalia D. Chichirova - department “Thermoelectric plants”, Kazan State Power Engineering University.

Received

December, 24 2018



WATER HEAT PUMP OPERATION UNDER CONDITIONS OF ICE FORMATION ON THE EVAPORATOR PIPE SURFACE

V.I. Maksimov, A. Saloum

National Research Tomsk Polytechnic University, Tomsk, Russia
amer-salom@hotmail.com

Abstract: We experimentally investigated the conditions and characteristics of ice formation on pipe surface of a heat pump evaporator which appears when using cold water (at a temperature lower than 280 K) as a low-grade energy source. During operation of such heat pump, we registered ice thicknesses, temperature of water in evaporator, and temperature of evaporation from pipe wall. The results allow us to make a conclusion on the possible use of water heat pump in practical applications under the conditions of partial ice coverage of evaporator surface at water heating in the condenser up to 313 K. It was experimentally shown that when initial water temperature in evaporator is decreased by 6 K, the maximum thickness of ice formed on the evaporator surface is increased by 30%. The ice formed on the evaporator, after reaching the maximum temperature of water in the condenser, completely melts over time. The relationship between Nusselt number and the natural convection heat exchange characteristics at phase change has been established.

Keywords: water heat pump, temperature, ice, evaporator, heat transfer during phase transitions, convection.

Acknowledgment: This work was supported by the project No. 18-79-10015 from the Russian Foundation for Basic Research.

For citation: Maksimov V.I., Saloum A. The water heat pump operation under frost conditions on the evaporator surface. *Proceedings of the higher educational institutions. ENERGY SECTOR PROBLEMS*. 2019; 21(3-4):44-51. (In Russ). doi:10.30724/1998-9903-2019-21-3-4-44-51.

Introduction

Heat pumps which use low-grade water energy source can provide the necessary heat load with high performance coefficient (2–4) [1]. Water heat exchange loop generates a significant part of the required heat load for the building. The systems based on heat pumps with water loop work quite effectively even under partial load conditions [2].

Water temperature of deep water bodies in cold seasons is higher than the ambient air temperature [3]. Therefore, thermal potential of energy sources for water heat pumps is higher than that for air heat pumps [4].

Nowadays, use of ground heat pumps increased dramatically [5], but their installation and maintenance have significant difficulties [6]. Besides this, such pumps have negative impact on soil temperature after a long operation period [7]. The low value of soil thermal conductivity is another disadvantage for this types of heat pumps [8]. All these problems can be avoided by the use of water as an energy source. But in this case, at low water temperatures, an ice may form on the evaporator pipe surface, which reduces the heat pump efficiency [9] in general.

The heat exchange process between the surface of spiral freon pipe of heat pump evaporator and water of low-potential heat source was studied in details by Zu S., Ni L., Yau W.

[10, 11]. But in experimental scheme [11] it was assumed that the surface temperature of evaporator pipe is higher than 273 K. Consequently, there has been no ice on the evaporator wall. And in these cases it has been concluded that the influence of vertical and horizontal pitch between the evaporator pipes on the intensity of heat transfer can be neglected.

It has been established that ice formation on evaporator pipe leads to an uneven temperature distribution in the liquid volume, which surrounds the pipes, and significantly reduces the heat transfer rate [12]. The results in [12] allow defining the heat pump temperature work range with full or partial ice coverage. For example, an ice layer with a thickness of 0.003 m reduces the heat flux between water and freon by 40 % [13]. Maintaining the water temperature at 277 K causes a natural convection current which increases the ice growth rate by 10–50 % (depending on the evaporator container height).

The purpose of this research is to study the working characteristics of heat pump under the conditions of ice formation on the evaporator pipe when using cold water as a low-grade energy source and to check the operation possibility of heat pump in the successive ice formation and melting cycles.

Experimental Facilities and Procedure Description

A series of experiments was conducted at water heat pump (HP) (fig.1) using the method described in [14]. Water temperature was measured at various vertical coordinates around the evaporator pipe using 15 thermocouples which were fixed with a step of 0,0154 m between every two of them. Also, 15 thermocouples were installed on the evaporator pipe wall surface with a distance of 0,23 m between each other by freon flow direction (fig. 1).

Thermocouples of Chromel/Alumel type with a junction point size of 0,001 m are connected to analog-to-digital converter and after that through a network adapter to a personal computer. A software is developed in the environment of National Instruments LabVIEW to record the real-time temperatures. The ice layer thickness formed on the surface of evaporator pipe is measured using a digital vernier caliper.

The temperature of water bodies which are used as energy source for heat pumps during the cold season is higher than the air temperature [15]. It has been established that the average water temperature in a lake varies in the range of 275–286 K for air temperature between 263–277 K [15]. In our experiments water around heat pump evaporator pipe has initial temperature (T_0^E) 280 K in the first stage and 286 K in the second one. For all cases, water initial temperature around the condenser pipe is 291 K in average. Freon pressure in evaporator pipe is 0,2 MPa and its flow rate is 0,002 kg/s. Under identical conditions, every experiment is repeated three times. The total relative systematic error of all temperature measurements does not exceed 4,6 % for the whole measurement range. Random error is less than 5 %.

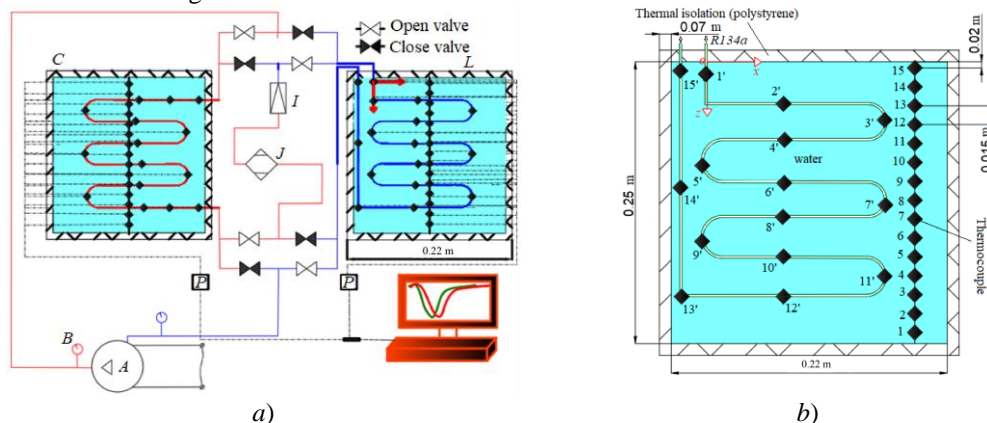


Fig. 1. The schematic diagram of experimental heat pump setup (a) and thermocouple installation points (b):
 a) A – compressor; B – manometer; C – condenser; J – filter; I – capillary pipe; L – evaporator;
 P – analog-to-digital converter; b) – the black squares represent the temperature measuring points

Experimental Results and Discussion:

In a few minutes after launching the experimental stand, we noticed a sharp decrease of wall temperature at the evaporator entrance (T_1) down to 258 K (fig. 2.). With the course of time, ($\tau \sim 1000$ s) T_1 begins to grow up due to the increase in water temperature around the condenser pipe. Also, when the heat pump panel is turned on the thermocouples 2'–5' registered a decrease in the evaporator wall temperature. Freon is evaporated and its vapour is heated in the evaporator pipe by absorbing energy from the water heat source. After 10000 s from the initial operating moment, the pipe wall temperature at the evaporator inlet exceeds 273 K, and as a result, the ice formed on the pipe starts to melt. Also, in the experimental procedure, the change in water temperature around the evaporator at various vertical levels is recorded (fig. 3.). The initial increase in water temperature in the first 600 s can be explained that freon temperature has the ambient value at the beginning of the experiment. After 600 s freon temperature increases along the evaporator pipe which causes a gradual cooling and freezing of water around its surface. The thermocouple 1, which is located close to the lower part of the evaporator, registers the lowest temperature in the first 6000 s compared with the readings of thermocouples 2–5 which are located higher (fig. 3)

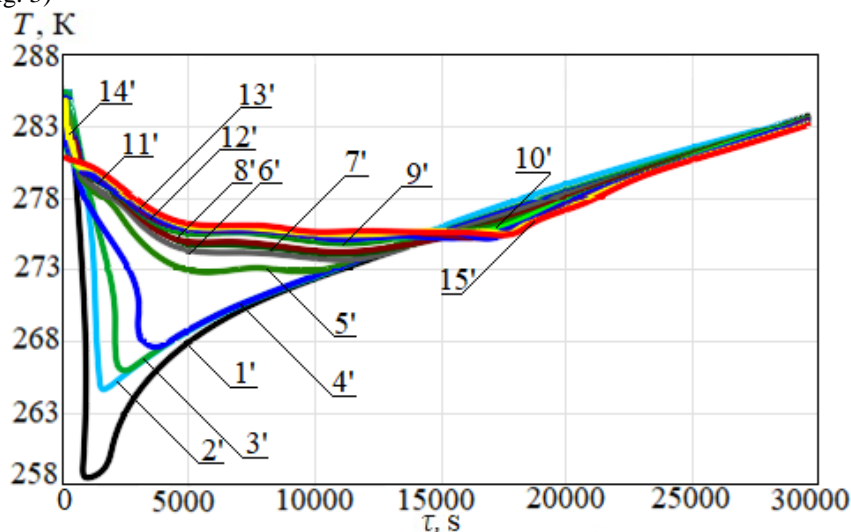


Fig. 2. The evaporator surface temperature change with time ($T_0^E = 286$ K):

1', 15' – Thermocouples located on the surface of the evaporator pipe at the inlet and outlet respectively; 2'–14' – Thermocouples located on the surface of the evaporator pipe at a distance of 0,230 m from each other

In time interval from 6000 to 10000 s, the water temperature in the lower part of the evaporator is about 277 K, and in the upper parts, it ranges from 274 to 276 K. This can be explained that the water has a maximum density at a temperature value of 277 K.

For working time higher than 11000 s, the water temperature in the evaporator starts to increase due to the growth in freon temperature in the evaporator because water in the condenser is already heated and it is not able to cool down freon to the liquid phase which affects its characteristics at the capillary pipe outlet.

The water temperature changes around the condenser pipe at various heights is shown in fig. 4. The water temperature increases from 291 to 308 K in a time period of 6000 s. Water heated up to these temperatures can be used in local heating systems “warm floor”. But such heating will be effective only when the ambient air temperatures are not lower than 283–290 K. If after 6000 s, this water is not cooled by using it in the heating system, its temperature will continue to increase to 313 K in the upper part of the condenser container. Under these conditions, freon is not cooled enough to finish its condensation process. After 11000–12000 s, freon temperature at the exit of the

capillary pipe increases exceeds 273 K which causes the melting of ice on the evaporator wall (fig. 5, 6).

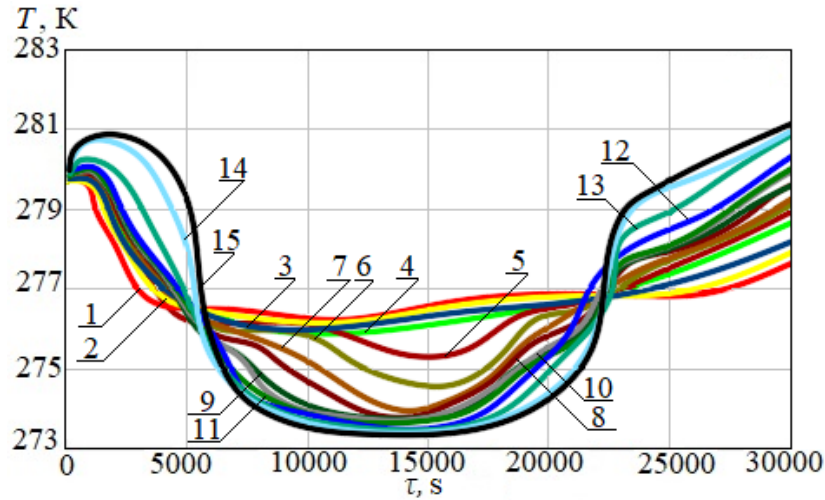


Fig. 3. The change in water temperature around the evaporator pipe with time at various vertical coordinates ($T_0^E = 286 \text{ K}$): 1 – Thermocouple at the lower part of the evaporator; 15 – Thermocouple located close to water surface; 2–14 – Thermocouples located at various vertical coordinates on the evaporator with a distance of 0,0154 m from each other

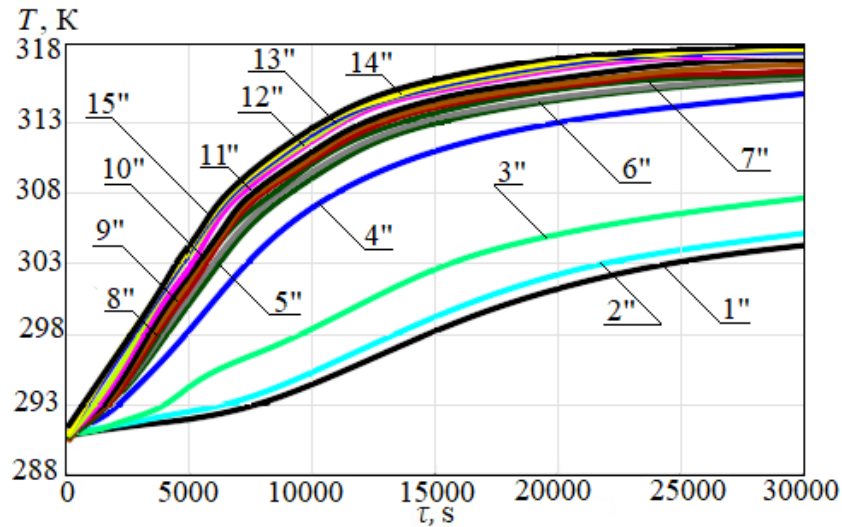


Рис. 4. The change of water temperature around the condenser pipe in time at various vertical coordinates ($T_0^E = 286 \text{ K}$): 1'' – Thermocouple located close to the lower part of the condenser; 15'' – Thermocouple located close to the water surface in the condenser; 2''–14'' – Thermocouples at various vertical coordinates in the water around the condenser pipe with a distance of 0,0154 m between each other

The ice which is formed in the first 8000 s, totally melts in the next 5000 s. And in this stage, the heat pump warms up the water from 291 to 313 K.

Basing on the experimental results, it can be concluded that for initial water temperature around the evaporator of 286 K, the thicknesses of ice in measuring points on the evaporator pipe surface are lower by 0,0024 m comparing to their values for an initial temperature 280 K. and the necessary time to remove the ice melting is 4000 s.

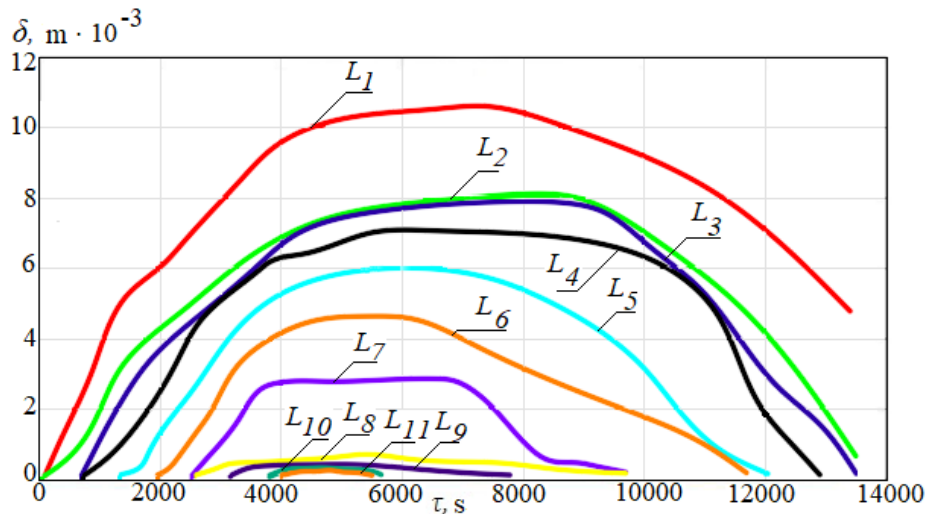


Fig. 5. The formed ice thickness change in time in various points along the evaporator pipe (the coordinates of ice thickness measuring points are given in the table, $T_0^E = 286 \text{ K}$)

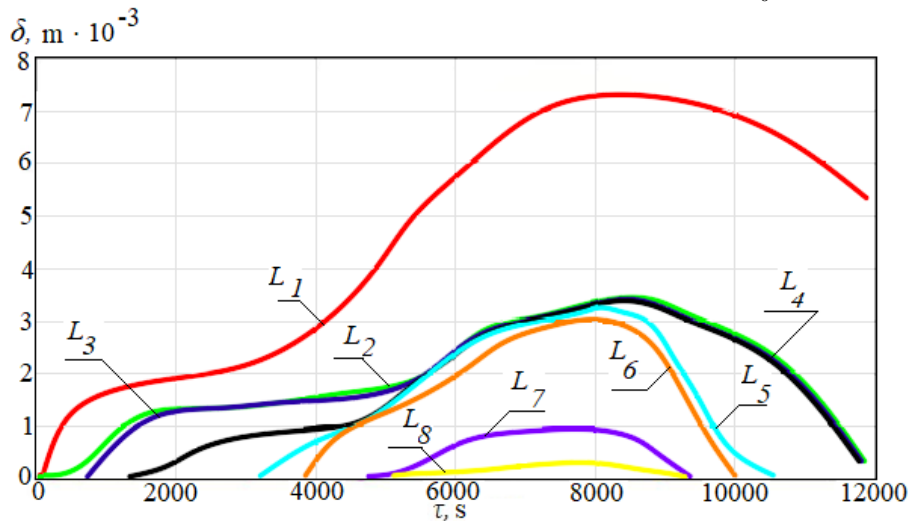


Fig. 6. The formed ice thickness change in time in various points along the evaporator pipe length (the coordinates of ice thickness measuring points are given in the table, $T_0^E = 286 \text{ K}$)

Table

The coordinates of the ice thickness measuring points

Measuring point	L_1	L_2	L_3	L_4	L_5	L_6	L_7	L_8	L_9	L_{10}	L_{11}	
The distance from the evaporator start point, m	0	0,11	0,26	0,44	0,59	0,77	0,92	1,11	1,25	1,43	1,58	
Cartesian coordinates, m	x	0	0,11	0,11	-0,07	-0,07	0,11	0,11	-0,07	-0,07	0,1	0,11
	y	0	0	0,14	0,14	0	0	0,14	0,14	0	0	0,14
	z	0	0,04	0,04	0,04	0,04	0,09	0,09	0,09	0,09	0,1	0,13

The experimental results show that the formed ice on the evaporator pipe surface of the water heat pump which operates in the conditions of the cold seasons (autumn, winter, spring) significantly reduces its efficiency during a working time period equals to two hours. The ice is

removed in 2–3 hours. After the full melting of ice, the working cycle is repeated again. The working efficiency of the heat pump unit decreases significantly when water around the condenser reaches its maximum temperature (313 K).

Analysis of the obtained water temperature values in the condenser and the evaporator for the heat pump experimental panel, showed the possibility to use this method to heat up water in the condenser to a temperature of 313 K which is enough for the heating system “warm floor” [16, 17]. But, under these working conditions, freon temperature in the evaporator decreases to values lower than 273 K, which causes an ice formation on its surface. When water in the condenser is heated to a maximum value (313 K), freon is partially condensed, and as a result, the temperature of the evaporator pipe wall becomes higher than the water freezing point. And the formed ice melts. The necessary time for ice to melt increases by 4 % for every decrease in the initial water temperature around the evaporator pipe for 1 K. When the ice is removed, the heat pump can be used again to heat up water from 291 to 313 K.

The obtained results can be used to develop the design of the evaporator, which operates in the conditions of ice formation on its surface. The thickness of ice layer formed on the evaporator pipe increases by 4 % for every 1 K decrease in water temperature in the evaporator.

To heat up water from 291 K to a higher temperature of 313 K, two heat pumps can be used. When one of them operates in a heating mode, the other one works in ice melting mode to keep water temperature equal to 313 K in the floor heating coil.

Conclusions

The research results prove the suggestion to use water heat pump station in mode of ice formation on the evaporator pipe surface when water temperature in evaporator corresponds to temperature of water surfaces in different Russian regions in the cold period of the year “autumn - winter - spring” to provide the heating system “warm floor” with hot water.

References

1. Liu X, Li F, Guo Q, et al. Experimental study of a new multifunctional water source heat pump system. *Energy Build.* 2016; 111:408-423. DOI: 10.1016/j.enbuild.2015.11.069.
2. Sayegh M. A., Jadwyszczak P., Axcell B.P., et al. Heat pump placement, connection and operational modes in European district heating. *Energy Build.* 2018; 166:122-144. DOI: 10.1016/j.enbuild.2018.02.006.
3. Liu Z, Tan H, Li Z. Heating and Cooling Performances of River-Water Source Heat Pump System for Energy Station in Shanghai. *Procedia Engineering.* 2017; 205:4074-4081. DOI: 10.1016/j.proeng.2017.09.898.
4. Piccolroaz S, Toffolon M, Majone B. A simple lumped model to convert air temperature into surface water temperature in lakes. *Hydrology and Earth System Sciences.* 2013; 8:3323-3338. DOI: 10.5194/hess-17-3323-2013.
5. Livingstone DM, Lotter AF. The relationship between air and water temperatures in lakes of the Swiss Plateau: a case study with palaeolimnological implication. *Journal of Paleolimnology.* 1998; 9(2):181-198. DOI: 10.1023/A:1007904817619.
6. Wu W, Skye HM. Progress in ground-source heat pumps using natural refrigerants. *International Journal*

Литература

1. Liu X., Li F., Guo Q., et al. Experimental study of a new multifunctional water source heat pump system // *Energy Build.* 2016. Vol. 111. pp. 408-423.
2. Sayegh M. A., Jadwyszczak P., Axcell B.P., et al. Heat pump placement, connection and operational modes in European district heating // *Energy Build.* 2018. Vol. 166. pp. 122-144.
3. Liu Z., Tan H., Li Z. Heating and Cooling Performances of River-Water Source Heat Pump System for Energy Station in Shanghai // *Procedia Engineering.* 2017. Vol. 205. pp. 4074-4081.
4. Piccolroaz S., Toffolon M., Majone B. A simple lumped model to convert air temperature into surface water temperature in lakes // *Hydrology and Earth System Sciences.* 2013. Vol. 8. pp. 3323-3338.
5. Livingstone D.M., Lotter A.F. The relationship between air and water temperatures in lakes of the Swiss Plateau: a case study with palaeolimnological implication // *Journal of Paleolimnology.* 1998. Vol. 9. P. 181–198.
6. Wu W., Skye H. M. Progress in ground-source heat pumps using natural refrigerants // *International Journal of Refrigeration.* 2018. Vol. 92. pp. 70-85.
7. Valizade L. Ground Source Heat Pumps // *Journal Clean Energy Technologies.* 2013. Vol. 3. pp. 216-219.

- of Refrigeration. 2018; 92:70-85. DOI: 10.1016/j.ijrefrig.2018.05.028.
7. Valizade L. Ground Source Heat Pumps. *Journal Clean Energy Technologies*. 2013; 1(3):216-219. DOI: 10.7763/JOCET.2013.V1.49.
8. Todoran TP, Balan MC. Long term behavior of a geothermal heat pump with oversized horizontal collector. *Energy Build*. 2016; 133:799-809. DOI: 10.1016/j.enbuild.2016.10.037.
9. Zhang N, Wang Z. Review of soil thermal conductivity and predictive models. *International Journal of Thermal Sciences*. 2017; 117:172-183. DOI: 10.1016/j.ijthermalsci.2017.03.013.
10. Kharchenko VV, Sychev AO. Use of Low Potential Heat of Surface Water in Heat Pump Heat Supply Systems Farmhouse. *Scientific Herald of NULES of Ukraine. Series: Technique and energy of APK*. 2014. 194(2):19-24 (in Ukraine).
11. Kharchenko VV, Sychov AO. Optimizaciya nizkotemperaturnogo kontura teplonasosnoj ustanovki na osnove teploty poverhnostnyh vod. *Alternativnaya Energetika i Ekologiya (ISJAE)*. 2013; 7(129):31-36 (in Russ).
12. Zhou C, Ni L, Yao Y. Heat transfer analysis of multi-row helically coiled pipe heat exchangers for surface water-source heat pump. *Energy*. 2018; 163:1032-1049. DOI: 10.1016/j.energy.2018.08.190.
13. Maksimov VI, Nagornova TA., Chernyshev VS. Conditions and characteristics of water crystallization on the working surface of evaporator heat pumps in reservoirs with low temperatures. *MATEC Web of Conferences: Heat and Mass Transfer in the Thermal Control System of Technical and Technological Energy Equipment*. Tomsk, 2015. Vol. 23, № 01051 (1-8). DOI: 10.1051/mateconf/20152301051.
14. Maksimov VI, Saloum A. An experimental study of the effect of water bodies temperature on water heat pump performance. *MATEC Web of Conferences*. 2018. Vol. 194, № 01050 (1-4). DOI: 10.1051/mateconf/201819401050.
15. Piccolroaz S., Toffolon M., Majone B. A simple lumped model to convert air temperature into surface water temperature in lakes. *Hydrology and earth system sciences*. 2013; 8:3323-3338. DOI:10.5194/hess-17-3323-2013.
16. Amoabeng K. O., Lee K. H., Choi M. J. A study on the performance characteristics of a testing facility for a water-to-water heat pump. *International Journal of Refrigeration*. 2018; 86: 113-126. DOI: 10.1016/j.ijrefrig.2017.11.013.
17. Sebarchievici C, Dan D, Sarbu I. Performance assessment of a ground-coupled heat pump for an office
8. Todoran T.P., Balan M.C. Long term behavior of a geothermal heat pump with oversized horizontal collector // *Energy Build*. 2016. Vol. 133. pp. 799-809.
9. Zhang N., Wang Z. Review of soil thermal conductivity and predictive models // *International Journal of Thermal Sciences*. 2017. No. 117. pp. 172-183. DOI: 10.1016/j.ijthermalsci.2017.03.013.
10. Харченко В. В., Сычѳв А.О. Использование низкопотенциальной теплоты поверхностного водотока в теплонасосной системе теплоснабжения сельского дома // *Науковий вiсник НУБiП України. Серiя: Технiка та енергетика АПК*. 2014. № 194-2. С. 19-24.
11. Харченко В.В., Сычѳв А.О. Оптимизация низкотемпературного контура теплонасосной установки на основе теплоты поверхностных вод // *Альтернативная энергетика и экология (ISJAE)*. 2013. № 7 (129). С. 31-36.
12. Zhou C., Ni L., Yao Y. Heat transfer analysis of multi-row helically coiled tube heat exchangers for surface water-source heat pump // *Energy*. 2018. Vol. 163. pp. 1032-1049.
13. Maksimov V.I., Nagornova T.A., Chernyshev V.S. Conditions and characteristics of water crystallization on the working surface of evaporator heat pumps in reservoirs with low temperatures // *MATEC Web of Conferences: Heat and Mass Transfer in the Thermal Control System of Technical and Technological Energy Equipment*. Tomsk, 2015. Vol. 23, № 01051 (1-8).
14. Maksimov V. I., Saloum A. An experimental study of the effect of water bodies temperature on water heat pump performance // *MATEC Web of Conferences*. 2018. Vol. 194, № 01050 (1-4).
15. Piccolroaz S., Toffolon M., Majone B. A simple lumped model to convert air temperature into surface water temperature in lakes // *Hydrology and earth system sciences*. 2013. Vol. 8. pp. 3323-3338.
16. Amoabeng K. O., Lee K. H., Choi M. J. A study on the performance characteristics of a testing facility for a water-to-water heat pump // *International Journal of Refrigeration*. 2018. Vol. 86. pp. 113-126.
17. Sebarchievici C., Dan D., Sarbu I. Performance assessment of a ground-coupled heat pump for an office room heating using radiator or radiant floor heating systems // *Procedia Engineering*. 2015. Vol. 118. pp. 88-100.
18. Bin H., Wang R.Z., Xiao B., et al. Performance evaluation of different heating terminals used in air source heat pump system // *International Journal of Refrigeration*. 2019. Vol. 98. pp. 274-282.

room heating using radiator or radiant floor heating systems. *Procedia Engineering*. 2015; 118:88-100. DOI: 10.1016/j.proeng.2015.08.407

18. Bin H, Wang RZ, Xiao B., et al. Performance evaluation of different heating terminals used in air source heat pump system. *International Journal of Refrigeration*. 2019; 98:274-282. DOI: 10.1016/j.ijrefrig.2018.10.014

Authors of the publication

Vyacheslav I. Maksimov – PhD, Associate Professor, The Butakov Research and Education Center, National Research Tomsk Polytechnic University.

Amer Saloum – PhD student, The Butakov Research and Education Center, National Research Tomsk Polytechnic University.

Received

January, 18 2019



A TEST-BENCH FOR POST-REPAIR TESTING OF ASYNCHRONOUS MOTORS OF VOLTAGE UP TO 1000 V

O.V. Vladimirov¹, I.V. Ivshin¹, M.F. Nizamiev¹, A.N. Tsvetkov¹, I.K. Usmanov²,
R.R. Gibadullin¹

¹Kazan State Power Engineering University, Kazan, Russia

² LLC «Tagras-Energoservis», Almetyevsk, Russia

Abstract: This article deals with the issues of an objective assessment of technical condition of asynchronous motors with voltage up to 1000 V. A new test-bench is proposed for post-repair tests. This test-bench allows one to conduct induction motor tests and to draw an objective conclusion on the technical condition and quality of the repair carried out automatically.

Keywords: technical condition assessment, test bench, asynchronous motors, software.

Acknowledgments: The work, which resulted in this article, was performed as part of research and development work under Contract No. 23/2015 of September 30, 2015, concluded between OOO Tagras-Energoservis and Kazan State Power Engineering University.

For citation: Vladimirov O.V., Ivshin I.V., Nizamiev M.F., Tsvetkov A.N., Usmanov I.K., Gibadullin R.R. Stand for after repair tests of asynchronous motors with voltage up to 1000 V. *Proceedings of the higher educational institutions. ENERGY SECTOR PROBLEMS*. 2019; 21(3-4):52-58. (In Russ). doi:10.30724/1998-9903-2019-21-3-4-52-58.

Nowadays, there is a problem of assessing the technical condition of asynchronous motors of voltage up to 1000 V, which are sent for repairs and returned from overhauls in order to plan the volume of future repairs.

The current existing test-benches for post-repair testing of motors up to 1000 V have a number of significant drawbacks (high cost, limited functionality and non-satisfaction of customer requirements). The applied programs of post-repair acceptance of motors, with “manual” parameter measurements, have low degree of reliability, lack of automation and the need for additional control over measurements and the correctness of filling in test reports.

Thus, it is advisable to use an automated test bench, which allows determining the technical condition of asynchronous motors after an overhaul, with the possibility of forming a conclusion about the quality of the repairs carried out in an automated mode, eliminating personnel errors. The analysis of existing test methods for asynchronous electric motors and the requirements of regulatory documents [1–7] showed the need to develop an automated test bench and test program to assess the quality of the repair performed.

In the context of cooperation between Kazan State Power Engineering University and OOO “TagraS-Energoservice”, a test-bench for post-repair testing of asynchronous motors up to 1000 V was developed and introduced into the production process. It performs a set of tests aimed at identifying defective electric motor units that are being repaired and overhauled in automatic mode.

The test bench consists of the following units (Fig. 1):

- Hardware-software complex, which includes a personal computer 1 and a printing device 2;

- Main shield 3, which includes control and measurement devices;
- Power supply system, which includes connector 4 for connecting electric motors of various dimensions and ensuring personnel safety, the motor under test 5 and the test table 6;
- Sensor system.

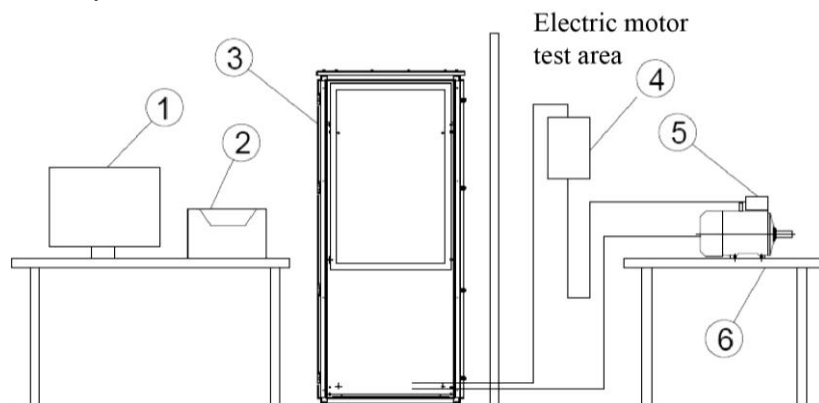


Fig. 1. Scheme of the test bench: 1 – Personal computer; 2 – Printing device; 3 – Main shield; 4 – Connector; 5 – Electric motor with installed sensors; 6 – Test table

Components of the test bench are located in a separate protected room. The test table 6 is located in the electric motor test area. The investigated object (electric motor) 5 is mounted on the test table. A sensor system is installed on the motor. The main shield 3 is at the top of the rack.

All electrical units are connected to each other and to the executive elements by power lines and information transmission lines. The electric motor is connected to the test bench via connector 4 mounted on the wall to ensure safety when connecting and disconnecting the test object.

Prior to testing, the test motor 5 is mounted on the test table 6 and connected by a power line to the main rack via connector 4. In addition, vibration sensors, temperature sensors and a shaft speed sensor are attached to the motor housing.

The main technical characteristics of the test bench are presented in Table 1.

Table 1

The main technical characteristics of the test bench

Characteristics	Value
Power supply voltage, V	380
Permissible relative error of RMS measurements of vibration velocity measured by IVD-3 sensors, %	±10
Accuracy class of measuring current transformers TTI	0.5S
The basic reduced error of voltage measurements,%	0.5
The basic reduced error of current measurements,%	0.25
The basic reduced error of temperature measurements,%	0.25
Maximum permissible error of motor turns measurements, rpm	±1
Maximum permissible error of insulation resistance measurements, %	±3
Maximum permissible error of measurements in mode of electrical strength test of insulation, %	±3
Noise level, dBL	43
Maximum time of continuous work, h	10
Mass of test table with equipment, kg	100
Mean Time Between Failures not less, h	1000

The test bench includes the following control and measurement devices:

- Megohmmeter M4122U-RS;
- Microhmmeter M4104RS;
- Electric network parameter meter ME110-220.3M;
- Module for analog signals input MV110-8A;
- Module for discrete signals output MU110-16R;
- Vibration sensor IVD-3Ts-3 K8M0;
- Tachometer TX01;
- Thermal converter of resistance DTS 014.

Megohmmeter M4122U-RS is used to measure the insulation resistance of motor electrical circuits by increased voltage. In addition, megohmmeter is used to calculate dielectric absorption coefficient and polarization index to identify the quality of insulation and its moisture content. This makes it possible to exclude windings state diagnostics by increased voltage from the test program and, therefore, to reduce the test duration.

Microhmmeter M4104RS is used to measure the resistance of motor windings to direct current, not being under voltage, in order to determine the correctness of its manufacturing and connection. This device is used to determine the magnitude and phase spread of the motor windings resistance.

The electric network parameter meter (ME110-220.3M) is used to measure voltage, current, frequency, power, phase angle and power factor consumed by the motor under test, to convert the measured parameters into a digital code and to transfer measurement results to a software package for further processing in order to determine the technical condition of electrical power unit.

The module for analog signals input MB1-8-8A is intended for converting into a digital code the results of measuring the ambient air temperature and the main elements of the motor under test, as well as the rotation frequency of the motor shaft obtained from a tachometer. The device is a universal 16-bit analog-to-digital converter, it works in the RS-485 network and is able to exchange information with all elements of the hardware-software complex.

The module for discrete signals output OVEN MU110-16R is used to control the actuators and to supply discrete control commands to measuring instruments. The device is controlled by the software of the test-bench.

The vibration sensor IVD-3Ts-3 K8M0 provides RMS measurement of vibration velocity in three directions perpendicular to each other.

The sensor works as follows:

- Converts the signal of the sensing element into voltage and current proportional to the vibration acceleration;
- Produces low-frequency and high-frequency filtering of the analog signal;
- Performs analog-to-digital conversion with a sampling frequency of 25,000 Hz;
- Integrates the acceleration and calculates the RMS of vibration velocity;
- Digitizes the received data and converts it into a form intended for transfer to the RS-485 interface for further processing by software.

The tachometer TX01 coordinates the shaft speed sensor of the motor under study and the analog signal input module MB110 for further digitization of the measured value.

Thermal converter of resistance DTS 014 is used for continuous measurement of electric motor temperature. This sensor converts a change in temperature into a change in electrical resistance to direct current. The sensor has a platinum sensitive element of Pt100 type and compensation of connecting wires resistance.

The appearance of the test bench is shown in Fig. 2

The control system of the test-bench is based on a personal computer with pre-installed software necessary for implementation of a unique control algorithm.

The test-bench works as follows. The network voltage is supplied to the main panel, from which according to the control system commands it is supplied to electric motor under study via

the power channel. Through the same channel, the main parameters of the motor winding are measured by re-switching. The control system receives from the motor under test the shaft rotational speed, the magnitude of vibration of front and rear bearings, as well as temperatures of front and rear bearings and winding.

The control system of the test-bench is based on the software implementation of the control algorithm. The algorithm is incorporated in the program code and allows one to run individual parts of the test program upon an operator's command.



Fig 2. Appearance of the test-bench

The software was created in the environment of the object-oriented programming VisualBasic and is an autonomously functioning module using standard libraries. The software has ample opportunities to customize the test process, set operating modes, calculate additional values based on the obtained data.

The obtained data is converted into a form used for further processing, display and archiving. The program implements solutions for visualization of the obtained and calculated data, which help the operator in the shortest possible time to determine the cause of defects that have appeared, displayed in the form of values that are outside the allowable limits.

The program has an error handling module that helps the operator to quickly debug and tune the system. The module shows code and decoding of the error that has occurred, as well as recommendations for eliminating it. This, in turn, reduces equipment downtime and overall test duration.

The program works as follows. Initially, all required procedures and communication devices are initialized. After launch, the program continuously monitors the communication ports and receives data from them. The main part of the program is the module of data exchange with devices, which receive data and send commands to actuators.

The program has a powerful graphical interface that allows one to visualize the process of testing and display the results in a readable form. The obtained data is stored in a file that has information about the date and time of test and the basic data of the test object. On the basis of the data obtained, a protocol is generated containing the test results and a conclusion on the state of the test object.

Fig. 3 shows the external interface of the program during the testing of an asynchronous motor.

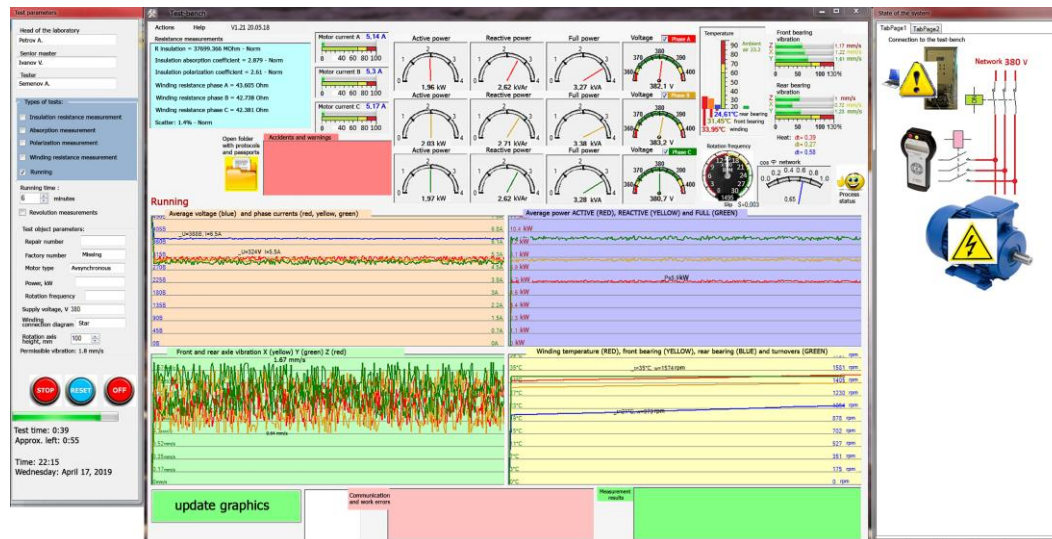


Fig. 3. Program working during test

The result of the program implementation is formation of a test report, a conclusion on the state of the asynchronous motor and its printing or storing it in the archive of protocols.

An example of a test report of a 15 kW power motor with a repair number AST135 is shown in Fig. 4.

Test protocol

Motor parameters:
Repair number: AST135
Serial number: Missing
Motor type: Asynchronous
Capacity: 15 kW
Rotation speed: 1500 rpm
Voltage: 380
Test duration: 33:42 min:s
Running duration: 30 minutes

1. Insulation resistance measurements, MOhm.
Device: M4122U-RS №4873

As per GD	Actual	Conclusion
≥ 1.0 MOhm	4144.961	Conforms

2. Absorption coefficient measurements.
Device: M4122U-RS №4873

As per GD	Actual	Conclusion
≥ 1.3	2.111	Conforms

3. Polarization coefficient measurements.
Device: M4122U-RS №4873

As per GD	Actual	Conclusion
≥ 1.0	----	Not measured

4. Winding resistance to DC, Ohm.
Device: M4104-RS №1369RS

Phase A	Phase B	Phase C	Allowable scatter	Actual scatter	Conclusion
43.375	43.557	43.095	≥2%	0.42	Conforms

5. Electric motor running.

Test mode	Current, A	Voltage, V	Stator temperature, °C	Conclusion
Idle run	0.31	216	22.1	Conforms

6. Electric motor vibration, mm/s.

Device: Vibration sensors IVD-3, № 544947, 544948

Meas. points	Front	Rare
Y - vertical, mm/s	0.49	0.28
X - horizontal, mm/s	0.37	0.37
Z - axial, mm/s	0.84	0.68
Bearing temp. C°	23	22

Maximum permissible vibration: 1.8 mm/s
 Conclusion Satisf.

Conclusion from test results

General conclusion Electric motor is accepted

Test conducted by: Semenov A.

Checked by senior master: Ivanov V.

Head of laboratory: Petrov A.

Fig. 4. The test report for the 15 kW motor with repair number AST135

The developed test bench allows one to carry out automated post-repair tests of asynchronous motors up to 1000 V with identification of its parameters compliance with nominal values. Also it generates test reports and conclusions on the state of the object with its printing or storing it in the archive of protocols.

References

1. Sharipov RR. Stend dlya posleremontnyh ispytaniy asinhronnyh dvigatelej do 1000 V. *Materials of the XXXVII International Scientific Conference «Actual scientific research 2018»*; April 27th 2018; Moscow, Russia; Moscow: Science Center «Olympus», 2018. pp.741-742. (In Russ).

2. Prikhodko VM, Luchkin VYu, Prikhodko IV. Vyyavlenie metodov posleremontnyh ispytaniy sudovyh elektricheskikh mashin. *Sbornik nauchnyh trudov ezhegodnoj nauchno-prakticheskoy konferencii professorsko-prepodavatel'skogo sostava FGBOU VO «GUMRF imeni admirala S.O. Makarova»*; 01 Apr-20 Okt 2017; Sankt-Peterburg, Russia; Sankt-Peterburg: izd-vo GUMRF im. adm. S. O. Makarova, 2017. pp. 383-391. (In Russ).

3. Kharlamov VV, Popov DI, Litvinov AV. Method of determining power and mathematical modeling of physical processes in testing traction induction motors by mutual loads. *The Russian Automobile and Highway Industry Journal*. 2016; 5(51):42-48. (In Russ).

4. Remezovsky VM, Vlasov AB, Mukhalyov VA. The method for controlling electric machine parameters based on the analysis of starting currents. *Vestnik of MSTU*. 2015; 18(1):143-148. Available at: http://vestnik.mstu.edu.ru/v18_1_n60/143_148_remez.pdf. (In Russ).

5. Kochin AE, Vasilchenko SA. Electrical machines testing system using the back-to-bact method. *Sbornik nauchnyh trudov Mezhdunarodnoj nauchno-prakticheskoy konferencii Tom. 1. Tekhnicheskie nauki*; 18-21 aprelya 2017; Rostov-on-Don, Russia. Rostov-on-Don: RGUPS, 2017. pp. 168-171. (In Russ).

6. Shashkov IV, Rudchenko YA. The Stand for Asynchronous Motors Testing in Self-Oscillatory Mode. *«Vestnik GGTU im. P.O.Suhogo»*. 2016; 2(65):86-93. (In Belarus).

7. Basak D., Tiwari A, Das SP. Fault diagnosis and condition monitoring of electrical machines-A Review. *2006 IEEE International Conference on Industrial Technology*; 15-17 December 2006; Mumbai, India. DOI: 10.1109/ICIT.2006.372719.

8. Kuzmenko NV, Kulikov VV, Demin AA. Razrabotka izmeritel'nogo stenda dlya uluchsheniya kachestva ispytaniy asinhronnyh dvigatelej. *Sovremennyye*

Литература

1. Шарипов Р.Р. Стенд для послеремонтных испытаний асинхронных двигателей до 1000 В // Материалы XXXVII международной научно-практической конференции «Actual scientific research 2018»; 27 апреля 2018 г., Москва: Научный центр «Олимп», 2018. С. 741-742.

2. Приходько В.М., Лучкин В.Ю., Приходько И.В. Выявление методов послеремонтных испытаний судовых электрических машин // Сборник научных трудов ежегодной научно-практической конференции профессорско-преподавательского состава ФГБОУ ВО «ГУМРФ имени адмирала С.О. Макарова»; 01 апреля-20 октября 2017 г., Санкт-Петербург. СПб.: изд-во ГУМРФ им. адм. С. О. Макарова, 2017. С. 383-391.

3. Харламов В.В. Попов Д.И., Литвинов А.В. Методика определения мощности и математическое моделирование физических процессов при испытании асинхронных тяговых двигателей методом взаимной нагрузки // «Вестник СибАД». 2016. № 5 (51). С. 42-48.

4. Ремезовский В.М., Власов А.Б., Мухалёв В.А. Метод контроля параметров электрического двигателя на основе анализа пусковых токов // Вестник МГТУ. 2015. Т. 18, № 1. С. 143-148.

5. Кочин А.Е., Васильченко С.А. Система для испытания электрических машин по методу взаимной нагрузки // Сборник научных трудов Международной научно-практической конференции Том. 1. Технические науки; Ростов-на-Дону, 18-21 апреля 2017. Ростов-на-Дону: РГУПС, 2017. С. 168-171.

6. Шашков И.В. Рудченко Ю.А. Стенд для испытания асинхронного двигателя в автоколебательном режиме // «Вестник ГГТУ им. П.О.Сухого». 2016. № 2 (65). С. 86-93.

7. Basak D., Tiwari A, Das SP. Fault diagnosis and condition monitoring of electrical machines-A Review // 2006 IEEE International Conference on Industrial Technology; 15-17 December 2006; Mumbai, India.

8. Кузьменко Н.В., Куликов В.В., Демин А.А. Разработка измерительного стенда для улучшения качества испытаний асинхронных двигателей // Современные технологии и научно-технический прогресс. 2017. Т.1. С.99-100.

9. Авилов В.Д., Попов Д.И., Литвинов А.В. Модернизированный стенд для испытания

tehnologii i nauchno-tehnicheskij progress. 2017; 1:99-100. (In Russ).

9. Avilov VD, Popov DI, Litvinov AV. Modernizirovannyj stand dlya ispytaniya asinhronnyh dvigatelej metodom vzaimnoj nagruzki. *Materialy IX Mezhdunarodnoj nauchno-tehnicheskoy konferencii «Povyshenie effektivnosti ekspluatatsii kollektornyh elektromekhanicheskikh preobrazovatelej energii»*; 05-06 Dec 2013; Omsk, Russia. Omsk: OSTU. pp. 137-141. (In Russ).

10. Kharlamov VV, Popov DI, Litvinov AV. Energy Efficient Universal Stand for Load Testing of Asynchronous Traction Motors and DC Motors. *Izvestia Transsiba (Journal of Transsib Railway Studies)*. 2016; 3 (27):58-66. (In Russ).

асинхронных двигателей методом взаимной нагрузки // Материалы IX Международной научно-технической конференции «Повышение эффективности эксплуатации коллекторных электромеханических преобразователей энергии»; Омск, 05-06 декабря 2013. Омск: ОмГУПС, 2013. С. 137-141.

10. Харламов В.В. Попов Д.И., Литвинов А.В. Универсальный энергоэффективный стенд для нагрузочных испытаний тяговых асинхронных двигателей и двигателей постоянного тока // Известия Транссиба. 2016. № 3 (27). С. 58-66.

Authors of the publication

Oleg V. Vladimirov – Department of Power supply of industrial enterprises of the Kazan State Power Engineering University.

Igor V. Ivshin – Head of the Department of Power supply of industrial enterprises of the Kazan State Power Engineering University.

Marat F. Nizamiev – Department of Power supply of industrial enterprises of the Kazan State Power Engineering University.

Alexey N. Tsvetkov – Department of Power supply of industrial enterprises of the Kazan State Power Engineering University.

Ilnur K. Usmanov – Head of the Production and Technical Department of LLC “TagraS-EnergoServis”.

Ramil R. Gibadullin – Department of Power supply of industrial enterprises of the Kazan State Power Engineering University.

Received

December, 14 2018.



SELECTION OF OPTIONS FOR RECONSTRUCTION OF POWER SUPPLY SYSTEM BASED ON THE FUZZY SETS THEORY AND THE CRITERIA OF DECISION- MAKING THEORY

A.V. Malafeev, A.I. Yuldasheva

Nosov Magnitogorsk State Technical University, Magnitogorsk, Russia

ORCID: <http://orcid.org/0000-0003-1471-9764>, malapheev_av@mail.ru

ORCID: <https://orcid.org/0000-0002-1403-4434>, alinayuldasheva1@gmail.com

Abstract: *The article proposes a method for selecting options for reconstruction of power supply system based on the criteria of decision-making theory. The reconstruction process is considered as a sequential game with two players: active and passive. The probability of possible states of the system is determined basing on the fuzzy sets theory. The main criterion for the choice of reconstruction option is the value of damage from the power supply interruption. The application of the proposed method is considered on the example of a large metallurgical enterprise.*

Keywords: *power supply system, fuzzy sets theory, decision-making theory, game flow chart, Bayes criterion, probable damage.*

For citation: Malafeev A.V., Yuldasheva A.I. Selection of options for the reconstruction of the power supply system based on the fuzzy sets theory and the criteria of decision-making theory. *Proceedings of the higher educational institutions. ENERGY SECTOR PROBLEMS.* 2019; 21 (3-4):59-67. (In Russ). doi:10.30724/1998-9903-2019-21-3-4-59-67.

Introduction

The increasing complexity of technology and consolidation of production has led to the need to apply various mathematical calculations for solving management problems. One of the issues that require application of a rather complex mathematical apparatus is planning of development and reconstruction of power systems in general, networks of main and territorial grid companies, and power supply systems of large industrial enterprises. The latter are characterized by a radical change in the scheme with complete replacement of equipment of any segment of electrical networks when replacing large energy-intensive technological equipment or introducing a new technological process (in particular, for metallurgical enterprises it is steelmaking and finishing of steel in electric arc furnaces, construction of new energy-intensive plants for flue gas cleaning, etc.). At the same time, during the process of construction and commissioning of new facilities, the terms of financing may change, the actually purchased equipment may not be as planned, there may be schematic changes, the actual load will differ from the design. This indicates the uncertainty in a number of factors; no statistical information is available, especially when introducing new technologies. The most convenient approach to accounting for such uncertainty is application of the fuzzy sets theory, which is quite a powerful strategic tool for managing complex systems. As noted in [1], in practice it is constantly necessary to make decisions in the context of incomplete information, and, since the mathematical apparatus of the fuzzy sets theory allows us to model human reasoning, the technologies and algorithms developed within this theory are universal in their applicability. Also the theory of fuzzy sets has found application for solving various problems in the field of energy: for making decisions in managing the reconstruction of power facilities; in determining the strategy for restoring power supply after

an accident; when diagnosing damage in networks, etc. [2]. In work [2] it is concluded that the use of fuzzy sets when choosing options for reconstruction power output schemes of power stations makes it possible to formalize this operation having information uncertainty and with inconsistent rules and criteria. In [3] an algorithm for solving multi-criteria optimization problems with uncertain information is presented on the example of choosing the optimal variant of efficiency increasing of overhead power lines operating in extreme environmental conditions. It is concluded that when making decisions, an integrated approach is needed to formulate and apply principles for evaluating the efficiency of investments in reconstruction projects (such as the domination principle, Pareto-optimal alternatives, formation of complex indicators, selection of the main indicator and transition of the rest to the category of restrictions, selection of non-dominant alternatives, additive convolution). In [4], the application of the fuzzy sets theory to assess production risks for an industrial power supply system was demonstrated. In [5], an algorithm was developed for selecting the optimal parameters of power supply systems, which allows one to solve planning problems in a multi-criteria formulation taking into account several uncertain factors. Discounted undersupply of electricity to consumers due to potential outages and net present value were taken as the criteria for efficiency and reliability. In addition, the work substantiates a rational set of uncertain factors and a method for obtaining additional information, which increases the efficiency of taking into account the uncertainty of the initial information in SES optimization problems and solving them using statistical methods, in particular, the Bayes criterion. The method of multi-criteria analysis of the models for development of power supply systems under conditions of uncertainty, presented in article [6], makes it possible to exclude subjectivity connected with the choice of the most probable value of power consumption and consider many options from the predicted range. A system of criteria for evaluating development models has been developed, which shows economical, technical, and architectural and town planning aspects (total discounted costs, technical losses of electricity, undersupply of electricity, length of transmission lines) and their mathematical models have been developed taking into account the information uncertainty. To assess the effectiveness of investment programs for reconstruction, the use of reliability models based on homogeneous Markov chains, which, however, requires detailed information on the results of reconstruction, is proposed in [7]. The work [8] is devoted to evaluating risks of a secure nature when planning the development of distributed generation taking into account uncertainty in load, generation, energy prices. In [9], a method is proposed for assessing such a risk during cascade development of an accident under conditions of extensive use in distribution networks of block-modular substations and other modern equipment based on the theory of D-S evidence. The use of method of sequential equivalence to assess the reliability is considered in [10].

When comparing options for reconstruction of the factory electrical network in case of production expansion, taking into account the damage from a power failure, uncertain (or partially uncertain) values include the following:

- 1) Deviation of actual load increase from the design value;
- 2) Nature of the emergency;
- 3) Disconnection time, taking into account finding the damage location.

This paper considers the first of these factors.

Methods for selecting options for reconstruction of power supply system

Large-scale reconstruction is accompanied, as a rule, by a stepwise commissioning of production facilities and individual sections of power supply system. During the process of commissioning of new and reconstructed facilities, it may become necessary to adjust decisions on implementation of the next stage. In this regard, it is necessary to consider the task of planning in such conditions as dynamic one. We represent this process as a sequential game [11] with participation of two players: an organization performing a complex of reconstruction works (active player A), and “nature” (passive player P).

The action of “nature” is determined by deviation of actual load of the object from the

design, the change in electricity prices in comparison with the forecast, the possibility of emergencies of various types and various time of their liquidation. Depending on the current situation, it is possible to take various decisions on further reconstruction, and therefore it is advisable to consider the reconstruction process as a game in mixed strategies, the number of moves in which is $2N$ (N is the number of stages). The probability of one or another state of “nature” (player P move) will be determined on the basis of the fuzzy sets theory, considering the actual load resulting from reconstruction of power supply system as a one-sided fuzzy number. For this we will use numbers with membership function specified by the Cauchy curve parametrized at a level of 0,5 [12]. In this case, it has the following form:

$$\mu(P) = \frac{1}{1 + \left(\frac{P - P_{bn}}{P_{av} - P_{bn}} \right)^2}, \quad (1)$$

where P is actual load as a result of reconstruction; P_{bn} is boundary value of load corresponding to the right boundary of the fuzzy interval core; as a boundary value we will take the design value of the calculated load; P_{av} is load corresponding to a 10 % excess of the actual load over the design value (an error of 10% corresponds to the definition of design loads by the method of design factors which is now used in design practice (see, for example, [12]); $P_{av} = 1,1 P_{bn}$.

It is necessary to minimize the loss of player A. We will accept the damage from violation of reliability of power supply during implementation of any option as the player A loss. Then the role of payment function will be played by player A loss after the next move.

The structure of the game graph for two stages of reconstruction is shown in Fig. 1.

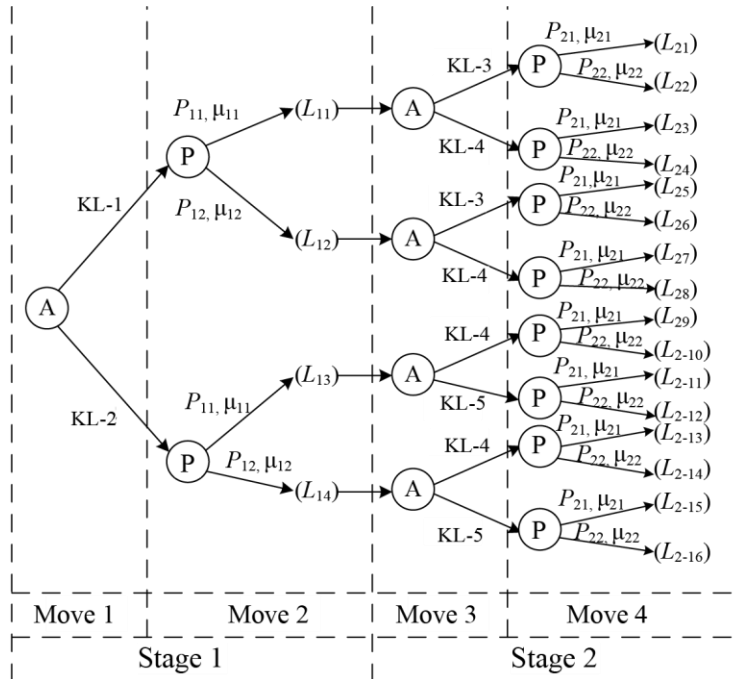


Fig. 1. General view of the game graph, corresponding to two-stages reconstruction of power supply system

Here KL-1 ... KL-5 are elements of the strategy being implemented – the input sections of the power supply system; P_{11} , P_{12} and P_{21} , P_{22} are possible load values of the reconstructed segment at the first and second stages, respectively, with probabilities p_{11} , p_{12} , p_{21} , p_{22} . D_{11} ... D_{14} are loss values corresponding to implementation of two options (construction KL-1 or KL-2) of

the first stage, when load is P_{11} or P_{12} ; $D_{21} \dots D_{2-16}$ are similar values for subsequent construction of KL-3 or KL-4 and load P_{21} (P_{22}). As loss D , we will use the reduced costs, taking into account the damage.

As a decision criterion, we take the Bayes criterion, which allows one to operate with subjective probabilities of the states of nature. As probabilities, we will use the values of membership function (MF) from expression (1). In this case, the loss at the i -th stage of reconstruction will be determined as follows:

$$L_{is}(i) = \sum_{i=1}^N \mu_{ia}(i) D_{is(i)a(i)}, \quad (2)$$

where $s(i)$ is number of the selected strategy; $a(i)$ is the state of nature at the i -th stage; $\mu_{ia}(i)$ is MF value for the state $a(i)$; $D_{is(i)a(i)}$ is loss, which includes investments, reduced to one year, and damage from power supply interruption when implementing strategy $s(i)$ and state of nature $a(i)$.

When taking into account the degree of confidence of player A to the accepted distribution, the Hodge-Lehmann criterion can be used, which is a combination of Bayesian and Wald criteria. The expression for loss in this case will be the following:

$$L_{is}(i) = \lambda \sum_{i=1}^N \mu_{ia}(i) D_{is(i)a(i)} + (1-\lambda) \max_{1 \leq i \leq N} (D_{is(i)a(i)}), \quad (3)$$

where $\lambda \in [0;1]$ is degree of confidence.

In the absence of any preferences (for $\lambda=0$) we obtain the Wald criterion:

$$L_{is}(i) = \max_{1 \leq i \leq N} (D_{is(i)a(i)}). \quad (4)$$

When using any of the specified criteria, the final version of the reconstruction will be selected by the criterion of minimum loss $\min L_{Ns}(N)$ at the last stage.

Practical implementation

As an example, the reconstruction of a large metallurgical enterprise is considered. It is planned to construct aspiration units, for power supply of which the construction of a new 110/10 kV PS-11 substation is envisaged. PS load will be $S_1= 80$ MVA. It is planned to carry out external power supply of PS-11 110kV from PS-60 and central electric station (CES); to provide more reliable power supply, construction of additional lines from substations is planned – 30, 62, 85.

Variants of PS-11 connection diagrams are shown in fig. 2

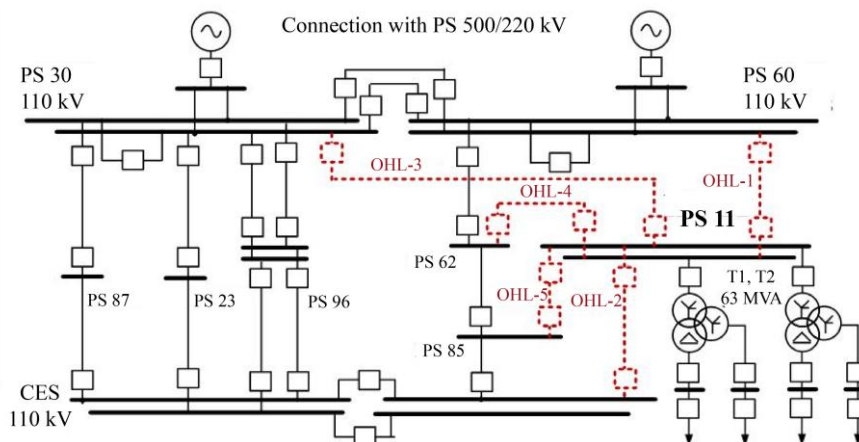


Fig. 2. Possible variants for PS-11 connection

For the proposed circuit solutions, a game graph is constructed (Fig. 3).

As noted above, the choice of final version of reconstruction is carried out based on the criterion of minimum total loss according to the accepted criterion (Bayes, Hodge-Lehmann, Wald) $\min L_{iS}$ at the last stage. In this case, the damage, as a component of the loss, is determined as follows:

$$Y_{is} = y_0 T_R \Delta P_{is}, \quad (5)$$

where y_0 is specific damage from undersupply of consumer electricity, determined by the time of interruption and the nature of production, rub./kW·h (for enterprises of ferrous metallurgy $y_0 = 18.3$ rub./kW·h [14]); T_R is recovery time; ΔP_{is} is power, unsupplied to the consumer due to a power failure, taking into account the MF value μ_{ij} when working with this value of P_{is} ($\Delta P_{is} = |P_1 - P_{is}| p_{is}$, where $P_1 = 64$ MW is design load).

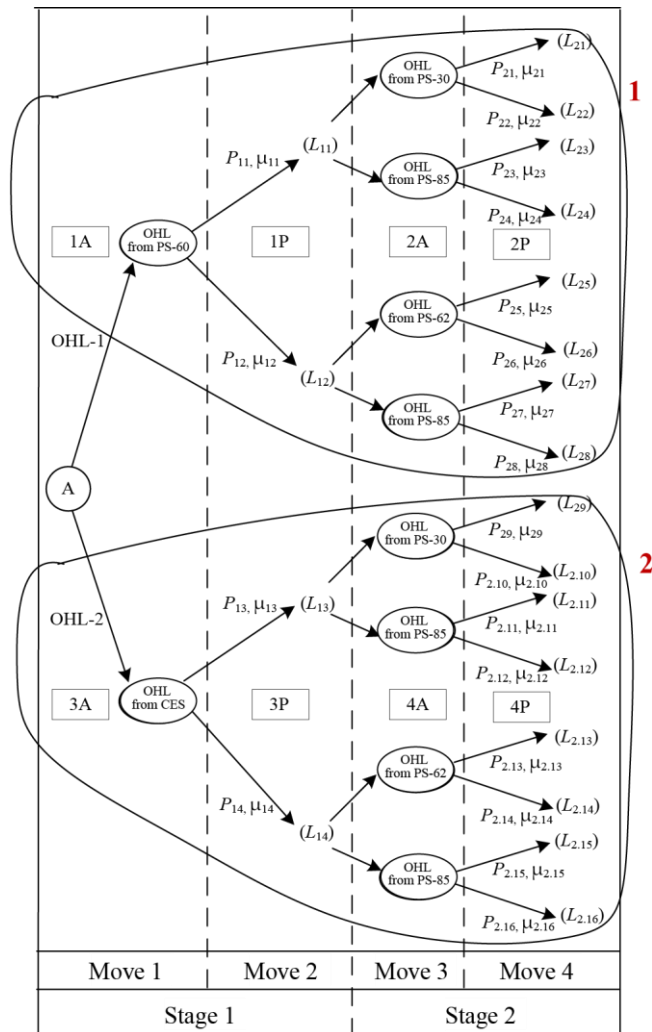


Fig. 3. The game graph corresponding to the construction of PS-11

For the proposed schemes, we estimated the capital investments K , and using the KATRAN software [15, 16], the reliability indicators (failure rate parameter ω and recovery time T_R) were calculated. The results are presented in Table. 1. In all considered options, we adopt construction of 110 kV power lines on metal poles using ASU-400 wires. Construction of 1 km of these wires will cost 0.55 million rub./km [17], its failure rate is $\omega = 0.0128$ 1/year per 1 km [17].

To correctly compare the obtained values, the capital investments were taken into account (the values are given in Table 1) in each of the reconstruction projects. Thus, the loss, which is reduced cost, taking into account damage Y_{is} , will be determined as follows:

$$L_{is} = Y_{is} + K_{is} E_N \tag{6}$$

where E_N is capital investment efficiency ratio $K_{is}(E_N = 0.12)$.

Table 1

PS-11 connectivity options and the corresponding investments and reliability indicators

Strategy	Constructed lines	Total length, km	Total capital investments, mln rub.	ω , 1/year	T_R , year
1	PS-60 – PS-11	5.2	2.86	0.000010	0.003948
	PS-60 – PS-11; PS-30 – PS-11	11.5	6.33	0.080650	0.000801
	PS-60 – PS-11; PS-85 – PS-11	12.3	5.45	0.060170	0.000801
	PS-60 – PS-11; PS-62 – PS-11	9.9	6.77	0.090890	0.000801
2	CES – PS-11	2.8	1.54	0.000005	0.003256
	CES – PS-11; PS-30 – PS-11	9.1	5.01	0.080645	0.000768
	CES – PS-11; PS-85 – PS-11	9.9	4.13	0.060165	0.000768
	CES – PS-11; PS-62 – PS-11	7.5	5.45	0.090885	0.000768

The results of loss calculation are shown in Table 2.

Table 2

The results of total loss calculation from the game graph

Strategy	Description of move	Load P_{ia}	MF value μ_{is}	Loss D_{is} , mln rub.	Total loss at P_{i1}	Total loss at P_{i2}		
1	1A: Construction of OHL-1 (from PS-60) 1P: Load growth	$P_{11}=1,2P_1$	0,2	10,064	10,064	34,364		
		$P_{12}=1,05P_1$	0,8	34,364				
	2A: Construction of OHL-3, 4, 5 (from PS-30, 62, 85) 2P: Load growth	From PS-30	$P_{21}=1,15P_1$ $P_{22}=1,3P_1$	0,31 0,1	3,667 1,828	13,731 11,892	38,031 36,192	
		From PS-85	$P_{23}=1,1P_1$ $P_{24}=0,85P_1$	0,5 –	5,173 –	15,237 –	39,537 –	
		From PS-62	$P_{25}=1P_1$ $P_{26}=0,9P_2$	– –	– –	– –	– –	
		From PS-85	$P_{27}=0,8P_1$ $P_{28}=1,2P_1$	– 0,06	– 1,331	– 11,395	– 35,695	
		2	3A: Construction of OHL-2 (from CES) 3P: Load growth	$P_{13}=1,2P_1$	0,2	8,201	8,201	4,527
				$P_{14}=1,3P_1$	0,1	4,527		
4A: Construction of OHL-3, 4, 5 (from PS-30, 62, 85) 4P: Load growth	From PS-30		$P_{29}=1,1P_1$ $P_{2,10}=1P_1$	0,5 –	4,933 –	13,134 –	9,46 –	
	From PS-85		$P_{2,11}=0,8P_1$ $P_{2,12}=1,15P_1$	– 0,31	– 3,283	– 11,484	– 7,81	
	From PS-62	$P_{2,13}=1P_1$ $P_{2,14}=1,3P_1$	– 0,1	– 1,678	– 9,879	– 6,205		
	From PS-85	$P_{2,15}=1,1P_1$ $P_{2,16}=0,95P_1$	0,2 –	2,492 –	10,693 –	7,019 –		

As follows from Table 2, the best strategy, characterized by least loss, is construction of an overhead line from CES, and at the second stage from PS-62.

Conclusions

The article presents an improved method for selecting options for multi-stage reconstruction of the power supply system based on the game theory approaches, which differs from the existing methods of taking into account the probabilities of possible states of an object as a result of implementation of each stage.

It is proposed to determine the probability of possible states of an object on the basis of fuzzy sets theory using numbers with the membership function defined by the Cauchy curve. The reconstruction process is represented as a sequential game involving an active player (the service responsible for planning reconstruction work) and a passive player (“nature”), which allows one to take into account all possible changes in external factors and combinations of decisions taken at each stage. The value of costs was chosen as the main criterion for selection of reconstruction option, taking into account the damage caused by loss of the power supply reliability. It is proposed to choose it based on the criterion of the minimum loss at the last stage. The technique allows correction of the adopted strategy based on the results of the implementation of any of the stages.

As an example, we considered two stages of reconstruction of power supply system of a large metallurgical enterprise during construction of a new energy-intensive consumer. The calculations based on the game graph, allowed us to choose the option characterized by the lowest loss value.

References

1. Konyshova LK, Nazarov DM. *Osnovy teorii nechetkikh mnozhestv*. Sankt Petersburg: Piter, 2011. (In Russ).
2. Kovalenko IV, Tremyasov VA. Application of the theory of fuzzy sets in the problem of reconstruction options selection for the main power distribution schemes of power plants. *Proceedings of the higher educational institutions. ENERGY SECTOR PROBLEMS*. 2004; 5-6:26-32. (In Russ).
3. Shevchenko NJ, Lebedeva JV, Havronichev SV. The algorithm for choice of optimal variant reconstruction of overhead power transmission lines of 110–220 kV. *Modern problems of science and education*. 2013; 5. (In Russ).
4. Malafeev AV, Yuldasheva AI. The fuzzy sets theory usage for production risk assessment for the mode control of industrial power supply systems. *Electrical energy industry through the eyes of young people: proceedings of VI Intern. scientific and technical conference, Nov 9–13 2015; Ivanovo, Russia*. Ivanovo: IGEU im. V.I. Lenina, 2015; V.2. pp. 294-297.
5. Metelkov AA. *Razrabotka metodiki planirovaniya sistem elektroснабzheniya rajonov s maloj plotnost'yu nagruzok s uchetom neopredelennosti iskhodnoj informacii* [dissertation]. Moscow; 2004. Available at: <https://search.rsl.ru/ru/record/01002663331>. Accessed: 21 Apr 2019. (In Russ).

Литература

1. Конишева Л.К., Назаров Д.М. Основы теории нечетких множеств. СПб: Питер, 2011. 192 с.
2. Коваленко И.В., Тремясов В.А. Применение теории нечетких множеств при выборе варианта реконструкции главных схем выдачи мощности электростанций // Известия высших учебных заведений. ПРОБЛЕМЫ ЭНЕРГЕТИКИ. 2004. № 5-6. С. 26-32.
3. Шевченко Н.Ю., Лебедева Ю.В., Хавроничев С.В. Алгоритм выбора оптимального варианта реконструкции воздушных линий электропередачи напряжением 110–220 кВ // Современные проблемы науки и образования. 2013. № 5.
4. Малафеев А.В., Юлдашева А.И. Использование теории нечетких множеств для оценки производственных рисков при управлении режимами промышленной системы электроснабжения // Электроэнергетика глазами молодежи: труды VI Междунар. науч.-техн. конф.; 9–13 ноября 2015 г., г. Иваново. В 2 т. 2Т. Иваново: ИГЭУ им. В.И. Ленина, 2015. С. 294-297.
5. Метельков А.А. Разработка методики планирования систем электроснабжения районов с малой плотностью нагрузок с учетом неопределенности исходной информации: Дис. ... канд. техн. наук. Москва; 2004. Доступно по: <https://search.rsl.ru/ru/record/01002663331>. Ссылка активна на 24 апреля 2019.
6. Семенова Л.А. Многокритериальный анализ

6. Semenova LA. Multi-criteria analysis of power systems development models in the face of uncertainty. *Cherepovets State University Bulletin*. 2016; 4:39-46. (In Russ).
7. Abdullazyanov EY, Vasiliev YA, Galiev IF. Enterprises power supplying schemes reliability models for investments efficiency. *Proceedings of the higher educational institutions. ENERGY SECTOR PROBLEMS*. 2009; 3:67-74. (In Russ).
8. Abapour S, Zare K, Mohammadi-ivatloo B. Evaluation of technical risks in distribution network along with distributed generation based on active management. *IET Generation, Transmission & Distribution*. 2014; 8(4):609-618. doi: 10.1049/iet-gtd.2013.0666.
9. Cunbin L, Gefu Q, Tingting Y. Operational Risk Assessment of Distribution Network Equipment Based on Rough Set and D-S Evidence Theory. *Journal of Applied Mathematics*. 2013. Article ID 263905. 7 p. <http://dx.doi.org/10.1155/2013/263905>.
10. Yuldasheva AI, Malafeev AV. Accounting the reliability index at planning the mode of industrial power supply system with own electric power stations. *Electrotechnical Systems and Complexes*. 2015; 3(28):36-40. (In Russ).
11. Duplyakin VM. *Teoriya igr*. Samara: Izd-vo Samar. aerokosm. un-ta, 2011. (In Russ).
12. Koroteev MV. Linguistic variables of economic indicators. *Audit and financial analysis*. 2012; 2:5. (In Russ).
13. Kudrin BI, Zhilin BV, Oshurkov MG. *Elektrosnabzhenie*. Rostov-on-Don: Feniks, 2018. (In Russ).
14. Nepomnyashchy VA. *Ekonomicheskie poteri ot narusheniya elektrosnabzheniya*. Moscow: MPEI, 2010. (In Russ).
15. Igumenshev VA, Malafeev AV, Panova EA, et al. *Kompleks avtomatizirovannogo rezhimnogo analiza KATRAN 9.0. Svidetel'stvo o gosudarstvennoj registracii programmy dlya EVM RUS №2015662725*. 30.11.2015. Byul. «Programmy dlya EVM, bazy dannyh, TIMS» №12. Available at: <https://elibrary.ru/item.asp?id=35632066>. Accessed: 20 Apr 2019.
16. Malafeev AV. Algoritm rascheta strukturnoj nadezhnosti sistem elektrosnabzheniya krupnyh promyshlennyh predpriyatij na osnove metoda posledovatel'nogo ekvivalentirovaniya. *Proceedings of the Russian Academy of Sciences. Power Engineering*. 2016; 4:62-72. (In Russ).
17. RUCABEL.RU [Internet]. Available at: http://www.rucabel.ru/asu/cabel_asu_400_93.html. Accessed: 20 Nov 2018.
18. Yuldasheva AI, Malafeev AV. Accounting the reliability index at planning the mode of industrial power supply system with own electric power stations. *Electrotechnical Systems and Complexes*. 2015; 3(28):36-40. (In Russ).
19. Abdullazyanov EY, Vasiliev YA, Galiev IF. Enterprises power supplying schemes reliability models for investments efficiency. *Proceedings of the higher educational institutions. ENERGY SECTOR PROBLEMS*. 2009; 3:67-74. (In Russ).
20. Abapour S, Zare K, Mohammadi-ivatloo B. Evaluation of technical risks in distribution network along with distributed generation based on active management // *IET Generation, Transmission & Distribution*. 2014. Vol. 8. Iss. 4. P. 609-618.
21. Cunbin L, Gefu Q, Tingting Y. Operational Risk Assessment of Distribution Network Equipment Based on Rough Set and D-S Evidence Theory // *Journal of Applied Mathematics*. Volume 2013. Article ID 263905. 7 p.
22. Юлдашева А.И., Малафеев А.В. Учет показателей надежности при планировании режима промышленной системы электроснабжения с собственными электростанциями // *Электротехнические системы и комплексы*. 2015. №3(28). С. 36-40.
23. Дуплякин В. М. Теория игр. Самара: Изд-во Самар. аэрокосм. ун-та, 2011. 191 с.
24. Коротеев М.В. Лингвистические переменные экономических показателей // *Аудит и финансовый анализ*. 2012. № 2. С 5.
25. Кудрин Б.И., Жилин Б.В., Ошурков М.Г. *Электроснабжение*. Ростов-на-Дону: Феникс, 2018. 382 с.
26. Непомнящий В.А. Экономические потери от нарушения электроснабжения. М: МЭИ, 2010. 187 с.
27. Игуменцев В.А., Малафеев А.В., Панова Е.А., и др. Комплекс автоматизированного режимного анализа КАТРАН 9.0. Свидетельство о государственной регистрации программы для ЭВМ № 2015662725. 30.11.2015. Официальный бюллетень «Программы для ЭВМ, базы данных, ТИМС» №12. Доступно по: <https://elibrary.ru/item.asp?id=35632066>. Дата обращения: 20 апреля 2019.
28. Малафеев А.В. Алгоритм расчета структурной надежности систем электроснабжения крупных промышленных предприятий на основе метода последовательного эквивалентирования // *Известия РАН. Энергетика*. 2016. №4. С. 62-72.
29. RUCABEL.RU [Электронный ресурс]. Доступно по: http://www.rucabel.ru/asu/cabel_asu_400_93.html. Ссылка активна на 20 ноября 2018.
30. РД 34.20.574. Указания по применению показателей надежности элементов энергосистем и

© *A.B. Малафеев, А.И. Юлдашева*

18. RD 34.20.574. Ukazaniya po primeneniyu pokazatelej nadezhnosti elementov energosistem i raboty energoblokov s paroturbinnymi ustanovkami [Internet]. Available at: http://www.xjob.ru/PД_34.20.574. Accessed: 20 Oct 2018.

работы энергоблоков с паротурбинными установками [Электронный ресурс]. Доступно по: http://www.xjob.ru/PД_34.20.574. Ссылка активна на: 20 октября 2018.

Authors of the publication

Aleksei V. Malafeev – Department of Industrial electric power supply, Nosov Magnitogorsk State Technical University.

Alina I. Iuldasheva – Department of Industrial electric power supply, Nosov Magnitogorsk State Technical University.

Received

December 29, 2018

**STATE ESTIMATION METHOD DEVELOPMENT FOR SCADA AND
SYNCHRONIZED PHASOR MEASUREMENTS INTEGRATION WITHIN POWER
SYSTEM**

P.I. Bartolomey, S.I. Semenko

**Ural Federal University named after the first President of Russia B.N.Yeltsin,
Yekaterinburg, Russia
sinissem@gmail.com**

Abstract: *In modern power systems, a special kind of measurement systems was actively implemented for the last 20 years. These measurement systems have a high-precision synchronized time stamp, which makes it possible to obtain, in addition to the effective value of line current and bus voltage, the electrical phase angles. In previous years, a large number of methods for steady state obtaining based on telemetry (state estimation) have been formed. These measurements are based on consideration of only modules of these quantities, as well as active and reactive components of injection power of nodes and flows in the branches. Most of these methods were based on the weighted least squares method, or other methods based on the maximum likelihood method, for which one requires determination of weighting factors of measurements, traditionally chosen on the basis of relative errors of these measurements. However, there is a problem of taking into account the electrical angles measurements, for which the relative error is fundamentally indeterminable. Also there is a problem associated with integration of phasor measurements with traditional measurement tools into a single measuring system due to a significant differences in accuracy and update frequency. This paper proposes an approach for combining phasor measurements with traditional SCADA measurements as a part of state estimation procedure, taking into account the described problems.*

Keywords: *static state estimation, synchronized phasor measurements, maximum likelihood method, choice of weighting factors, linear state estimation.*

For citation: Bartolomey P.I., Semenko S.I. State estimation method development for SCADA and synchronized phasor measurements within power system. *Proceedings of the higher educational institutions. ENERGY SECTOR PROBLEMS*. 2019; 21 (3-4):68-78. (In Russ). doi:10.30724/1998-9903-2019-21-3-4-68-78.

Introduction

Classical methods of state estimation (SE) are based on measurements of effective currents and voltages of nodes, measurements of active and reactive components of capacities of nodes and branches. Due to the nonlinearity of relationship between current, voltage, and power, the SE task turns out to be nonlinear, which introduces considerable difficulties in its practical implementation. The methods for solving this problem turn out to be iterative, non-robust, insufficiently reliable, and potentially long to calculate. As a conclusion, the issues of transition from iterative to direct solution of ES problem became relevant. The main way of such a transition is to get rid of power measurements. The development and implementation of synchronized phasor measurement (SPM) tools allowed one to use only measurements of complex currents and voltages in SE tasks, which ensured the emergence of integrated linear state estimation (LES) methods [1–3].

The most popular SE methods use weighting factors measurement, which are selected

based on the measurement instrument errors. All measurements included in the classic SE have data on relative error. However, for measurements of phase angles of currents and voltages which appeared in the SPM system, it is impossible to record the relative error due to their nature. This issue is particularly relevant for the problem of the specified complex linear SE. Consequently, the important issue is combined usage of phase angles measurements and other classical methods.

There are power systems [1–3] in which complete observability is provided entirely by SPM. In such networks, the idea of using the complex currents and voltages received from measuring devices for LSE solving is implemented. For the Russian energy systems, which are characterized by branching and large length, at present there is no possibility to implement the LSE idea, due to the lack of sufficient number of PMU devices to ensure observability. Moreover, the very possibility of LSE is not yet justified.

Currently, SPM are not ubiquitous, due to their high prices in the past, as well as inertia of transition to new technologies. Accordingly, it is necessary to consider issues of smooth transition to the joint use of SPM and SCADA, which requires development of hybrid SE methods. The present work is devoted to these questions. In addition, this article discusses the issues on SE development so that when a local network segment observed by PMU appears, it becomes possible to use LSE the most effectively.

Maximum likelihood method in SE task

Despite recent publications on non-quadratic methods [4], and evolution of computational procedures [5], the weighted least squares method is the most used method in practice for SE. It consists in minimizing the weighted sum of squares of deviations of estimated related quantities from measurements, which can be written in the form [6–7]:

$$\Phi_2(X) = \sum_{i=1}^M \alpha_i \cdot (y_i(X) - y_i^{\text{TM}})^2 \rightarrow \min \quad (1)$$

$$\{h_j(X) = 0, \quad j = 1 \dots K,$$

where X is vector of basic state parameters, of dimension N , through which all other parameters can be expressed, M is the number of measurements used in SE task, y_i^{TM} is telemetry parameter, $y_i(X)$ is analytical expression of the parameter being measured through independent variables X , α_i is weighting factor, $\{h_j(x) = 0, \quad j = 1 \dots K$ is limitations showing information that is known to be accurate. Observability requires measurement redundancy, or $M > N$, when the system is nondegenerate $\{y_i(X) = y_i^{\text{TM}}, \quad i = 1 \dots M$. As applied to the power system, X , most often, refers to the vector of modules and phase angles of voltages; y_i^{TM} refers to measurements of nodal and linear values of current modules, active and reactive power components, nodal voltage modules; $y_i(X)$ is analytical expression of the parameter being measured only through modules and phases of voltages, $\{h_j(x) = 0, \quad j = 1 \dots K$ is substation limitations with zero power takeoff, limitations on power factors.

The effectiveness of SE procedure directly depends on the choice of coefficients α_i . Each time the coefficients α_i are selected on the basis of operating experience (empirically), by an expert, based on recommendations for their choice (heuristically) [1, 8]. Nowadays, these recommendations suggest setting α_i values inversely proportional to the square of relative measurement error θ_i , which is indicated in the passport of the measuring device. Until recently, these methods of choosing weight coefficients effectively coped with the task, presumably due to the accumulated operating experience of the corresponding software systems. Moreover, to date, the errors of all instruments for measuring the characteristics of a power

system are metrologically normalized by the relative error. The recently introduced SPM devices, making it possible to measure phase electric angle of complex values, which cannot be normalized by relative error, have revealed a new problem when taking into account these angles in SE.

In order to substantiate the approach to the choice of weighting factors for measuring dissimilar parameters, we consider the least squares method from the standpoint of the maximum likelihood method. We consider power system for which SE task is performed. We assume that M telemetry is performed in a power system as in the previous task. Since all these measurements have errors, we suppose that for all these errors, probability densities $\rho_i(\Delta y_i)$ are given, where i is measurement number from 1 to M , Δy_i is a random error value, which is usually taken as continuous. Then it turns out that

$$y_i = y_i^{\text{TM}} + \Delta y_i, \quad (2)$$

where y_i is the estimated value of the characteristic being measured. From (1) it follows that

$$\Delta y_i = y_i - y_i^{\text{TM}}. \quad (3)$$

We suppose that all measurements are carried out independently of each other, that is, measurement errors are independent random variables. Then, to determine the probability density of the entire measurement system $\rho_p(\Delta Y)$, the probability density of vector of such values ΔY are multiplied [9], and, therefore,

$$\rho_p(\Delta Y) = \prod_{i=1}^M \rho_i(\Delta y_i). \quad (4)$$

This function is most often taken as the likelihood function in the maximum likelihood method [9].

Also, we suppose that it is reliably known that parameters y_i are interconnected by a system of equations:

$$\left\{ f_j(X, Y) = 0, \quad j = 1 \dots L, \right. \quad (5)$$

where $f_j(X, Y)$ is interconnection functions, which are determined by information about specific physical phenomena and objects, L is the number of interconnection equations. Therefore, the optimization problem for the maximum likelihood method can be written as:

$$\begin{aligned} \Phi(Y) = \prod_{i=1}^M \rho_i(y_i - y_i^{\text{TM}}) \rightarrow \max \\ \left\{ f_j(X, Y) = 0, \quad j = 1 \dots L. \right. \end{aligned} \quad (6)$$

The solution of this optimization problem is estimation of X parameters.

If we assume that all random variables Δx_i are normally distributed, in other words, we can write:

$$\rho_i(\Delta y_i) = \frac{1}{\sqrt{2 \cdot \pi \cdot \sigma_i}} \cdot \exp\left(-\frac{\Delta y_i^2}{2 \cdot \pi \cdot \sigma_i^2}\right), \quad (7)$$

Where σ_i is dispersion of random variable Δy_i , then, given that the exponential function and multiplication by a positive constant do not affect the order relation, and knowing that at exponent multiplication its degrees are added, we can rewrite expression (5) in the form of the least squares method

$$\Phi(Y) = \sum_{i=1}^M \frac{1}{\sigma_i^2} \cdot (y_i - y_i^{\text{TM}})^2 \rightarrow \min \quad (8)$$

$$\left\{ f_j(X, Y) = 0, \quad j = 1 \dots L. \right.$$

The transition from maximization (5) to minimization (7) was accomplished by changing the sign in the exponent. Problem (8) is itself a weighted least squares problem. To finally transform expression (8) into expression (1), it is additionally required to assume that there is an equivalent transformation

$$\left\{ f_j(X, Y) = 0, \quad j = 1 \dots L \right. \Rightarrow \left\{ \begin{array}{l} y_j(X) = y_j, \quad j = 1 \dots M, \\ h_j(X) = 0, \quad j = 1 \dots K. \end{array} \right. \quad (9)$$

From expressions (1)–(8) it can be seen that the method of least squares (1) is a special case of the maximum likelihood method. Consequently, the weighting factors α_i are completely equivalent to the reciprocal of the square of dispersion $1 / \sigma_i^2$.

Further we list the assumptions made during transition from the maximum likelihood method to the method of least squares:

1. The probability density of all errors is predeterminedly known, unchanged in time and is a normal distribution.
2. The system of constraints in the form of equalities in optimization problem should be performed under any conditions and there should be no doubt about its correctness.
3. The dispersions must be constant and known in advance.
4. There should be no, or should be known in advance the magnitude of systematic measurement error σ_i .

All these assumptions are used in the least squares method (1) described at the beginning of the section, although they were implicitly accepted there.

The choice of weights for the method of weighted least squares for SE task

As already noted, for all measurements the instrument passport normalizes the relative error θ_i . Traditionally, in the least squares method (1), it is recommended [1, 8] to choose weighting factors as

$$\alpha_i = \frac{1}{(\theta_i \cdot m_i)^2}, \quad (10)$$

where m_i is the scaling coefficient of measurement, which is selected based on the physical nature of the measured value. For example, for voltage modules, current modules and power components, this coefficient will differ because they are dissimilar. Strictly speaking, the main problem of the described method is that it is fully applicable only under the condition that θ_i is not relative, but absolute error, but usually it is applied to relative errors. This problem was not previously manifested, due to the fact that all measurements were normalized to relative error. However, the relatively recent appearance of SPM has led to the possibility of measuring characteristics that can in principle be normalized only by absolute error, namely, the phase angles of electrical quantities. The application of the old approach (9) to new measurement systems leads to the fact that the accumulated experience, on the basis of which the scaling coefficients m_i were chosen, is inapplicable and, as a conclusion, this can lead to an unpredictable mode distortion as a result of its SE. Worse, for the current SE paradigm it is impossible even to normalize this mode distortion, since the measure of mode deviation from

the standard turns out to be uncertain.

In this paper, it is proposed to replace the traditional method of choosing weight coefficients. The purpose is to take into account the heterogeneity of parameters, which, first of all, manifests itself in combined usage of modules and phase angles of electrical quantities. The essence of the proposed method is that all measurements should be divided into M_{Θ} measurements with normalized absolute error Θ_i , $i = 1 \dots M_{\Theta}$, and M_{θ} measurements with normalized relative error θ_i , $i = 1 + M_{\Theta} \dots M$. For measurements with normalized absolute error, it is proposed to calculate the weighting factor as

$$\alpha_i = \frac{1}{\Theta_i^2}, \quad (11)$$

and for measurements with normalized relative error it is proposed to calculate the weighting factor as

$$\alpha_i = \frac{1}{(\theta_i \cdot y_i^{\text{TM}})^2}. \quad (12)$$

Accordingly, the objective function and the constraint system will take the form:

$$\begin{aligned} \Phi(Y) &= \sum_{i=1}^M \alpha_i \cdot (y_i - y_i^{\text{TM}})^2 \rightarrow \min \\ \{ f_j(X, Y) &= 0, \quad j = 1 \dots L, \end{aligned} \quad (13)$$

where α_i is weighting factor corresponding to (11) for measurements with normalized absolute error and to (12) for measurements with normalized relative error.

Further we show how the transition was made from expression (8), where $1/\sigma_i^2$ are used as weights, to weights written in expressions (11)–(12). For this we take the first group of assumptions: normalized absolute errors correspond to the confidence interval of the measured value. This can be mathematically written as

$$\Theta_i = S_i \cdot \tau_i \approx \sigma_i \cdot \tau'_i, \quad (14)$$

where S_i is sample standard deviation corresponding to the series of measurements assumed to be performed for instrument calibration, τ_i is the Student's coefficient corresponding to the performed series of measurements and the required reliability of measurements (for example 99%) τ'_i is the Student's coefficient corresponding to infinite number of measurements and the same reliability as for τ_i . The equality sign in (14) shows that measuring devices are assumed to be verified by a series of tests on a more accurate device, and an approximate equality sign indicates that an infinite number of tests were made during such verification [10]. Taking into account that the largest error [10] is indicated in the instrument passports, these assumptions seem to be acceptable for further reasoning.

The second group of assumptions is: the normalized relative error can be calculated as

$$\theta_i = \frac{S_i \cdot \tau_i}{y_i^e} \approx \frac{\sigma_i \cdot \tau'_i}{y_i^e} \approx \frac{\sigma_i \cdot \tau'_i}{y_i^{\text{TM}}}, \quad (15)$$

where y_i^e is etalon value of the parameter being measured, y_i^{TM} is actual measurement value with an error. The first equality sign of expression (15) means the assumption that the measuring

devices are assumed to be verified by a series of tests using a more accurate instrument normalized by reference values. The following sign of approximate equality shows the assumption that an infinite number of tests were performed during calibration. The second sign of approximate equality shows the assumption made in this paper that the reference value is approximately equal to telemetry.

Coordinate conversion to perform linear SE

When considering SE with SPM, it became possible to formulate the LSE task. In foreign publications [1–3] the following approach to LSE is considered. PMUs are assumed to provide real and imaginary values for currents and voltages. We assume that in the branch of power system connecting the nodes s and t , the node s has a PMU, which measures complex values of voltage of node s and current of $s-t$ branch. In this case, for this PMU, one can write a fragment of the objective function and the system of constraints (13):

$$\begin{aligned} \phi_{PMU}(Y) = & \alpha_{U_{sR}} \cdot (y_{U_{sR}} - y_{U_{sR}}^{TM})^2 + \alpha_{U_{sI}} \cdot (y_{U_{sI}} - y_{U_{sI}}^{TM})^2 + \alpha_{I_{sR}} \cdot (y_{I_{sR}} - y_{I_{sR}}^{TM})^2 + \alpha_{I_{sI}} \cdot (y_{I_{sI}} - y_{I_{sI}}^{TM})^2 \\ & \begin{cases} -g_{ss} \cdot U'_s + b_{ss} \cdot U''_s + g_{st} \cdot U'_t - b_{st} \cdot U''_t = I'_{st}, \\ -b_{ss} \cdot U'_s - g_{ss} \cdot U''_s + b_{st} \cdot U'_t + g_{st} \cdot U''_t = I''_{st}, \\ y_{U_{sR}} - U'_s = 0, \quad y_{U_{sI}} - U''_s = 0, \\ y_{I_{sR}} - I'_{st} = 0, \quad y_{I_{sI}} - I''_{st} = 0, \end{cases} \end{aligned} \quad (16)$$

where U'_s and U''_s are real and imaginary part of the node s voltage; U'_t and U''_t are real and imaginary part of the node t voltage; I'_{st} and I''_{st} are real and imaginary part of current, entering the node s from the branch $s-t$; g_{ss} and b_{ss} are real and imaginary part of intrinsic conductance of $s-t$ branch in the node s ; g_{st} and b_{st} are real and imaginary part of intrinsic conductance of $s-t$ branch in the node t ; $\alpha_{U_{sR}}$, $\alpha_{U_{sI}}$, $\alpha_{I_{sR}}$ and $\alpha_{I_{sI}}$ are measurements weights of real and imaginary parts of current and voltage, respectively.

A serious advantage of this approach is the ability to reformulate system (16) in terms of classical formulation of the problem of the method of least squares (1). If in the considered power system there is complete observability using only PMU, then this approach leads to solving systems of linear equations, which makes the SE task itself to be solved quickly, robustly and without using iterative methods.

However, an equally serious drawback of this approach is the uncertainty of measurements weights. From the point of view of the above approach of the maximum likelihood method (13), this way of formulating the objective function and the constraint system turns out to be incorrect, since SPM does not indicate the errors of the real and imaginary components of the vector dimensions, but one specifies relative errors of its modules and absolute errors of its angles.

We write the fragment of the objective function and the system of constraints (16) for the case when the measurements are modules and angles of complex parameters

$$\begin{aligned} \phi_{PMU}(Y) = & \alpha_V \cdot (y_V - y_V^{TM})^2 + \alpha_\delta \cdot (y_\delta - y_\delta^{TM})^2 + \alpha_I \cdot (y_I - y_I^{TM})^2 + \alpha_\psi \cdot (y_\psi - y_\psi^{TM})^2 \\ & \begin{cases} -g_{ss} \cdot V_s \cdot \cos(\delta_s) + b_{ss} \cdot V_s \cdot \sin(\delta_s) + g_{st} \cdot V_t \cdot \cos(\delta_t) - b_{st} \cdot V_t \cdot \sin(\delta_t) = I_{st} \cdot \cos(\psi_{st}), \\ -b_{ss} \cdot V_s \cdot \cos(\delta_s) - g_{ss} \cdot V_s \cdot \sin(\delta_s) + b_{st} \cdot V_t \cdot \cos(\delta_t) + g_{st} \cdot V_t \cdot \sin(\delta_t) = I_{st} \cdot \sin(\psi_{st}), \\ y_V - V_s = 0, \quad y_\delta - \delta_s = 0, \\ y_I - I_{st} = 0, \quad y_\psi - \psi_{st} = 0, \end{cases} \end{aligned} \quad (17)$$

where V_s and δ_s are module and angle of voltage of node s ; V_t and δ_t are module and angle

of voltage of node t ; I_{st} and ψ_{st} are module and angle of current, entering node s from branch $s-t$; α_V , α_δ , α_I and α_ψ are weights for voltage module, voltage angle, current module and current angle as a complex value.

The approach (17) described in [1], despite the correctness of formulation, has an important disadvantage compared to the approach (16), it assumes an iterative solution of a system of nonlinear equations, regardless of what type of measurement (SCADA or SPM) is used.

In order to combine the linearity of approach (16) and statistical correctness of approach (17), the formulation of the problem presented in (18) is proposed. It is important to note that in formulation (18) an assumption is made that is not crude, namely: it is assumed that the deviation of measurements of modules and angles of the complex values from their reference values turned out to be small values. This made it possible to rotate the coordinate system of the real and imaginary components of the complex parameters so that the actual components u'_s and i'_{st} correspond to the module measurements, and the imaginary components u''_s and i''_{st} correspond to the angle measurements multiplied by the module measurements

$$\phi_{PMU}(Y) = \alpha_V \cdot (y_V - y_V^{TM})^2 + \alpha_\delta \cdot (y_\delta - y_\delta^{TM})^2 + \alpha_I \cdot (y_I - y_I^{TM})^2 + \alpha_\psi \cdot (y_\psi - y_\psi^{TM})^2$$

$$\left\{ \begin{array}{l} -g_{ss} \cdot U'_s + b_{ss} \cdot U''_s + g_{st} \cdot U'_t - b_{st} \cdot U''_t = I'_{st}, \\ -b_{ss} \cdot U'_s - g_{ss} \cdot U''_s + b_{st} \cdot U'_t + g_{st} \cdot U''_t = I''_{st}, \\ y_V - u'_s = 0, \quad y_\delta - \frac{1}{y_V^{TM}} \cdot u''_s = 0, \\ u'_s = U'_s \cdot \cos(y_\delta^{TM}) - U''_s \cdot \sin(y_\delta^{TM}), \\ u''_s = U'_s \cdot \sin(y_\delta^{TM}) + U''_s \cdot \cos(y_\delta^{TM}), \\ y_I - i'_{st} = 0, \quad y_\psi - \frac{1}{y_I^{TM}} \cdot i''_{st} = 0, \\ i'_{st} = I'_{st} \cdot \cos(y_\psi^{TM}) - I''_{st} \cdot \sin(y_\psi^{TM}), \\ i''_{st} = I'_{st} \cdot \sin(y_\psi^{TM}) + I''_{st} \cdot \cos(y_\psi^{TM}). \end{array} \right. \quad (18)$$

Formulation (18), in conjunction with the maximum likelihood approach, allows one to perform the state evaluation, upon condition that the network is observable from the SPM point of view, as follows:

$$diag(Y^{TM})^{-1} \cdot A \cdot X = D, \quad (19)$$

where Y^{TM} is telemetry vector, A is information matrix, X is state parameters vector, D is vector, the elements of which are equal to one.

The essence of the method indicated in (19) consists in the complex estimation of state, where the complex values of measurements themselves are given as weights in equations. This gives grounds to call it as “a linear method of state estimation weighted by measurements” (Measurements Weighted Linear State Estimation), which we will abbreviate as “MWLSE”.

In [11], the SE method is shown, in which it is assumed that each measurement group has its own estimation procedure: linear for SPM measurements and non-linear for SCADA. The first one to be performed is linear SE on more accurate SPM measurements. This will be the first level of SE. The second performed is non-linear SE with fixing the results of the first SE level as constants. The test calculations performed for this method showed that a two-level SE leads to a significant increase in the computational speed, with a high accuracy of the obtained flow distribution.

The proposed MWLSE method allows one to more accurately perform the linear SE required for a two-level SE. Thanks to the choice of weighting factors specified in (19), the linear SE performed for the data from SPM becomes more accurate, which is critical for performing the second level of non-linear SE according to SCADA.

Computational experiment

We consider electrical network shown in Figure 1, where the etalon current distribution mode is shown in section a), etalon mode with indication of flow distribution is shown in b), and c) is an example of measurements with errors. It is assumed that PMUs are installed in nodes 1 and 3, which measure voltages at these nodes and currents in lines 1-2 and 2-3 from the PMU side.

For this network and for this composition of measurements, we will perform a linear SE using two methods. The first method involves formulation of the objective function according to the approach (16). Due to the fact that the choice of weighting factors used in (16) is not presented in the literature, in this example the coefficients were chosen in the same manner as described in [1], where this method is called “Linear State Estimation” (LSE). The result of such an SE is shown in Figure 2, where the resulting current distribution a) and flow distribution b) are labeled with a superscript “LSE”. The box shows the result of comparison of the calculated mode using SE with the reference mode in accordance with the criterion

$$S = \sum_{i=1}^L \left(\left(|\dot{S}_{in}^{LSE} - \dot{S}_{in}^e| \right)^2 + \left(|\dot{S}_{ik}^{LSE} - \dot{S}_{ik}^e| \right)^2 \right), \quad (20)$$

where L is amount of lines, and subscripts “s” and “f” correspond to start and finish of the line.

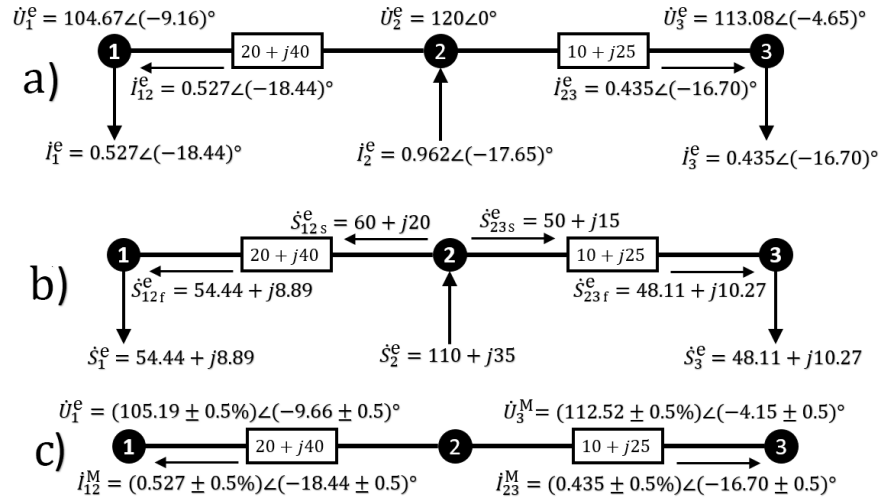


Fig. 1. An example of an electrical network of 110 kV for matching SE

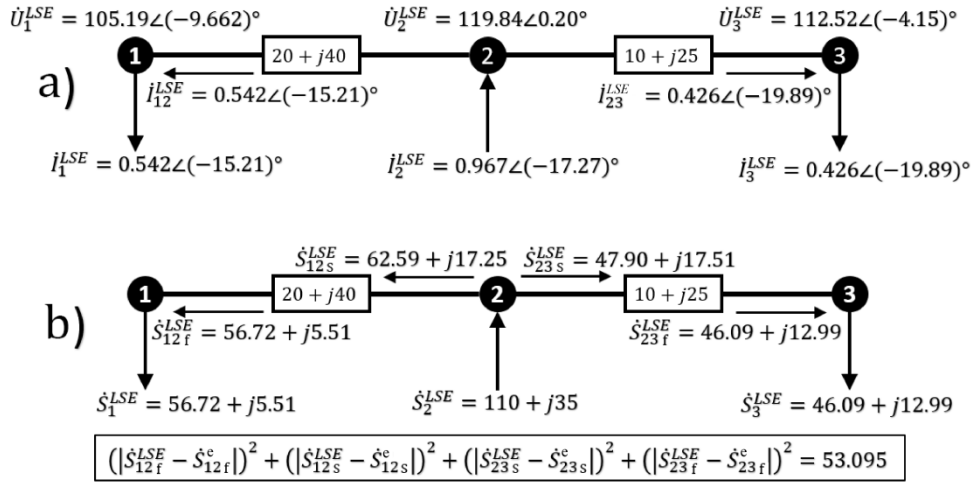


Fig. 2. The SE result for measurements shown in Figure 1, c) according to the first method

The specified criterion (20) shows the deviation measure of the estimated mode from etalon for lines power, which to the greater extent shows error in mode calculation when choosing control actions related to the change in flow distribution. As a result of calculation by the first method, the value of this criterion turned out to be 53.095.

As a second method, the proposed MWLSE method (19) was considered, which was tested on the same circuit and for the same measurements for the purpose of comparison with the first method. The calculation result is shown in Figure 3, where, also, the current distribution a) and flow distribution b), are marked with a superscript "LSE". For this method, the value of the criterion (20) turned out to be 0.826, which is almost two orders of magnitude less than that for the first method. As it can be seen from comparison of two final results from two SE methods, one can confidently judge the much higher accuracy of the MWLSE method.

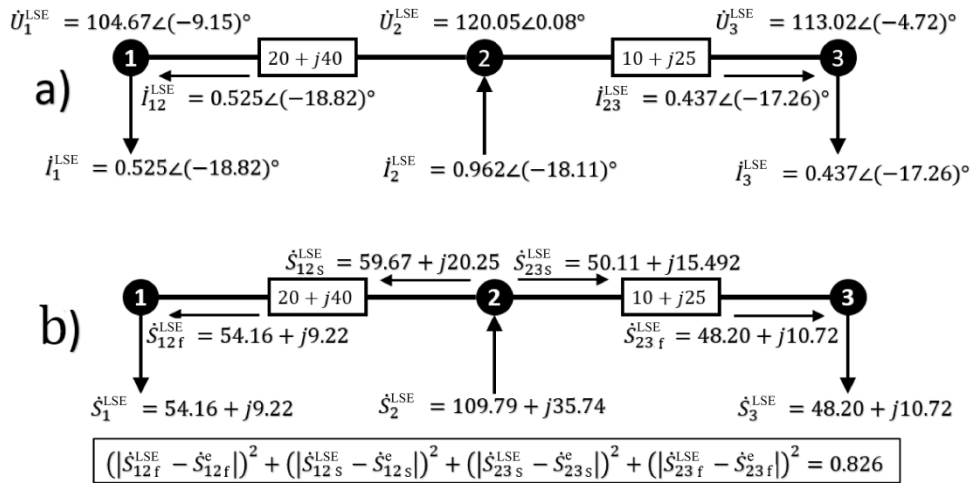


Fig. 3. SE result for measurements depicted in Figure 1 using the MWLSE method

For persuasiveness, the method has been tested on a number of IEEE test problems, namely, for IEEE-14, IEEE-RTS96, IEEE-30, IEEE-57, IEEE-118 networks. The test results

showed a higher accuracy of MWLSE, and the following was revealed. Firstly, it turned out that the accuracy of the proposed method in comparison with the LSE method is the higher, the higher the voltage class of the network under consideration is. Secondly, it was noticed that the comparative accuracy of the proposed method decreased with the weighting of mode, but still, it remained higher than for other methods.

Conclusions

As it is known, in EES for the state estimation by SCADA telemetry, the least-squares weighted method finds the greatest application. The SPM systems that have emerged in recent years have made it possible to move to an accelerated linear state estimate LSE. However, this method does not guarantee high accuracy of the final result.

The proposed state estimation method, called MWLSE, is intended for networks that are monitored using PMUs in the WAMS information support system. It is as robust and computationally fast as the linear state estimation method LSE used in foreign power systems, but it turned out to be much more accurate for all the cases considered.

References

1. Houghton DA, Heydt GT. A Linear State Estimation Formulation for Smart Distribution Systems. *IEEE Transactions on Power Systems*; May 2013. 28(2):1187-1195. <http://dx.doi.org/10.1109/TPWRS.2012.2212921>.
2. Zhang L, Bose A, Jampala A., et al. Design, Testing, and Implementation of a Linear State Estimator in a Real Power System. *IEEE Transactions on Smart Grid*; July 2017. 8(4):1782-1789. DOI: 10.1109/TSG.2015.2508283.
3. Ghiocel SG., Stefopoulos G, Chow JH., et al. Phasor-Measurement-Based State Estimation for Synchrophasor Data Quality Improvement and Power Transfer Interface Monitoring. *IEEE Transactions on Power Systems*; March 2014; 29, (2):881-888. DOI: 10.1109/TPWRS.2013.2284098.
4. Khokhlov MV. Robastnoe ocenivanie sostoyaniya elektroenergeticheskikh sistem na osnove nekvadraticnykh kriteriev [dissertation]. Yekaterinburg; 2010. Available at: <http://elar.urfu.ru/handle/10995/19860>. Accessed: 25 Feb 2019. (In Russ).
5. Maksimenko DM, Mashalov EV, Neuimin VG. Ocenivanie sostoyaniya na baze optimizacionnogo algoritma v PK RastrWin3. *Izvestiya NTC Edinoj energeticheskoy sistemy*. 2013; 2(69):36-44. (In Russ).
6. Gamm AZ. *Statisticheskie metody ocenivaniya sostoyaniya elektroenergeticheskikh system*. Moscow: Nauka, 1976. (In Russ).
7. Schweppe FC, Wildes J. Power system static state estimation. Part 1: exact model. *IEEE Transactions On Power Systems*. 1970; 1:120-125.
8. Prikhno VL, Chernenko PA. *Operativnyj raschet rezhima energosistemy po dannym telezmerenij*. Irkutsk: SEI SB AS USSR, 1982. (In Russ).

Литература

1. Houghton D.A., Heydt G.T. A Linear State Estimation Formulation for Smart Distribution Systems // *IEEE Transactions on Power Systems*; May 2013. Vol. 28, iss. 2. pp. 1187-1195.
2. Zhang L, Bose A, Jampala A., et al. Design, Testing, and Implementation of a Linear State Estimator in a Real Power System // *IEEE Transactions on Smart Grid*; July 2017. Vol. 8, iss. 4. pp. 1782-1789.
3. Ghiocel S.G. et al. Phasor-Measurement-Based State Estimation for Synchrophasor Data Quality Improvement and Power Transfer Interface Monitoring // *IEEE Transactions on Power Systems*; March 2014. Vol. 29, iss. 2. pp. 881-888.
4. Хохлов М.В. Робастное оценивание состояния электроэнергетических систем на основе неквадратичных критериев: Дис. ... канд. техн. наук. Екатеринбург; 2010. Доступно по: <http://elar.urfu.ru/handle/10995/19860>. Ссылка активна на 25 февраля 2019.
5. Максименко Д.М., Машалов Е.В., Неймин В.Г. Оценивание состояния на базе оптимизационного алгоритма в ПК RastrWin3 // *Известия НТЦ Единой энергетической системы*. 2013. №2(69). С. 36-44.
6. Гамм А.З. Статистические методы оценивания состояния электроэнергетических систем. М.: Наука, 1976. 220 с.
7. Schweppe F.C., Wildes J. Power system static state estimation. Part 1: exact model // *IEEE Transactions On Power Systems*. 1970. №1. pp. 120-125.
8. Прихно В.Л., Черненко П.А. Оперативный расчет режима энергосистемы по данным телеизмерений. Иркутск: СЭИ СО АН СССР, 1982. С.70-75.

9. Nikulin MS.; Vinogradov IM., ch. editors. Likelihood Relations Criterion. *Mathematical Encyclopedia*. Moscow: Soviet Encyclopedia, 1984; 4: 151-1216. (In Russ).

10. GOST R 8.000-2015. Gosudarstvennaya sistema obespecheniya edinstva izmerenij (GSI).

11. Bartolomey P.I., Semenenko S.I. Power Systems State Estimation Acceleration on the Basis of the Synchronized Phasor Measurements in the Power System Steady State Control Tasks. *International Youth Scientific and Technical Conference Relay Protection and Automation (RPA); 27-28 Sep 2018; Moscow, Russia*. Moscow; 2018. pp. 1-10.

9. Никулин М.С. Отношения правдоподобия критерий // Математическая энциклопедия / Виноградов И. М. (гл. ред.). М.: Советская энциклопедия, 1984. Т. 4. С.151-1216.

10. ГОСТ Р 8.000-2015. Государственная система обеспечения единства измерений (ГСИ). Основные положения.

11. Bartolomey P.I., Semenenko S.I. Power Systems State Estimation Acceleration on the Basis of the Synchronized Phasor Measurements in the Power System Steady State Control Tasks // International Youth Scientific and Technical Conference Relay Protection and Automation (RPA); 27-28 September 2018; Moscow, Russia. Moscow, 2018. pp. 1-10.

Authors of the publication

Petr I. Bartolomey – doctor of sciences (techn.), full professor, Department “Automated Electrical Systems”, Ural Federal University.

Sergey S. Semenenko – senior lecturer, Department “Automated Electrical Systems”, Ural Federal University.

Received

January, 09 2019



ASSESSMENT OF EFFICIENCY INDICATORS OF THE STEAM-TURBINE MINI-THERMAL POWER PLANTS BURNING COAL

D.T. Nguyen, D.N. Fam, G.R. Mingaleeva

Kazan State Power Engineering University, Kazan, Russia

mingaleeva-gr@mail.ru

Abstract: We present results of calculations of main units of steam-turbine mini-thermal power plants of low power (6, 11.4, 12, 20 and 25 MW), intended for operation in autonomous mode. Basing on material, thermal and exergy balances we defined efficiency indicators: exergy efficiency and specific fuel expenses. The units of 6, 20 and 25 MW have the highest exergy efficiency at the level of 33 %. This fact testifies to a possibility of efficient combination of boiler and turbine equipment of this power as well as integration of technological schemes of mini-thermal power plants on the basis of drying and mill equipment, steam boilers and turbines of low power.

Keywords: mini-thermal power plant, fuel preparation, steam boilers, steam turbines.

Acknowledgments: This work was supported by the project No. 17-08-00295 "A" from the Russian Foundation for Basic Research.

For citation: Nguyen D.T., Fam D.N., Mingaleeva G.R. Assessment of indicators of efficiency of the steam-turbine mini-thermal power plants burning coal. *Proceedings of the higher educational institutions. ENERGY SECTOR PROBLEMS*. 2019; 21(3-4):79-89. (In Russ). doi:10.30724/1998-9903-2019-21-3-4-79-89

Introduction

According to the expert estimates, the share of energy costs in the cost of production of various industries ranges from 3 to 55 %, which basically exceeds the world level in the relevant industries. The highest share of fuel and energy costs is observed in the refining industry - up to 54,7 %. In addition, the dynamics of growth in tariffs for heat and electricity exceeds the growth rate of prices for products, which contributes to an increase in the share of expenditures on energy resources [1]. Construction of a personal source for production of electrical and thermal energy, i.e. a small thermal power plant (mini-TPP), will help to achieve stabilization of costs for this item of expenditure.

Mini-TPPs can be used in remote and underdeveloped regions that are far from centralized power supply (approximately 50–70 % of the Russia territory), in order to meet own needs of certain facilities - residential or industrial, as well as in the event of an emergency.

The relevance of development of small distributed power engineering is also associated with economic recovery in the areas of centralized power supply and, accordingly, with difficulties in operational connection or lack of technological capabilities to connect to power grids.

Nowadays the fuel and energy balance of Russia is significantly shifted to the use of natural gas, whose share in production of heat and electricity exceeds 70 %. Along with the well-known and indisputable advantages of this type of fuel compared to others, this situation poses a real threat to the country's energy security [2]. The main type of fuel for the European part of Russia and the Ural regions, where more than 82 % of the population lives, is natural gas. It is known that

the supplied fuel is produced mainly in one gas producing region of the Tyumen region and is transported over a distance of more than 2 thousand km. The existing gas transmission system has a complex and extensive structure and “bottlenecks”, the accidental or intentional damage of which can cause enormous damage to the economy of the country. In addition, the gas transmission system itself, the basis of which was formed during the existence of the Soviet Union, is significantly worn out [3]. It is noted that more than 70 thousand km (42 % of the total length) of gas pipelines have been in operation for more than 30 years and require reconstruction. A similar situation occurred with compressor stations.

Under such conditions, the new energy facilities being commissioned should be diversified to the maximum extent by the type of fuel used, and small distributed energy facilities should be oriented by local, cheaper fuel in order to be competitive at the cost price of the energy produced. The development of small distributed generation is evidenced by the fact that at present, despite the reforms in the energy sector, competition remains extremely weak and the consumer, even quite large, does not have a choice of supplier of heat and electricity. The available analytical estimates confirm that the cost of centralized power supply is compared with the price of its own generation [4]. At the same time, distributed sources of energy supply can already constitute a significant competition in the energy market and contribute to the establishment of lower prices.

At present, the share of small autonomous energy in Russia is estimated for about 5–7 %, mainly these are diesel power plants with a unit capacity of 340 kW and a total of 17 million kW, producing up to 50 billion kWh and consuming about 17 million tons of fuel equivalent per year [5].

World experience shows that the share of small autonomous energy in the production of electrical energy can be at least 2 times higher, as it is in industrialized countries, where this trend is supported by law. In the UK, for example, part of taxes is returned to owners of environmentally “clean” mini-power plants, in Germany there are benefits and compensations for owners of power plants, and centralized networks receive surplus energy from them at favorable rates. Owners of autonomous energy sources are also exempt from taxes in some US states, they are also compensated for a part of capital expenditures [6, 7]. Thus, in many countries whose governments are interested in developing healthy competition in the energy market, the development of small autonomous energy is ensured by legislative and organizational measures.

At the federal level, in the perspective until 2030, it is planned to significantly increase the share of coal and other solid fuels in production of heat and electricity, since its explored reserves are huge and amount to 193,3 billion tons (of which brown coal is 101,2, coal is 85,3 and anthracite is 6,8 billion tons), which provides the Russian economy with this type of fuel for 550 years [8].

Currently, mini-TPPs actually exist and, although they are designed and built for specific operating conditions, some typical schemes can be identified and classified according to the main equipment: steam boilers with steam turbines, gas turbines with waste-heat boilers and diesel generators [5]. Solid fuel (coal, peat, industrial carbon-containing waste) in these schemes can be burned in the furnaces of steam boilers or processed into energy gas, which is then burned in furnaces of gas boilers or combustion chambers of gas turbines. Equipment for thermal processing of solid fuels – gas generators and pyrolysers – is not yet commercially available. Therefore, introduction of technologies of small distributed autonomous generation, using coal and other types of solid organic fuel, is advisable to start from traditional for Russian energy schemes with steam turbine plants.

Main part

Further we consider the technological scheme of a steam turbine mini-TPP, shown in Fig. 1 [9].

The fuel (Kuznetsky lean coal) in a pulverized state enters the burners of a steam boiler, which is equipped by a two-stage steam superheater, which is designed to prepare steam with the required parameters for a steam turbine. Two stages of economizer and air heater are interstaged into the boiler backpass. In addition, to control the steam temperature before the second stage, a

surface steam cooler is installed, to which feed water flows after the first stage of economizer. Feed water and condensate are heated in heaters of low (LPH) and high (HPH) pressure. Network water is heated by steam from a turbine extractor in the main boiler. In peak mode, hot steam from a reduction and cooling unit (RCU) is used to heat the network water.

The algorithm for calculation this scheme assumes the sequence of actions shown in Fig. 2

Kuznetsk coal (T grade) is used as fuel. At the first stage, a steam turbine is selected that corresponds to the required power, which is determined taking into account the redundancy of the units. According to the flow rate and parameters of steam which must be supplied to the turbine, a steam boiler operating on solid fuel is selected. The quality characteristics of the coal used as fuel determine the type and composition of the dust preparation system. Calculation of this block is the most time-consuming, so here it is given in details. Key performance indicators are calculated based on provisions of exergy analysis, which allows one to compare multi-purpose objects, for example, producing heat and electricity, as well as by-products [10, 11].

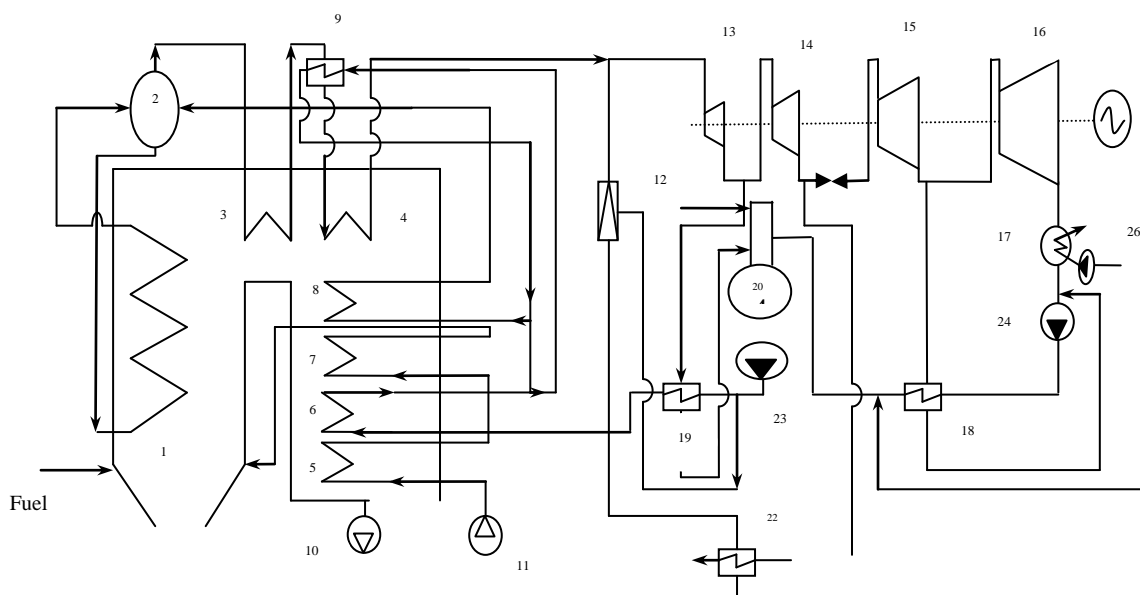


Fig. 1. Technological scheme of a steam turbine mini-TPP: 1 – Furnace; 2 – Boiler drum; 3, 4 – The first and second stages of steam superheater, respectively; 5, 7 – The first and second stages of air heater; 6, 8 – The first and second stages of water economizer; 9 – Steam cooler; 10 – Smoke pumps; 11 – Blower fan; 12 – CU; 13, 14, 15, 16 – Turbine compartments; 17 – Turbine condenser; 18 – PND; 19 – LDPE; 20 – Deaerator; 21 – Mains heater; 22 – Peak heater; 23 – Feed pump; 24, 25 – Condensate pumps; 26 – Circulation pump; 27 – Network pump

The steam turbine was selected according to the required power and in conjunction with the parameters of steam produced in the steam boiler. The existing range of low-power steam turbines (up to 25 MW) is not very diverse. These turbines are manufactured by the Kaluga Turbine Plant.

The calculation of steam boiler during combustion of Kuznetsk coal (grade T) was carried out in accordance with the regulatory method [12]. For drying and coal pulverizing from typical

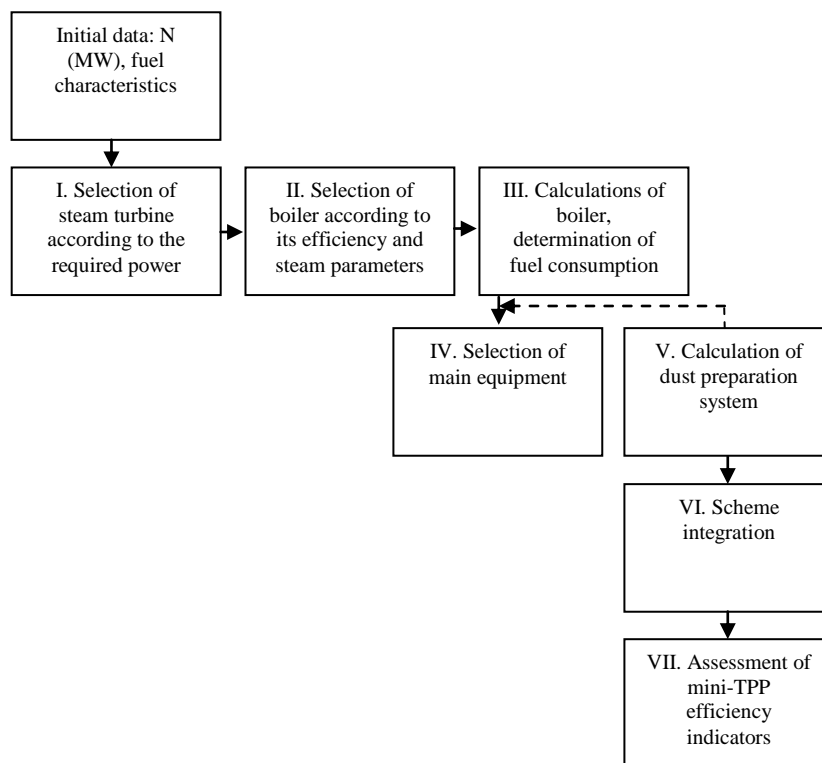


Fig. 2. The algorithm for calculating the technological scheme of the steam turbine mini-TPP

schemes we have chosen the most compact closed individual system with direct injection of coal dust into the boiler furnace and air drying under pressure. For this system we determined the flow rate of the drying agent (air). In such systems, three types of grinding mills can be used: ball drum (BDM), hammer (HM) and mid-roll (MRM). From the existing size range, only ball drum and hammer mills are suitable for mini-TPP.

The heat balance of this type of system is written as follows (all components are indicated in kJ per 1 kg of raw fuel):

$$q_1 + q_{meh} - q_{evap} - q_2 - q_h - q_5 = 0. \quad (1)$$

where q_1 , q_2 is heat of drying agent at the inlet to mill and at the outlet from it, respectively; q_{meh} is heat released from grinding bodies of mill; q_{evap} is heat consumed for fuel moisture evaporation; q_h is sensible heat of fuel; q_5 is heat losses to the outside environment through the equipment walls.

Since the system operates under pressure, the component associated with the external air intakes into the system is not taken into account. The calculation of the heat balance components is as follows.

First, we set the temperature of drying agent at the mill inlet. When the fuel is dried with hot air, the upper limit of initial temperature of the drying agent is determined by 10 °C below the air temperature behind the air preheater based on data from [13].

Then we determine the amount of heat released as a result of mill grinding bodies operation q_{meh} . During calculation of q_{meh} we determine the energy costs of grinding. At this, the type of mill is taken into account. If BDM is installed in the system of this type, then the specific energy consumption for grinding, kWh/t, is determined by the formula

$$E_{gr} = \frac{N_n + N_{add}}{B}, \quad (2)$$

where N_n is power consumed by electric motor from the network, kW, and it equals to:

$$N_n = \frac{N_{v.l.}}{e_{em}}, \quad (3)$$

e_{em} is electric motor efficiency, which is in the range 0,92–0,94; N_{add} is additional power consumed for cooling and exciting of motor, for drive of oil pumps and some other needs, kW (for synchronous motors $N_{add} \approx 50$ kW, for high-speed asynchronous motors $N_{add} \approx 15$ kW).

In expression (2) B is grinding efficiency of mill determined by the formula

$$B = K_n K_{ven} a \varphi^{0,8} \Psi_d^{0,6} V_d, \quad (4)$$

Where $K_n = K_{arm} K_{ek}$ is coefficient equal to a product of the following values: K_{arm} is armor form factor equal to 1,0 for unworn wavy armor; K_{ek} is coefficient taking into account the decrease in the performance of mill during operation (assumed to be 0,9); K_{ven} is coefficient taking into account the influence of drum ventilation on the mill performance, its value is determined using graphs based on the results of industrial operation of systems [14]; a is auxiliary value, depending on fuel properties and the resulting dust; Ψ_d is degree of drum filling with balls; V_d is internal volume of the mill drum. All components in the formula (4) are determined according to the relationships presented in [14].

When determining the ventilation coefficient K_{ven} for ventilated BDM, the optimal flow rate of drying agent through the mill is calculated taking into account the grinding conditions, , according to the following relationship, m³/h:

$$V_{MVopt} = \frac{0,9V_d}{\varphi} \left(1000 \sqrt[3]{K_{lo}} + 36R_{90} \sqrt{K_{lo}} \sqrt[3]{\Psi_d} \right) \quad (5)$$

where φ is dimensionless value, which characterizes drum rotation frequency [14]; K_{lo} is grinding form factor; R_{90} is share of particles, remaining at the sieve with particle dimensions of 90 μm.

The mill fan is selected in such a way that its performance is close to V_{MVopt} , i.e. $K_{ven} \approx 1,0$.

In (3) the power consumed by drum rotation (MW), reduced to the motor shaft, is calculated from

$$N_{v.d} = \frac{1}{\eta_{dr}} \left(0,122 D_d^3 L_d n_d \rho_{db} \Psi_d^{0,9} K_{br} K_{tl} + 1,86 D_d L_d n_d S_d \right), \quad (6)$$

where η_{dr} is drive efficiency without taking into account the electric motor efficiency (for gear-driven mills and gearbox $\eta_{dr} = 0,865$, for friction-driven mills and gearboxes, as well as for gearless gears without gearbox $\eta_{dr} = 0,885$, for mills with friction drive without gearbox = 0,905); $\rho_{db} = 0,4,9$ t/m³ is bulk density of the balls; K_{tl} is coefficient, which takes into account the properties of the grinding fuel; it can be determined from the reference data [14], depending on the fuel type and degree of drum filling with balls; L_d is drum internal length, m; n_d is drum rotation frequency, rpm; S_d drum wall thickness, including armor (along the midline of waves), m.

While determining heat consumption for fuel heating q_h , the temperature t_2 behind the mill is determined from the reference data depending on the criterion of fuel explosiveness K_f [14].

When a hammer mill (HM) is installed into the system, the energy costs for fuel grinding are determined by the formula

$$E = \frac{N}{B} = \frac{N_i N_{i,r.}}{B}, \quad (7)$$

Where relative power N_i is determined from

$$N_i = N_{i0} k_{ab} k_{kon}, \quad (8)$$

where N_{i0} is relative power, which depends on the rotor speed and the type of separator, is selected according to the reference data [14, 16] (deviation of N_{i0} from the values determined by the schedule is allowed within 15 %); k_{ab}, k_{kon} are operational factors [14].

In (7) $N_{i,r.}$ is idle run power (9 kW), which is determined from:

$$N_{i,r.} = 7 \cdot 10^{-5} u^3 D L \beta c_b \sqrt{m_D} \quad (9)$$

where D is rotor diameter; c_b is coefficient, which takes into account the grinding chamber construction (for mills with open grinding chamber $c_b = 1$, for mills with closed grinding chamber with rotor closing angle of at least 260° $c_b = 0,6$); L is rotor length, m; m_D is the number of hits on a circle, pcs; β is coefficient, which takes into account the relative height of beater:

$$\beta = 1 - 0,7 \left(1 - \frac{2h}{D} \right)^4, \quad (10)$$

where h is total beater height, including lugs, m.

The performance of hammer mills with centrifugal and inertial separators is determined by the formula [14], t/h:

$$B = c \cdot 10^{-5} u^3 L m_D^{0,25} (1,43 N_i - 1)^{0,7} P_f P_v K_{ex} K_{cl}, \quad (11)$$

where B is capacity, t/h; c is coefficient, which takes into account the influence of separator design on mill operation (for mills with inertial separator $c = 1,5$, for mills with centrifugal separator $c = 1,4$); u is circumferential rotor speed, m/s; L is rotor length, m; m_D is amount of beaters on a circle, pieces; N_i is relative mill power; P_f is coefficient, which takes into account the influence of fuel physical properties and dust particle size on mill performance; P_v is coefficient taking into account the influence of ventilation on mill performance; K_{ex} is coefficient taking into account the decrease in mills performance in operating conditions due to wear and tear (usually $K_{ex} = 0,85$); K_{cl} is coefficient taking into account the influence of rotor degree of closure (for open-rotor mills $K_{cl} = 1$, for closed-rotor mills $K_{cl} = 0,7$).

For thermal calculation of coal-preparation plant, one takes into account only relationship between dust humidity, temperature of drying agent at the end of installation and initial moisture fuel. Such connection is detected separately for conditions of fuel drying with a mixture of flue gases with air and for fuel drying by hot air. When conducting a thermal calculation of the dust system, the dust humidity is taken according to combustion conditions in boiler, and the temperature at the end of the installation is selected according to the graphs [14].

After thermal calculation, the accepted value of t_2 must be consistent with the relative humidity of drying agent leaving the installation. In all cases, the agent temperature t_2 must be higher than the dew point temperature of water vapor. If the adopted temperature t_2 does not satisfy the specified conditions, then the thermal calculation is repeated, the amount of the drying agent increases, or its initial temperature decreases.

At known temperatures at the inlet to the installation and at the outlet from it, according to the reference data, the heat capacity of dry air (at the inlet) and moist (at the outlet) are determined [14, 16].

A preliminary calculation of drying agent flow rate at the intake to the installation is carried out. Then, the moisture content of the drying agent at the outlet of the installation, calculated to 1 kg of dry gas, is calculated. The weight and volume amount of wet drying agent at the end of installation is determined when drying with hot air.

After the calculations, it is necessary to verify the obtained value of the drying capacity of the mill, t/h , according to the formula

$$B_s = \frac{V_2}{1000V_{wet}}, \quad (12)$$

Where V_{wet} is amount of wet air, m^3/kg ; V_2 is amount of wet drying agent at the end of installation, m^3/h , which is calculated depending on the designed mill capacity B_{design} :

$$V_2 = 1000V_{wet}B_{design}. \quad (13)$$

The drying capacity must be higher or equal to the designed one, i.e. $B_s \geq B_{design}$. If the available V_2 (for example, the capacity of a mill fan or a fan mill) is less than that obtained from (13), then it is necessary to increase the value adopted earlier or to increase the temperature of the drying agent t_1 . In the absence of this capability, the plant capacity will be limited by the drying conditions.

The capacity of the mill fan V_{MF} , m^3/h , installed in front of the pressure mill, is determined by the formula:

$$V_{MF} = \frac{1000g_1B_{design}}{\rho_{0air}} \cdot \frac{273+t}{273}, \quad (14)$$

where t is air temperature before fan, °C; g_1 is air consumption at the inlet to installation, kg/kg of wet coal; ρ_{0air} is air density, kg/nm^3 .

The design capacity for selection of mill fan is taken with a margin of 5 %. According to the technical characteristics of the selected fan is determined by the pressure created by it in the system.

On the basis of the obtained calculated data on the energy and material flows entering into each element of the installation and leaving it, their exergy, exergy efficiency of individual units and the whole technological scheme were determined.

The exergy method is the most common method of thermodynamic study of various energy conversion processes. It allows one to visually determine the degree of perfection and sources of losses in installations and find ways to improve them.

This method is widely used in studies of systems operating on the principle of combined generation of heat and electrical energy [10, 11], however, it is extremely rare applied to small-scale energy facilities operating on solid fuels.

The most important components of exergy are physical and chemical, and in the whole they give thermal exergy E_t . Physical exergy E is the result of a mismatch between temperature and pressure of the considered substance and that of the environment. Exergy, arising from the difference in compositions, is chemical exergy E_{ch} . Chemical exergy of coal can be determined in various ways [17]. In this work, the specific chemical exergy of coal e_{ch} , kJ/kg, is determined by the ratio proposed by V.S. Stepanov [18]:

$$e_{ch} = \left[1,009 + \frac{0,131O + 0,116W}{100 - (A + W)} \right] Q_i^P, \quad (15)$$

where O is oxygen content in coal in terms of work mass, %; W and A is humidity and ash-content in terms of work mass, %; Q_l^p is low calorific value of coal, kJ/kg.

The main process in coal pulverization systems is drying combined with grinding in coal-grinding mills. All components of exergy balance of drying and grinding processes can be determined by the known dependencies (J/s or W) [5], exergy efficiency $\eta_{s.m.}$ is calculated by the formula:

$$\eta_{s.m.} = \frac{E''_{coal} + E_{evap} + E''_{dr.a.}}{E'_{dr.a.} + \sum_{i=1}^n L_i + E'_{coal} + E_{meh}}, \quad (16)$$

where L_i is electric power spent on equipment for drying and grinding; n is amount of devices having an electric drive; E_{evap} is exergy, spent on evaporation of moisture from coal; $E'_{dr.a.}$, $E''_{dr.a.}$ is exergy of the drying agent at the inlet and at the exit of the mill, E'_{coal} , E''_{coal} is exergy of coal entering the mill, and ground coal, E_{meh} is exergy of heat released during grinding of coal.

The exergy efficiency of the steam boiler is calculated using the expression:

$$\eta_{s.b.} = \frac{E''_s}{E'_{p.c.} + E''_{f.w.}}, \quad (17)$$

$E''_{f.w.}$ is exergy of feed water, supplied to waste heat recovery boiler; E''_s is exergy of steam, produced in waste heat recovery boiler; $E'_{p.c.}$ is exergy of combustion products, supplied to waste heat recovery boiler.

Exergy efficiency of steam turbine is determined as follows:

$$\eta_{s.t.} = \frac{N_e + E''_{s.t.}}{E''_s + \sum_{i=1}^m L_i}. \quad (18)$$

N_e is electric power generated by steam turbine generator; $E''_{s.t.}$ is exergy of steam sent for heat; E''_s is exergy of steam supplied to the steam turbine from waste heat recovery boiler; L_i is electric power spent for auxiliary equipment; m is amount of auxiliary equipment units of a steam turbine having an electric drive.

For a more complete assessment of efficiency of a mini-TPP operating on solid fuel and generating heat and electricity, the exergy efficiency of a steam turbine mini-TPP is used, which does not include internal flows of a steam turbine plant:

$$\eta_{miniTPP} = \frac{N_e + E''_{s.t.}}{E'_{coal} + \sum_{i=1}^k L_i + E'_v + E'_{f.w.} + E_{meh}}, \quad (19)$$

where k is the total number of auxiliary equipment units of mini-TPP, having an electric drive. The remaining designations in formula (19) are the same as in formulas (16)–(18).

Results and discussion

The selection of equipment was carried out on the basis of well-known methods for calculating and designing fuel preparation systems, boiler plants and steam turbines, the chosen brands for boilers, steam turbines and mills are presented in Table. 1. Analysis of the presented results shows that efficiency of waste-heat recovery boilers of various capacities in the steam

generation range from 25 to 90 t/h is approximately at the level of 48 %, with the exception of the KE 25-14-225C boiler, which has lower rates. Exergy efficiency of low-power steam turbines differ significantly. The highest value corresponds to the turbine P-6-1.2 / 0.5 of 6 MW capacity. Turbines of 11 and 12 MW capacities have lower exergy efficiency – 44,5 and 46,9%, respectively. Also, low efficiency possess the HMT 1300/2300/735 and BDM 250/390 coal mills, which are selected for mini TPP with capacities of 12 and 20 MW, respectively.

Exergy efficiency of mini-TPP and specific coal consumption are considered as performance indicators, the results are presented in Table. 2

Table 1

Main equipment for steam-turbine mini-TPP

№	Electrical capacity of mini TPP, MW	Waste heat recovery boiler	Exergy efficiency of boiler, $\eta_{s,b}$, %	Steam turbine	Exergy efficiency of turbine $\eta_{s,t}$, %	Coal grinding mill	Exergy efficiency of drying-mill unit, $\eta_{d,m}$, %
1	6	KE 25-14-225C	42,1	П-6-1.2/0.5	79,7	HMT 1000/710/980	27,88
2	11,4	E 65-3.9-440 KT	48,2	К 11-1. (KTZ)	44,5	BDM 220/330	27,07
3	12	KE 65-3.9-440 KT	48,2	К 12-4.2	46,9	HMT 1300/2300/735	24,74
4	20	E 75-3.9-440 KT	48,3	STU-20	67,5	BDM 250/390	24,26
5	25	E 90-3.9-440 KT	47,7	STU-30	70,4	HMT 1300/2030/735	28,68

Table 2

Performance indicators of mini-TPP

№	Electrical capacity of mini TPP, MW	Coal consumption, kg/s	Exergy efficiency of mini-TPP, %	Specific coal consumption, g/MW
1	6	0,757	33,6	126
2	11,4	2,25	21,3	197
3	12	2,246	22,4	187
4	20	2,6	32,3	130
5	25	3,112	33,7	124

Conclusions

The units of 6, 20 and 25 MW have the highest exergy efficiency at the level of 33 %, which indicates the possibility of effectively combining the boiler and turbine equipment of this capacity, as well as completing the technological mini-TPP schemes based on the corresponding drying and mill plants, steam boilers and turbines of small power.

References

- Ivanov VA. Analiz energozatrat v razlichnyh otraslyah promyshlennosti [Internet]. *Naukovedenie*. 2015; 7(1):1-18. Available at: <http://naukovedenie.ru/PDF/144TVN115.pdf>. Accessed: 01 Mar 2018. (In Russ).
- Senderov SM, Rabchuk VI, Edelev AV. Osobennosti formirovaniya perechnya kriticheski vazhnyh ob"ektov gazotransportnoj seti Rossii s uchetom trebovanij

Литература

- Иванов В.А. Анализ энергозатрат в различных отраслях промышленности [Электронный ресурс] // *Науковедение*. 2015. Т.7, №1. С.1-18.. Доступно по: [http://naukovedenie.ru/PDF/144TVN115 .pdf](http://naukovedenie.ru/PDF/144TVN115.pdf). Ссылка активна на 01 марта 2018.
- Сендеров С.М., Рабчук В.И., Еделев А.В. Особенности формирования перечня критически

energeticheskoj bezopasnosti i vozmozhnye mery minimizacii negativnyh posledstvij ot chrezvychajnyh situacij na takih ob'ektah. *Proceedings of the Russian Academy of Sciences. Power Engineering*. 2016; 1:70-78. (In Russ).

3. Sukharev MG, Kulik VS. Vliyanie nedostovernosti informacii pri planirovanii rezhimov sistem gazosnabzheniya i prinyatii reshenij po ih razvitiyu. *Proceedings of the Russian Academy of Sciences. Power Engineering*. 2015; 4:69-83. (In Russ).

4. Veselov FV, Solyanik AI. Sostoyanie i perspektivy investicionnoj deyatel'nosti v postreformennoj elektroenergetike. *Proceedings of the Russian Academy of Sciences. Power Engineering*. 2015; 1:105-83. (In Russ).

5. Afanasyeva OV, Mingaleeva GR. *Modeling of technological schemes of mini-thermal power plant*. Moscow: MPEI publishing house, 2014. (In Russ).

6. Kotler VR. Mini cogeneration stations: Foreign experience. *Thermal Engineering*. 2006; 53(8):659-662.

7. Ghioca L, Panait L, Pressel S, et al. Conditii tehnice si economice de rentabilizare a unor centrale termice si de termoficare, mici, din cadtul RENEL. *Energetica*. A. 1993; 41(5):214-223.

8. Energeticheskaya strategiya Rossii na period do 2030 [Internet]. Available at: <https://minenergo.gov.ru/node/1026>. Accessed: 03 Nov 2017. (In Russ).

9. Kler AM, Marinchenko AYu, Sushko SN. Optimization of steam-turbine power unit of a coal mini-HPP with variable schedule of heat and electric energy loads. *Thermophysics and Aeromechanics*. 2006; 2:283-293.

10. Gao L, Jin H, Liu Z. Exergy analysis of coal-based polygeneration system for power and chemical production. *Energy*. Elsevier, 2004; 29(12):2359-237. DOI: 10.1016/j.energy.2004.03.046.

11. Ghosh S, De S. Energy analysis of a cogeneration plant using coal gasification and solid oxide fuel cell. *Energy*. Elsevier. 2006; 31(2):345-363. DOI: 10.1016/j.energy.2005.01.011.

12. Kuznecov NV., editor. *Teplovoj raschet kotel'nyh agregatov. Normativnyj metod*. Moscow: EKOLIT, 2011. (In Russ).

13. Lipov YuM., et al. *Komponovka i teplovoj raschet parovogo kotla*. Moscow: Energoatomizdat, 1988. (In Russ).

14. Nazmeev YuG, Mingaleeva GR. *Sistemy toplivopodachi i pyleprigotovleniya TES*. Moscow: MEPI publishing house, 2005. (In Russ).

15. RD 153-34.1-03.352-99. *Pravila vzryvo-bezopasnosti toplivopodachi i ustanovok dlya prigotovleniya i szhiganiya pylevidnogo topliva*. Moscow:

важных объектов газотранспортной сети России с учетом требований энергетической безопасности и возможные меры минимизации негативных последствий от чрезвычайных ситуаций на таких объектах // Известия академии наук. Энергетика. 2016. №1. С.70-78.

3. Сухарев М.Г., Кулик В.С. Влияние недостоверности информации при планировании режимов систем газоснабжения и принятии решений по их развитию // Известия академии наук. Энергетика. 2015. №4. С.69-83.

4. Веселов Ф.В., Соляник А.И. Состояние и перспективы инвестиционной деятельности в постреформенной электроэнергетике // Известия академии наук. Энергетика. 2015. №1. С.105-83.

5.Афанасьева О.В., Мингалева Г.Р. Моделирование технологических схем мини-ТЭС. М.: Издательский дом МЭИ, 2014. 220 с.

6. Котлер В.Р. Мини-ТЭЦ: зарубежный опыт // Теплоэнергетика. 2006. № 8. С. 69-71.

7. Ghioca L., Panait L., Pressel S., et al. Conditii tehnice si economice de rentabilizare a unor centrale termice si de termoficare, mici, din cadtul RENEL // Energetica. A. 1993. Vol. 41. No 5. P. 214-223.

8. Энергетическая стратегия России на период до 2030 [Электронный ресурс]. Доступно по: <https://minenergo.gov.ru/node/1026>. Ссылка активна на 03 ноября 2017.

9. Клер А.М., Маринченко А.Ю., Сушко С.Н. Оптимизация паротурбинного энергоблока угольной мини-ТЭЦ с учетом переменных графиков тепловых и электрических нагрузок // Теплофизика и аэромеханика. 2006. №2. С. 303-314.

10. Gao L., Jin H., Liu Z. Exergy analysis of coal-based polygeneration system for power and chemical production // Energy. 2004. Vol. 29. pp. 2359-2371.

11. Ghosh S., De S. Energy analysis of a cogeneration plant using coal gasification and solid oxide fuel cell // Energy. 2006. 31. pp. 345-363.

12. Тепловой расчет котельных агрегатов. Нормативный метод / под ред. Н.В. Кузнецова и др. М.: ЭКОЛИТ, 2011.

13. Липов Ю.М. и др. Компоновка и тепловой расчет парового котла: учеб.пособие для вузов. М.: Энергоатомиздат, 1988.

14. Назмеев Ю.Г., Мингалева Г.Р. Системы топливopодачи и пылеприготовления ТЭС: Справочное пособие. М.: Издательский дом МЭИ, 2005. 480 с.: ил.

15. РД 153-34.1-03.352-99. Правила взрывобезопасности топливopодачи и установок для приготовления и сжигания пылевидного топлива. М.:

ОАО РАО УЭС, 1999. (In Russ).

16. Raschet i proektirovanie pyle-prigotovitel'nyh ustanovok kotel'nyh agregatov. Moscow: СКТИ, 1971. (In Russ).

17. Eisermann W, Johnson P, Conger W. Estimating Thermodynamic Properties of Coal, Char, Tar and Ash. *Fuel Processing Technology*. 1980; 3:39-53.

18. Stepanov VS. Himicheskaya energiya i eksergiya veshchestv. Novosibirsk: Nauka, 1990. (In Russ).

РАО «ЕЭС России», 1999.

16. Расчет и проектирование пыле-приготовительных установок котельных агрегатов. М.-Л.: ЦКТИ, 1971.

17. Eisermann W, Johnson P, Conger W. Estimating Thermodynamic Properties of Coal, Char, Tar and Ash // *Fuel Processing Technology*, 1980. 3. pp.39-53.

18. Степанов В.С. Химическая энергия и эксергия веществ. Новосибирск: Наука, 1990. 163 с.

Authors of the publication

Nguyen Dyk Tuoang – Power engineering department, Kazan State Power Engineering University, Kazan, Russia.

Fam Dang Nyat – Power engineering department, Kazan State Power Engineering University, Kazan, Russia.

Guzel R. Mingaleeva – Head of Power engineering department, Kazan State Power Engineering University, Kazan, Russia.

Received

January, 31 2019.



ASSESSMENT METHODOLOGIES FOR SYNCHRONOUS MOTORS STABILITY UNDER THREE-PHASE FAULTS IN POWER SUPPLY GRIDS

A.I. Fedotov, R.M. Mudarisov, R.E. Abdullazyanov

Kazan State Power Engineering University, Kazan, Russia

Ramil.mudarisov@litsey7.com

Abstract: This article presents research of three-phase short circuit impact on synchronous motors stability in external power supply grids. The analysis of the work performed on this topic revealed that the following issues in motor operation during the fault are not taken into account: voltage sag on busbars occurred during short circuit; the relationship between busbars voltage and distribution of currents in the elements of the power supply system; the impact of sag through excitation system. As part of the work, short circuits in adjacent lines are considered and the law of voltage sag on the busbars of the backbone substation during short-circuit is revealed. A synchronous motor model was developed to take into account the impact of neglected factors on the motor stability. The article proposes the methodology developed to assess synchronous motor stability under three-phase short circuit faults occurring in electric grids. Research results could be used to calibrate protective relays used in power supply grids with powerful synchronous motors.

Keywords: Short-break power supply; short circuit; stability; synchronous motor; critical fault duration; methodology.

Acknowledgments: This research was funded by the Ministry of Education and Science of the Russian Federation as a part of federal targeted programme “Research and Development in Priority Areas of Development of the Russian Scientific and Technological Complex for 2014-2020”. Grant subsidy agreement № 075-02-2018-190 – 1 stage, unique ID of applied scientific research (project) is RFMEFI57418X0188.

For citation: Fedotov A.I., Abdullazyanov R.E., Mudarisov R.M. Synchronous motors stability estimation methodologies under three-phase faults in power supply grids. *Proceedings of the higher educational institutions. ENERGY SECTOR PROBLEMS*. 2019; 21(3-4):90-99. (In Russ). doi:10.30724/1998-9903-2019-21-3-4-90-99.

The motors stability maintenance during short-break in power supply resulting from short circuits (SC) in electric grids is one of the key problems in power supply systems equipped by synchronous motors (SM). This problem is solved by the installation and correct regulation of fast automatic load transfer switches (FALTS) and by the electric transmission line relay protections that detect the fault and restore electric power supply before motors lose their synchronism [1, 2].

In both cases the stability of motors can be provided only if critical fault duration is calculated using correct methodologies. Critical fault duration is the maximum time interval corresponding to the operation of SM under the short-break power supply caused by the three-phase short circuits without the loose in synchronism.

The existing practical criteria and methodologies used to assess stability of motors [3, 4], and researches which are performed to calculate the critical fault duration for the motors operating under the short circuits are based on assessment of motors stability with the following

assumptions: it is performed under electric power supply interruption and the subsequent supply recovery [1, 2, 5]; it neglects the transient DC component of the voltage sag [6-9]; it doesn't take into account real distribution of symmetrical current and voltage components over the elements of power supply grid [7,10]; it doesn't take into account the operation of excitation system i.e. neglect the impact of sag on the motors excitation winding [3–6].

However, short-break in power supply mainly occurs because of short circuits in the transmission lines connected to the same busbars of the backbone substation as the synchronous motors [12].

At the same time, all the above-mentioned assumptions affect the assessment of the reliable duration of a power failure, since during short circuits appearing in the electric grids, motors operate under the voltage sags with transient DC component, moreover distribution of current over the power supply elements during sag effects the motors voltage value and phase. Besides that, powerful synchronous motors are mainly equipped with static excitation systems that are connected to the same busbars as the motors which they excite, and it means that voltage sag also affects the operation of motors through their excitation.

Fig. 1. shows synchronous motors electrical power supply system schematic diagram. It has the following elements: *EG* – Electric grid; *L*₁ – electric transmission line feeding the motor; *L*₂ – transmission line with short-circuit (*SC*); *T*₁ – step down transformer of industrial substation with *SM*; *BUS-1* – busbars of the backbone substation; *BUS-2* – busbars of the industrial step-down substation.

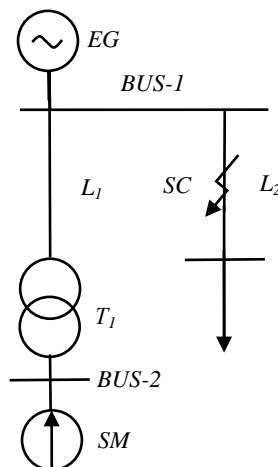


Fig. 1. Power supply grid schematic diagram

Further we consider voltage sags appearing in power supply grids those load consists of synchronous motors by 25–30 % of transformers power (*T*₁ in fig. 1). According to the Russian state standard GOST 52735-2007 “Short circuits in electrical installations” that defines the methods of short circuit current calculations in the electric grids, when calculating the initial effective value of AC component of the three-phase short-circuit current, it is allowed to neglect synchronous motors if they are separated from the short-circuit point by power transformers. Therefore equations of the periodic AC component of the current and the voltage of phase A on busbars of backbone substation (*BUS-1* in fig.1) during the 3-phase short circuit in the line *L*₂ can be expressed as follows:

$$i_p(t) = \frac{E\sqrt{2} \sin(\omega t + \alpha - \varphi_K)}{\sqrt{3}\sqrt{(R_1 + R_2)^2 + (X_1 + X_2)^2}} = \sqrt{2}I_P \sin(\omega t + \alpha - \varphi_K), \quad (1)$$

$$u_P(t) = \frac{E\sqrt{2}\sqrt{(R_2^2 + X_2^2)} \sin(\omega t + \alpha - \varphi_1)}{\sqrt{3}\sqrt{(R_1 + R_2)^2 + (X_1 + X_2)^2}} = \sqrt{2}U_P \sin(\omega t + \alpha - \varphi_1). \quad (2)$$

Transient DC-components of the current and the voltage on the busbars of backbone substation can be calculated by equations:

$$i_A(t) = I_A e^{-t/T}, \quad (3)$$

$$u_A(t) = (R_2 i_A(t) + \frac{X_2}{\omega} \frac{di_A(t)}{dt}) = (R_2 - \frac{X_2}{\omega T}) I_A e^{-t/T}. \quad (4)$$

Symbols used in equations (1–4) have the following meanings: R_1 and X_1 are active and reactive resistances of the electric grid (EG in fig.1), respectively; R_2 and X_2 are active and reactive resistances of the line with fault (L_2 in fig.1); E is electromotive force (EMF) of electric grid; T is transient time constant of DC component; ω is angular frequency of electric grid voltage and current; α is short circuit appearance angle; φ_1 and φ_K are phase angles related to the scheme diagram resistances; I_A is initial value of short circuit current transient component. Value of the current I_A can be calculated as the difference between current AC-component before fault and immediately after it:

$$I_A = I_M \sin(\alpha - \varphi) - \sqrt{2} I_P \sin(\alpha - \varphi_K) \quad (5)$$

Symbols in the equation (5) are: I_M is magnitude of current periodic AC component before the fault; φ is phase angle related to current AC component before the fault. It is clear that the DC component of current and voltage achieve their maximum if the magnitude of current before the fault in the equation (5) equals to zero. This corresponds to case when transmission line with fault doesn't have the load in prefault conditions. If we rewrite equation (4) by using equation (5) for the conditions with the maximum DC component when I_M is zero we obtain equation (6):

$$u_A(t) = -(R_2 - \frac{X_2}{\omega T})(\sqrt{2} I_P \sin(\alpha - \varphi_K)) e^{-t/T} = -U_A e^{-t/T}. \quad (6)$$

Then the residual voltage (u_R) of the backbone substation busbars (BUS-1 in fig.1) will be written as equation (7) and have periodic (U_P) and transient DC (U_A) components:

$$u_R(t) = \sqrt{2} U_P \sin(\omega t + \alpha - \varphi_1) - U_A e^{-t/T}. \quad (7)$$

Figs. 2–3 show relationships between DC-component residual voltage (U_{A*}) and phase angle φ_1 and AC-component residual voltage (U_{P*}). Table 1 shows phase angles φ_K corresponding to various values of the DC component transient time constants varying from 0,02 s to 0,2 s. In figs. 2–3 and table 1 transient DC-component voltage (U_{A*}), periodic AC-component voltage (U_{P*}) and DC component transient time constant (T^*) are expressed in relative units. AC current period (0,02 s) is taken as the base unit for the transient time constant. These calculated values are given for 6 values of voltage DC component time constants and correspond to electric grids with 110–220 kV voltage ratings those 3-phase short circuit currents on the backbone substation busbars vary from 4 to 40 kA. Dependencies in figs. 2–3 show that for the considered classes of power supply systems, the DC-transient component of voltage is greater, the greater the voltage sag and the shorter the decay time constant are.

Phase angle φ_K for various time constants T_*

T_* , r.u.	1	2	3	4	5	10
φ_K , °	81	85	87	88	88	89

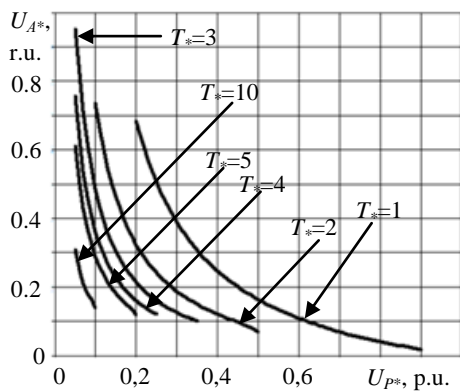


Fig. 2. Relationship between voltage of DC-component (U_{A^*}) and voltage of AC-component (U_{p^*})

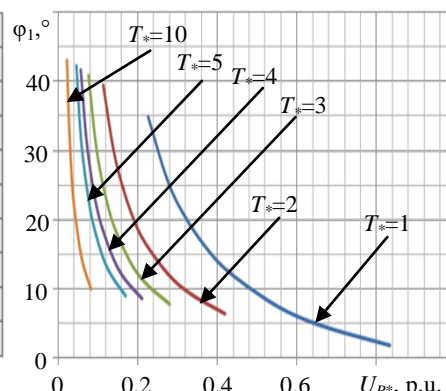


Fig. 3. Relationship between phase angle φ_1 and voltage of AC-component (U_{p^*}).

The synchronous motor model shown in fig. 4 is developed to assess motors stability. The distinct feature of this model from its analogues is that it takes into account features in motors operation under 3-phase short circuit conditions such as: sag is described by residual voltage equation (7) with DC-component; it calculates current flow in power supply grid elements and therefore accounts the influence of current on the motor voltage; it calculates the impact of voltage sag on the motors excitation winding.

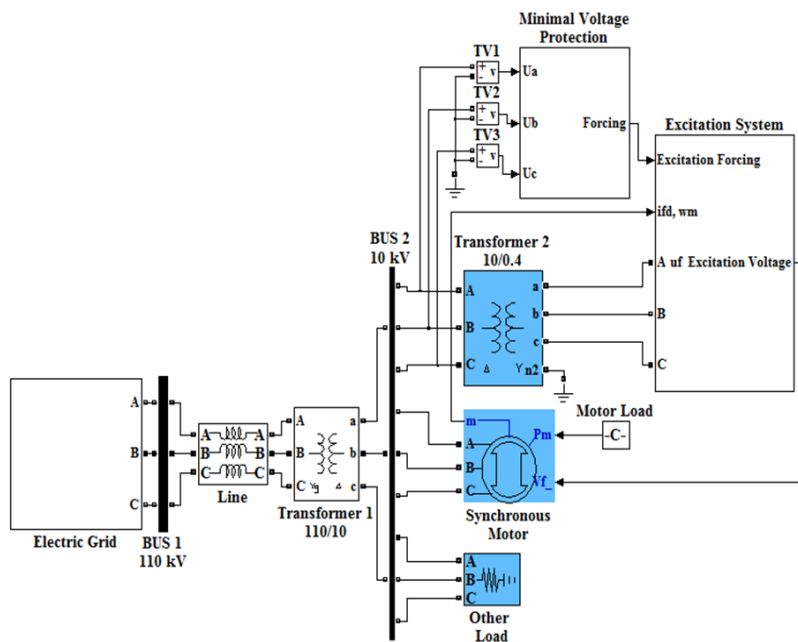


Fig.4. The Simulink model of SM and its power supply grid

In order to calculate the influence of voltage sag on the motors excitation winding the model includes elements of “TE8-320” excitation systems (“Excitation System” element in fig. 4). These elements implement the basic functions of excitors such as: field forcing, switching on the starting resistor that limits voltage surges on the rectifier and starting resistor circuit switching off function.

In order to prove advantages of aforementioned model we have calculated critical fault duration of SM under 3-phase short circuits. Calculation was done using practical criteria and motor models, designed by other researchers. Calculations were performed for the STD-8000 synchronous motor with the following properties of prefault conditions: equivalent load moment of inertia $J_{LOAD}=250 \text{ kg}\cdot\text{m}^2$, load factor $m_L=0,7 \text{ r.u.}$, system voltage $U=0,997 \text{ r.u.}$ (SM voltage $U_{SM}=1,081 \text{ r.u.}$), synchronous EMF $E_q E_q=1,598 \text{ r.u.}$, load angle $\delta=62,8^\circ$. Motor is connected to 110 kV electric grid ($Z_1=j15,88 \text{ Ohm}$) through TDN-16000/110 transformer.

Table 2 shows results of critical fault duration research that was carried out using simplified motor models from other researchers.

Table 2

Calculation of stability using simplified motor models

№	Motor model type	Calculation 1: $U_{p*}=0, U_{A*}=0, T^*=0$ (SC on backbone substation busbars)		Calculation 2: $U_{p*}=0,111, U_{A*}=0,256, T^*=5 \text{ r.u.}$ ($U=110 \text{ kV}$, SC in transmission line: AS-240, $L=4,7 \text{ km}$)		Calculation 3: $U_{p*}=0,227, U_{A*}=0,579, T^*=1$ ($U=110 \text{ kV}$, SC in transmission line: AS-70, $L=7,1 \text{ km}$)		Calculation 4: $U_{p*}=0,431, U_{A*}=0,217, T^*=1$ ($U=110 \text{ kV}$, SC in transmission line: AS-185 $L=26,3 \text{ km}$)		Total error of all calculations $\Delta t_c, \%$
		$t_c, \text{ ms}$	$\Delta, \%$	$t_c, \text{ ms}$	$\Delta, \%$	$t_c, \text{ ms}$	$\Delta, \%$	$t_c, \text{ ms}$	$\Delta, \%$	
1	Test model	160	0,0	211	0,0	231	0,0	831	0,0	0,0
2	Model 1	172	7,5	215	1,9	232	0,4	932	12,2	22,0
3	Model 2	172	7,5	206	2,4	217	6,1	698	16,0	31,9
4	Model 3	178	11,3	210	0,5	223	3,5	933	12,3	27,5
5	Model 4	245	53.1	314	48,8	1249	440,7	3934	373,4	916,0

Explanations for table 2:

- Test model is full model of the electrical power supply system diagram, shown in fig. 1, that includes electric grid (EG), electric transmission line feeding the motor (L_1), step-down transformer (T_1), synchronous motor (SM), excitation system, adjacent transmission line with short circuit (L_2) and the element that simulates the 3-phase short circuit fault;
- Model 1 is a developed model, which, instead of a three-phase circuit system and unit in an adjacent line, takes into account the law of change of residual voltage on busbars of backbone substation (BUS-1 in fig. 1.) according to expression (7). The model also includes feeding transmission line (L_1), step-down transformer (T_1), motor (SM), operation of excitation system under voltage sag.
- Model 2 is the same as the model 1, but doesn't take into account the transient DC component of the residual voltage equation (7);
- Model 3 is the same as the model 1, but doesn't take into account the transient DC

component of the residual voltage equation (7) and the impact of sag on the operation of the excitation, exciter voltage is assumed to be constant and equal to exciter voltage before the fault;

- Model 4 is based on distribution of currents in the elements of the power supply system depending on the busbars voltage of backbone substation (*BUS-1* in fig. 1), electric grid, adjacent transmission line with fault (L_2), feeding transmission line (L_1), step-down transformer (T_1) are simulated as voltage source that generates voltage sag without transient DC component on the busbars of industrial step-down substation, i. e. this model neglects the impact of current flow over the power supply grid elements on the value and phase of motor voltage.

Results of research show that correct stability assessment over full range of voltage sag is possible only within the full model (test model in table 2) and within the developed models (models 1 and 2 in table 2) which are based on distribution of currents in the elements of the power supply system depending on the busbars voltage of backbone substation (*BUS-1* in fig. 1), which take into account: equation of voltage on the busbars of backbone substation, impact of current flow over the power supply grid elements on the motor voltage, and operation of excitation system under voltage sag. The developed model also has the following advantages when comparing it with full models: it accounts less elements, which results in reduction of time needed to prepare electrical power supply system model, and enables to calculate critical fault duration relatively to the voltage sag values which is used to adjust adaptive relay protection systems.

Table 3 shows critical fault duration that were calculated by practical criteria used to assess motors stability such as: method of equal areas, criterion of transient stability under break in power supply [3, 4]. These results are calculated for the motor with decelerating torque (m_D) caused by excitation field and with field forcing (synchronous EMF of motor with field forcing $E_q = 1,75E_{q,NOM} = 4,0$ r.u.). In calculations it is assumed that motor is working under voltage sags described in the calculations 3 and 4 presented in table 2 (in calculation 3 $U_{P*} = 0,227$ r.u., in calculation 4 $U_{P*} = 0,431$ r.u.).

Table 3

Calculation of SM stability using practical criteria

Criterion	Method of equal areas t_A , s			Transient stability under break in power supply t_{CR} , s		
	$E_q = \text{const}$	$E'_q = \text{const}$	$E''_q = \text{const}$	$m_D = 0$ $E_q = E_{q1}$	$m_D \neq 0$, $E_q = 4$ r.u.	$m_D = 0$, $E_q = 4$ r.u.
Calculation assumptions:						
Critical fault duration in calculations 3/4, s	0,151/ 0,209	0,233/ 0,095	0,083/ 0,047	0,232/ 0,232	0,213/ 0,213	0,292/ 0,292
Errors of calculations 3/4, %	34,6/74,8	0,9/88,6	64,1/94,3	0,4/72,1	7,8/74,4	26,4/64,9

Results of research prove that aforementioned practical stability criteria don't assure accuracy requirements in calculations of critical fault duration over full range of voltage sag values caused by 3-phase short circuits appearing in the electrical grids. Further we consider characteristic properties of stability assessment in the synchronous motor models that take into account the aforementioned recommendations.

In order to observe the impact of fault appearance time on the motor stability under three-phase short circuit, the motor operation is simulated with 0,001 s shift in fault appearance time which is determined by the phase angle α in the voltage equation (7). The results of this research

are presented in fig. 5 as a critical duration vs fault appearance time curve. These results are obtained for the STD-8000 synchronous motor model operating at previously mentioned prefault conditions and under voltage sags described for the calculation 3 presented in table 2 ($U_{P*}=0,227$ r.u). In fig. 5: curve 1 corresponds to the results obtained using the full model (testing model in table 2), when motor is connected to the electric grid through the transformer (TDN-16000/110); curve 2 corresponds to the results obtained using the full model (test model), when motor is connected to the electric grid through the transformer (TDN-16000/110) and feeding transmission line (conductor of AS-70 type, length 20 km); curve 3 corresponds to the results obtained by the developed model (model 2 in the table 2) that doesn't account the transient DC-component of the voltage equation (7) for the motor connected to the electric grid through the transformer (TDN-16000/110) and feeding transmission line (conductor of AS-70 type, length is 20 km).

As it is seen from fig. 5, the distinction between the minimum and the maximum critical fault durations is less than 2 % (approximately 3 ms). This result assures that fault appearance time could be neglected during the assessment of SM stability under 3-phase short-circuit faults.

Fig. 6 shows relationship between critical fault duration and residual voltage obtained in the developed model of the STD-8000 synchronous motor connected to 110 kV electric grid through the transformer (TDN-16000/110) and feeding transmission line (conductor type is AS-70) of 20 km length. Motor operates with the following prefault conditions: equivalent load moment of inertia $J_{LOAD}=250$ kg·m², load factor $m_L=0,7$ r.u., system voltage $U=0,995$ r.u. (SM voltage $U_{SM}=1,07$ r.u.), synchronous EMF $E_q=1,587$ r.u., load angle $\delta=64,8^\circ$. In fig. 6: curve 1 corresponds to the results obtained by the developed model (model 2 in table 2) that doesn't account the transient DC-component of the voltage equation (7); curves 2–6 correspond to the results obtained by the developed model (model 1 in table 2) that takes into account the transient DC-component of the voltage equation, transient time constants of these curves are equal to (1–5) periods of voltage AC-component consequently.

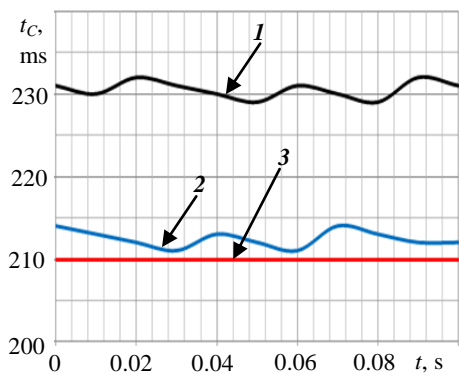


Fig. 5. Critical duration vs fault appearance time

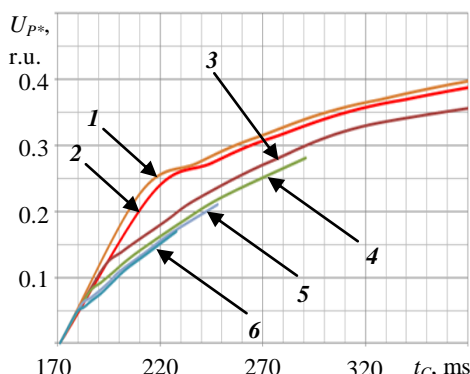


Fig. 6. Critical duration vs residual voltage

It is seen from fig. 6 that transient DC-component of voltage increases the critical fault duration. Thus stability assessment without transient DC-component of voltage sag equation provides calculation of the combined stability zone that includes stability zones with all transient time constants of transient voltage DC-component.

Fig. 7 shows relationship between critical duration and phase angle φ_1 obtained without transient DC-component of the voltage sag equation. Calculation is carried out for the STD-8000 synchronous motor model, prefault condition of which are described in the previous research presented in fig. 5. During the fault motor operates under the voltage sag without transient DC

voltage component described in calculation 3 presented in table 2 ($U_{p*}=0,227$ r.u.).

As it seen from fig. 7, critical fault duration calculated for the fault with the fixed value of AC-component residual voltage ($U_{p*}=0,227$ r.u.) can change up to 36 % depending on the phase angle φ_1 . It should be noticed that real values of φ_1 phase angle vary from 0 to 90° and that increase in this angle increases the critical fault duration. Hence critical fault duration should be calculated for the possibly lower values of the phase angle φ_1 .

Fig. 8 shows relationship between phase angle φ_1 and AC-component residual voltage for various values of electric grid resistances and types of transmission line conductor. This curves are plotted for the 110–220 kV electric grids for which three-phase short circuit currents vary from 4 to 40 kA. In fig. 8: curve 1 corresponds to 110 kV transmission line with AS-70 conductor type; curve 2 corresponds to 110 kV transmission line with AS-95 conductor type; curve 3 corresponds to 110 kV transmission line with AS-150 conductor type; curve 4 corresponds to 110 kV transmission line with AS-300 conductor type; curve 5 corresponds to 220 kV transmission line with AS-300 conductor type; curve 6 corresponds to 220 kV transmission line with AS-400 conductor type. From fig. 7–8 it can be concluded that motors stability assessment must be calculated for φ_1 phase angles corresponding to transmission lines with higher cross-section area of conductors and according to curves in fig. 8.

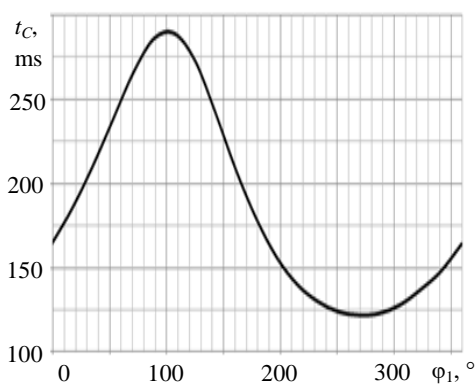


Fig. 7. Relationship between critical duration and phase angle φ_1

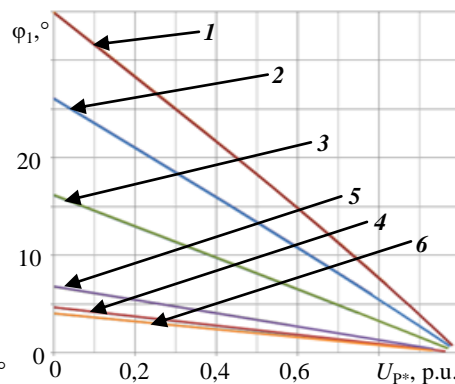


Fig. 8. Relationship between phase angle φ_1 and AC-component voltage (U_{p*})

All results obtained in studies described above are used to develop stability assessment methodology. Methodology assures calculation of critical fault duration of SM under three-phase short circuits appearing in the electrical grids and consists of the following principles:

1) SM computing model should take into account the distribution of currents in the elements of the power supply system depending on the busbars voltage of backbone substation (*BUS-1* in fig. 1), electric grid and transmission line with the fault can be simulated as voltage source that generates voltage on the busbars of backbone substation according to equation (7). The model must also take into account feeding transmission line (L_1), step-down transformer (T_1) of industrial substation and excitation system operating under voltage sag.

2) Stability assessment of synchronous motors for full range of residual voltage and possible values of transient time constants should be carried out in the form of combined stability zone (fig. 6) which is computed by the developed SM model (fig.4) according to the residual voltage equation (7) without transient voltage component.

3) Calculation of critical fault duration of synchronous motors operating under three-phase short circuit faults appearing in the electric grids could be done without regard to the fault appearance time (angle α in the equation (7));

4) Assessment of stability of synchronous motors should to be done with regard to real values of phase angle φ_1 according to the curves in fig. 8, corresponding to transmission lines connected to the backbone substation busbars and having higher cross-section area of conductors.

The developed methodology could be used during designing and adjustment of protective relays used in electric grids and designing the elements of power supply grids with regard to the stability of synchronous motors. This will enhance reliability of SM operation under short-break power supply caused by the three-phase short circuits in electric grids.

References

1. Pupin VM, Zhukov VA, Safonov DO. Modernizacii skhemy vkladyeniya elegazovogo vyklyuchatelya dlya obespecheniya neotklyuchenij pogruzhnyh nasosov. *University news. North-caucasian region. Technical sciences series*. 2013; 1:56-60. (In Russ).
2. Alekseev VYu. Zashchita ot poteri pitaniya na perekachivayushchih nasosnyh stanciyah [dissertation]. Ufa; 2012. Available at: https://www.ugatu.ru/media/uploads/MainSite/Science/dissovet/02/2011/20.02.12/alekseev_avtoreferat.pdf. Accessed: 20 Feb 2019. (In Russ).
3. Golodnov YuM. *Samozapusk elektrodvigatелеj*. Moscow: Energoatomizdat, 1985. (In Russ).
4. Venikov VA. *Perekhodnye elektro-mekhanicheskie processy v elektricheskikh sistemah*. Moscow: Vysshaya shkola, 1985. (In Russ).
5. Shabanov VA, Yusupov RZ, Alekseev VYu. Device for adaptive automatic to reserve source on oil pumping stations. *Electrical and data processing facilities and systems*. 2016; 2(12):16-22. (In Russ).
6. Marini P. Immunity to voltage dips for synchronous motors. *Paper submitted to the International Conference on Power Systems Transients (IPST2013); 18-20 July 2013; Vancouver, Canada*. Vancouver, 2013.
7. Hyla M. Impact of voltage dips on the operations of a high-power synchronous motor with a reactive power controller. *Mining-Informatics, Automation and Electrical Engineering*. 2016; 2:5-13.
8. Abramovich BN, Ustinov DA, Sychev YuA, et al. The dynamic stability of electrotechnical complexes with synchronous and asynchronous motors in oil and gas enterprises. *Neftgazovoe delo*. 2011; 3:17-25. (In Russ).
9. Alipoor J, Doroudi A, Ghaseminezhad M. Detection of the Critical Duration of Different Types of Voltage Sags for Synchronous Machine Torque Oscillation. *Energy and Power Engineering*. 2012; 4: 117-124. DOI:10.4236/epe.2012.43016.
10. Carlsson F, Sadarangani C. Behavior of Synchronous Machines Subjected to Voltage Sags of Type A, B and E. *European Power Electronics and Drives Journal (EPE)*. 2005; 15(4):35-42. <https://doi.org/10.1080>

Литература

1. Пупин В.М., Жуков В.А., Сафонов Д.О. Модернизации схемы включения элегазового выключателя для обеспечения неотключений погружных насосов // Известия высших учебных заведений. Северо-Кавказский регион. Серия: Технические науки. 2013. №1. С. 56-60.
2. Алексеев В.Ю. Защита от потери питания на перекачивающих насосных станциях: Дис. ... канд. техн. наук. Уфа; 2012. Доступно по: https://www.ugatu.ru/media/uploads/MainSite/Science/dissovet/02/2011/20.02.12/alekseev_avtoreferat.pdf. Ссылка активна на 20 февраля 2019.
3. Голоднов Ю. М. *Самозапуск электродвигателей*. М.: Энергоатомиздат, 1985. 136 с.
4. Веников В.А. *Переходные электромеханические процессы в электрических системах*. М: Высш. шк., 1985. 536 с.
5. Шабанов В.А., Юсупов Р.З., Алексеев В.Ю. Устройство адаптивного автоматического включения резерва на нефтеперекачивающих станциях // Электротехнические и информационные комплексы и системы. 2016. Т. 12, №2. С. 16-22.
6. Marini P. Immunity to voltage dips for synchronous motors // Paper submitted to the International Conference on Power Systems Transients (IPST2013); 18-20 July 2013; Vancouver, Canada. Vancouver, 2013.
7. Hyla M. Impact of voltage dips on the operations of a high-power synchronous motor with a reactive power controller // Mining-Informatics, Automation and Electrical Engineering. 2016. N2. pp. 5-13.
8. Абрамович Б.Н., Устинов Д.А., Сычев Ю.А., и др. Динамическая устойчивость электромеханических комплексов с синхронными и асинхронными двигателями на предприятиях нефтедобычи // Нефтегазовое дело. 2011. №3. С. 17-25.
9. Alipoor J., Doroudi A., Ghaseminezhad M. Detection of the Critical Duration of Different Types of Voltage Sags for Synchronous Machine Torque Oscillation // Energy and Power Engineering. 2012. N4. pp. 117-124.
10. Carlsson F., Sadarangani C. Behavior of Synchronous Machines Subjected to Voltage Sags of Type

11. Alipoor J, Doroudi A, Hosseinian SH. Identification of the Critical Characteristics of Different Types of Voltage Sags for Synchronous Machine Torque Oscillations. *Electric Power Components and Systems*. 2014; 13(42).

2. Fedotov AI, Rozhentsova NV, Vagapov GV, et al. Metodika proverki effektivnosti tokoogranichivayushchego ustrojstva dlya snizheniya glubiny provala napryazheniya. *Industrial Power Engineering*. 2016; 12:28-33. (In Russ).

A, B and E // *European Power Electronics and Drives Journal (EPE)*. 2005. Vol. 15, no 4. P. 35-42.

11. Alipoor J, Doroudi A, Hosseinian S.H. Identification of the Critical Characteristics of Different Types of Voltage Sags for Synchronous Machine Torque Oscillations // *Electric Power Components and Systems*. 2014. Vol. 13, N 42.

12. Федотов А.И., Роженцова Н.В., Вагапов Г.В., и др. Методика проверки эффективности токоограничивающего устройства для снижения глубины провала напряжения // *Промышленная энергетика*. 2016. №12. С. 28-33.

Authors of the publication

Alexander I. Fedotov – D.Sc., Professor, Engineering center “Computer simulation and engineering in the field of power engineering and power engineering machinery”.

Rustem E. Abdullazyanov - PhD in Engineering sciences, assistant professor at “Relay protection and automation of electric power systems” department.

Ramil M. Mudarisov - graduate student, Kazan State Power Engineering University.

Received

March, 10 2019



**DETERMINATION OF THERMAL CAPACITY OF PROCESSED SORBENTS
FROM RESIDUAL BIOMASS OF CHLORELLA SOROKINIANA
AND DUCKWEED LEMNA MINOR**

**E.L. Shaburov¹, O.V. Derevianko¹, A.V. Fedyukhin²,
Yu.A. Smyatskaya¹, N.A. Politaeva¹**

¹Peter the Great St. Petersburg Polytechnic University, St. Petersburg, Russia

²National Research University Moscow Energy Institute, Moscow, Russia

derevyanko_ov@spbstu.ru

Abstract: *Our article reviews the issues arising during the process of wastewater purification and utilization of spent adsorbents. We are offering different ways of utilization of spent sorbents produced from residual biomass of Chlorella Sorokiniana microalgae and Lemna Minor duckweed. We review the technology of adsorbent production from agricultural waste (carbonized millet husks), wastes of the thermally expanded graphite and chitosan biopolymer production, and residual biomass of Chlorella Sorokiniana microalgae and Lemna Minor duckweed, which is formed after all the valuable components have been extracted from the algae and duckweed. We have conducted a thermogravimetric analysis that demonstrated that the spent sorbents' decomposition when exposed to high temperatures results in a variety of exothermic effects in the 300 to 500 °C range. This fact allows us to recommend application of spent sorbents as a fuel for energy generation. For the first time we determine the specific heat of combustion of spent sorbents used in wastewater purification from oils (22857–25220 kJ/kg) and from heavy metal ions (19 079–21 117 kJ/kg). We demonstrate that the value of specific heat of combustion of spent sorbents produced from residual biomass is not less than that of classic fuels such as coals and brown coals. The specific heat value of combustion of spent sorbents used in wastewater purification from oils is higher than that of those used in wastewater purification from heavy metal ions because of the oil carbohydrates adsorbed on sorbents, which increases the material's calorific value.*

Keywords: *spent sorbents' utilization, fuel, residual biomass of Chlorella Sorokiniana microalgae and Lemna Minor duckweed, water purification.*

Acknowledgments: *The research was conducted within the Federal Target Program “Research and Development of Priority Directions of Development of Scientific and Technological Complex of Russia from 2014 to 2020”, project topic “Development and Implementation of Innovative Biotechnologies of Processing of Chlorella Sorokiniana Microalgae and Lemna Minor Duckweed” (AGREEMENT #14.587.21.0038, July 17, 2017) Unique project ID RFMEFI58717X0038.*

For citation: Shaburov E.L., Derevianko O.V., Fedyukhin A.V., Smyatskaya Yu.A., Politaeva N.A. Determination of thermal capacity of processed sorbents from residual biomass of Chlorella Sorokiniana and duckweed Lemna Minor. *Proceedings of the higher educational institutions. ENERGY SECTOR PROBLEMS*. 2019; 21(3-4):100-106. (In Russ). doi:10.30724/1998-9903-2019-21-3-4-100-106.

Introduction

Purification of wastewaters and waste utilization are among the most important ecological problems. Few of the priority tasks of modern industry are closed-cycle water purification and waste-free production technologies. In order to reduce the toxicity level of wastewaters, we are using efficient sorption purification methods. Some prospective and profitable sorbents can be produced using secondary materials (lignin and cellulose-containing waste), which will allow solving two problems simultaneously: water purification and waste processing. The process of consumption of impurities (heavy metal ions from the wastewaters of the oil production industry) by the adsorbent cannot go on indefinitely as at some point the adsorbent reaches its saturation state and needs to be replaced. Thus, among the ecological problems of the sorption water purification are desorption (regeneration) and utilization of the sorbent. It is very important not only to purify the wastewaters of the industry, but also to achieve the minimal amount of the wastes for utilization, for them to be non-toxic and not harmful for the environment [1–4].

The employees of the Peter the Great St. Petersburg Polytechnic University have developed a technology for production of valuable components from the *Chlorella Sorokiniana* microalgae and *Lemna Minor* duckweed [5, 6]. After extraction of all the valuable components (lipids, carotenoids, pigments), a waste (remaining biomass) is formed, from which some sorption material were produced. In order to increase the sorption capacity of the sorbent, we have added some agricultural wastes (carbonized millet husk) [7-10], wastes from the thermally expanded graphite production [11–13], and a chitosan biopolymer was used as a binder [14–16].

We have obtained three types of sorbents:

- 1 – thermally expanded graphite plus chitosan plus remaining biomass;
- 2 – chitosan plus remaining biomass;
- 3 – chitosan plus remaining biomass plus carbonized millet husk.

Obtained sorption materials were used to purify wastewaters from heavy metal ions (HMI) and oil products (OP). The process of regeneration of used sorbents is ecologically unsafe and economically unsound. Thus, we have reviewed possible ways of utilization of spent sorbents while obtaining goods that are important for agriculture following the scheme at the figure 1:

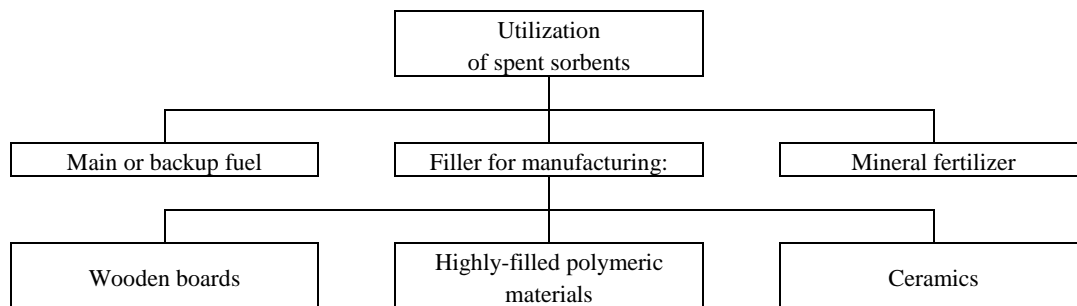


Figure 1. The scheme of utilization of spent sorption materials based on the wastes of agricultural complex

The goal of this work is researching the possibility of utilization of spent sorbents as main or secondary fuel for solid fuel boilers.

Devices and methods

Thermogravimetric research of spent sorbents was conducted using the “Derivatograph” device OD-103 produced by the Hungarian company “MOM”. A sample weight (0,2 g) was placed in fused alumina crucibles and heated in air to 1000° C at the rate of 10 degrees per minute. Calcined alumina was used as a reference; the temperature was recorded using a Pt-Pt/Rh thermocouple. Sample preparation of the analysis consisted of grinding the spent sorbents in an agate mortar until a powder state was reached.

Tests to determine the specific heat of combustion of spent sorbents were carried out in the laboratory of the Hamburg University of Technology (Germany) using an IKA C 5000 calorimeter. The device used is an adiabatic jacket calorimeter according to DIN EN 51900-3. Spent sorbents are pre-dried at 45 °C until their mass becomes constant, then ground to sizes less than 0,25 mm.

According to DIN EN 51900-1, the calorific value $H_{o,v}$ can be determined as the ratio of the amount of heat released in the case of complete combustion and the mass of the sample under the following assumptions:

- burning occurs at a constant volume;
- the temperature of the fuel before combustion and the temperature of its products of combustion is 25 °C;
- water present in the fuel before combustion, and water formed when hydrogen-containing compounds of combustible fuel are present in a liquid state after combustion;
- products of combustion of carbon and sulfur are present as carbon dioxide and sulfur dioxide in the gaseous state;
- nitrogen oxidation does not occur.

$H_{o,v}$ is determined using a calorimeter following the method described below. The calorimetric bomb is placed in a water-filled calorimetric vessel, which is located in an adiabatic insulating jacket. When the temperatures of calorimetric bomb and water in the calorimetric vessel equalize, the fuel sample is ignited. The rate of increase in temperature is recorded. From the temperature difference, the calorific value of the sample was calculated taking into account the heat capacity of the calorimeter:

$$H_{o,v} = \frac{C \cdot \Delta T - (Q_N + Q_S + Q_Z)}{m_p}, \quad (1)$$

where $H_{o,v}$ is the calorific value of the sample, J/g; ΔT is the temperature change value, K; Q_N is the evolution of heat through the formation of nitric acid, J; Q_S – Heat generation Q_Z through the formation of SO₂, J; Q_Z is the amount of external heat, J; m_p is the sample mass, g;

C determines the heat capacity of the calorimetric system. J/K, according to the equation (2):

$$C = \frac{H_{o,v} \cdot m_B + Q_Z}{\Delta T}, \quad (2)$$

where: $H_{o,v}$ is the heat of combustion of the reference substance in joules per gram; m_B is the mass of the reference substance in grams; Q_Z is the amount of external heat in joules; ΔT is the temperature rise determined in calibration in Kelvin.

The measurement is done in two stages. First, temperature compensation begins between the calorimetric bomb and calorimetric water. This compensation time is called a preliminary experiment. Subsequently, the main experiment begins with the ignition of the combustion sample and the determination of the increase in temperature.

From the given value of the heat of combustion and the element content, the calorific value can be calculated using equations (3) and (4):

$$H_{u,p} = H_{o,v} - [k \cdot H + 0,8 \cdot (N + O) + k_1 \cdot w], \quad (3)$$

$$N + O = 100 - (w + A + C + H + S), \quad (4)$$

where: k is the heat of evaporation, taking into account the volume work of water produced from hydrogen during combustion at $25\text{ }^\circ\text{C} = 23,727\text{ J}/\%$; k_1 is the specific heat of evaporation of water at constant pressure at $25\text{ }^\circ\text{C}$, $k_1 = 24,4\text{ J}/\%$; w is the analytical moisture content of the fuel, % by mass; A is the ash content of fuel, % by mass; C is the carbon content of fuel, % by mass; H is the hydrogen content of fuel, % by mass; S is the sulfur content of fuel, % by mass [17].

The measurement error does not exceed 2,5 %.

Results and discussion

Spent sorbents after purification of oil products were subjected to thermogravimetric analysis (measurement error did not exceed 2,5 %). The data of differential thermogravimetric analysis (DTA) of the spent sorbents of first composition, after purification of wastewater from OP, (Fig. 2) show that water removal occurs up to 120 °C, weight loss lies in range from 0 to 7 %. The beginning of the decomposition of the components of the spent sorbents begins at 300 °C, when the decomposition of hydrocarbons (OP) adsorbed from the wastewater occurs. Analysis of the DTA curve shows that decomposition of the spent adsorbent under the influence of temperature is accompanied by exothermic effects in the temperature range of 360–500 °C. This confirms the possibility of using spent sorption materials as fuel for energy generation.

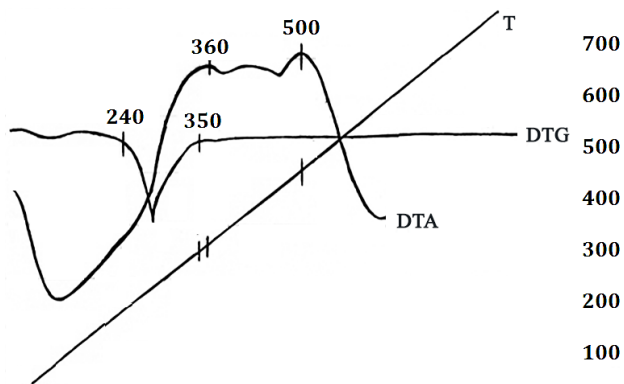


Figure 2. Thermogravimetric analysis of spent sorbents after wastewater purification from OP.

Using the IKA C 5000 calorimeter and formulas 1 to 4 we have determined the specific heat of combustion of spent sorbents after purification of wastewater from HMI and OP (see Table 1).

Table 1

Comparative data of the specific heat of combustion of spent sorbents and classic fuel

№	Sorbent composition	Specific heat of combustion of spent sorbents after purification of wastewater from HMI, kJ/kg	Specific heat of combustion of spent sorbents after purification of wastewater from OP, kJ/kg
1	Thermally expanded graphite plus chitosan plus remaining biomass	21 117 ± 21	25 220 ± 15
2	Chitosan plus remaining biomass	20 674 ± 20	23 432 ± 23
3	Chitosan plus remaining biomass plus carbonized millet husk	19 079 ± 19	22 857 ± 22
For comparison			
	Fuel type	Specific heat of combustion, kJ/kg	

4	Charcoal	29 600
5	Coal	20 200
6	Brown coal, lignite	16 300

The table shows that the values of specific heat of combustion of spent sorbents made of residual biomass are not inferior to the classical types of fuel – coal and brown coal. The specific heat of combustion of spent sorbents after purification of wastewater from OP is higher (22 857–25 220 kJ/kg) than the specific heat of combustion of used sorbents after purification of wastewater from HMI. This fact is explained by the presence of petroleum hydrocarbons adsorbed on sorbents, which increase the caloric content of the substance. As a result of the analysis, it is possible to recommend the use of spent sorbents as fuel.

Conclusions

As a result of this work, we have reviewed the methods of utilization of spent sorbents made of residual biomass of *Chlorella Sorokiniana* microalgae and *Lemna minor* duckweed. Thermogravimetric analysis demonstrated that the exothermic effects in the temperature range of 360–500 C accompany decomposition of the spent sorbents under the influence of temperature. This allows us to recommend the use of spent adsorption materials as fuel for energy generation.

For the first time, the specific heat of combustion of the spent sorbents after purification of wastewater from OP was determined (22 857–25 220 kJ/kg) and from HMI (19 079–21 117 kJ/kg). We demonstrate that the values of specific heat of combustion of spent sorbents made of residual biomass are not inferior to the classical types of fuel – coal and brown coal. The specific heat of combustion of spent sorbents after purification of wastewater from OP is higher than the specific heat of combustion of used sorbents after purification of wastewater from HMI. This is due to the presence of petroleum hydrocarbons adsorbed on sorbents, which increase the caloric content of the substance.

References

1. Zhumaeva DZ. Ugol'nye adsorbenty dlya ochistki stochnyh vod i ih vtorichnoe ispol'zovanie // *Universum: Himiya i biologiya: ehlektron. nauchn. zhurn.* 2016; 11(29). Available at: <http://7universum.com/ru/nature/archive/item/3851>. Accessed: 30 Jan 2019. (In Russ).
2. Litvinova TA, Cokur OS, Zubenko YuYu., et al. Reshenie problemy utilizatsii neftesoderzhashchih othodov s вовлечением их в resursooborot // *Sovremennye problemy nauki i obrazovaniya.* 2012; 6. Available at: <http://online.rae.ru/1272>. Accessed: 23 Feb 2019. (In Russ).
3. Misun LV, Misun IN, Grishchuk VM. *Inzhenernaya ehkologiya v APK.* Minsk: BSATU, 2007. (In Russ).
4. Jumaeva DJ, Toirov OZ. The obtainment of carbon adsorbents and their composition for clearing industrial wastewater. *Austrian Journal of Technical and Natural Sciences.* 2016; 3–4:67-70.
5. Politaeva N, Kuznetsova T, Smyatskaya Y., et al. *Chlorella Microalga Biomass Cultivation for Obtaining Energy in Climatic Conditions of St. Petersburg.* In book: *International Scientific Conference Energy Management of Municipal Transportation Facilities and Transport EMMFT 2017, series: Advances in Intelligent Systems and Computing; 10–13 April 2017; Khabarovsk, Russia.* Springer International Publishing, vol.692, 2018. pp.555-

Литература

1. Жумаева Д.Ж. Угольные адсорбенты для очистки сточных вод и их вторичное использование // *Universum: Химия и биология: электрон. научн. журн.* 2016. № 11(29). Доступно по: <http://7universum.com/ru/nature/archive/item/3851>. Ссылка активна на 30 января 2019.
2. Литвинова Т.А., Цокур О.С., Зубенко Ю.Ю., и др. Решение проблемы утилизации нефтесодержащих отходов с вовлечением их в ресурсооборот // *Современные проблемы науки и образования.* 2012. № 6. Доступно по: <http://online.rae.ru/1272>. Ссылка активна на 23 февраля 2019.
3. Мисун Л.В., Мисун И.Н., Грищук В.М. *Инженерная экология в АПК.* Минск.: БГАТУ, 2007. 302 с.
4. Jumaeva D.J, Toirov O.Z. The obtainment of carbon adsorbents and their composition for clearing industrial wastewater. *Austrian Journal of Technical and Natural Sciences.* Vienna, 2016. № 3-4. pp. 67-70.
5. Politaeva N., Kuznetsova T., Smyatskaya Y., et al. *Chlorella Microalga Biomass Cultivation for Obtaining Energy in Climatic Conditions of St. Petersburg.* In book: *International Scientific Conference Energy Management of Municipal Transportation Facilities and Transport EMMFT 2017, series: Advances in Intelligent Systems and*

562. DOI: 10.1007/978-3-319-70987-1_59.

6. Politaeva N., Kuznetsova T., Smyatskaya Y., et al. Impact of various physical exposures on *Chlorella Sorokiniana* microalgae cultivation. *International Journal of Applied Engineering Research*. 2017; 12 (21):11488-11492.

7. Sobgajda NA, Ol'shanskaya LN, Makarova YuA. Vliyanie modifitsirovaniya sheluhi pshenicy na ee sorbtsionnye svoystva k ionam Pb²⁺, Cd²⁺, Zn²⁺ i Cu²⁺. *Izvestiya vysshikh uchebnykh zavedenij. Seriya: Khimiya i khimicheskaya tekhnologiya*. 2010; 53(11):36-40. (In Russ).

8. Sobgajda NA, Ol'shanskaya LN, Makarova YuA. Ochistka stochnykh vod ot ionov tyazhelykh metallov s pomoshch'yu sorbentov—otodov derevoobrabatyvayushchej i sel'skohozyajstvennoj promyshlennosti. *Himicheskoe i neftegazovoe mashinostroenie*. 2009; № 9:43-45. (In Russ).

9. Sobgajda NA., Makarova YuA. Vliyanie prirody svyazuyushchego materiala na sorbtsionnye svoystva sorbentov, izgotovlennykh iz otodov agropromyshlennogo kompleksa. *Vestnik Saratovskogo gosudarstvennogo tekhnicheskogo universiteta*. 2011; 1(52):116-122. (In Russ).

10. Sobgajda NA, Olshanskaja LN, Makarova YA. Cleaning petroleum products from waste water with composite filters based on waste products. *Chemical and Petroleum Engineering*. 2010; 46(3):171-177. DOI: 10.1007/s10556-010-9313-x.

11. Sobgajda NA, Olshanskaja LN, Nikitina TV. Fiber and carbon materials for removing oil products from effluent. *Chemical and Petroleum Engineering*. 2008; 44(1):41-44. DOI: 10.1007/s10556-008-9011-0.

12. Politaeva N, Bazarnova J, et al. Impact of carbon dopants on sorption properties of chitosan-based materials. *Journal of Industrial Pollution Contro*. 2017; 33(2):1617-1621.

13. Olshanskaya AA, Sobgajda NA, Popova SS, et al. New materials for sorption of hydrogen. *Russian Journal of Applied Chemistry*. 2004; 77(9):1505-1509.

14. Taranovskaya EA, Sobgajda NA, Markina DV. Technology for Obtaining and Using Granulated Absorbents Based on Chitosan. *Chemical and Petroleum Engineering*. 2016; 52(5-6):357-361. DOI: 10.1007/s10556-016-0200-y.

15. Politaeva NA, Slugin VV, Taranovskaya EA, et al. Granulated sorption materials for waste waters purufucation from zink ions (Zn²⁺). *Izvestiya Vysshikh Uchebnykh Zavedenii, Seriya Khimiya i Khimicheskaya Tekhnologiya*. 2017; 60(7):85-90. (In Russ).

16. Taranovskaya EA, Sobgajda NA, Markina DV., et al. Technology for Obtaining and Using Granulated

Computing; 10–13 April 2017; Khabarovsk, Russia. Springer International Publishing, vol.692, 2018. pp.555-562

6. Politaeva N., Kuznetsova T., Smyatskaya Y., et al. Impact of various physical exposures on *Chlorella Sorokiniana* microalgae cultivation // *International Journal of Applied Engineering Research*, Vol. 12, No.21 (2017). pp. 11488-11492.

7. Собгайда Н.А. Ольшанская Л.Н., Макарова Ю.А. Влияние модифицирования шелухи пшеницы на ее сорбционные свойства к ионам Pb²⁺, Cd²⁺, Zn²⁺ и Cu²⁺ // *Известия высших учебных заведений. Химия и химическая технология*. 2010. Т.53, №11. С.36-40.

8. Собгайда Н.А., Ольшанская Л.Н., Макарова Ю.А. Очистка сточных вод от ионов тяжелых металлов с помощью сорбентов - отходов деревообрабатывающей и сельскохозяйственной отраслей промышленности // *Химическое и нефтегазовое машиностроение*. 2009. № 9. С.43-45.

9. Собгайда Н.А., Макарова Ю.А. Влияние природы связующего материала на сорбционные свойства сорбентов, изготовленных из отходов агропромышленного комплекса // *Вестник Саратовского государственного технического университета*. 2011. Т. 1, № 1 (52). С. 116-122.

10. Sobgajda N.A., Olshanskaja L.N., Makarova YA. Cleaning petroleum products from waste water with composite filters based on waste products // *Chemical and Petroleum Engineering*. 2010. Vol. 46, № 3. P. 171-177.

11. Sobgajda N.A., Olshanskaja L.N., Nikitina T.V. Fiber and carbon materials for removing oil products from effluent // *Chemical and Petroleum Engineering*. 2008. Vol. 44, №.1. pp. 41-44.

12. Politaeva N.A., Bazarnova J.G., et al. Impact of carbon dopants on sorption properties of chitosan-based materials // *Journal of Industrial Pollution Contro*. 2017. № 33 (2). pp. 1617-1621.

13. Olshanskaya A.A., Sobgajda N.A., Popova S.S., et al. New materials for sorption of hydrogen // *Russian Journal of Applied Chemistry*. 2004. Vol. 77, № 9. pp. 1505-1509.

14. Taranovskaya E.A., Sobgajda N.A., Markina D.V. Technology for Obtaining and Using Granulated Absorbents Based on Chitosan // *Chemical and Petroleum Engineering*. 2016. №52(5-6). pp. 357-361.

15. Politaeva N.A., Slugin V.V., Taranovskaya E.A., et al. Granulated sorption materials for waste waters purufucation from zink ions (Zn²⁺) // *Izvestiya Vysshikh Uchebnykh Zavedenii, Seriya Khimiya i Khimicheskaya Tekhnologiya*. 2017. 60(7). pp. 85-90.

16. Taranovskaya E.A., Sobgajda N.A., Markina

Absorbents Based on Chitosan. *Chemical and Petroleum Engineering*. 2016; 52(5-6):357-361. DOI: 10.1007/s10556-016-0200-y.

17. Абрютин А. А. и др. *Тепловой расчет котлов. Нормативный метод. ГОСТ 147-2013 Топливо твердое минеральное. Определение высшей теплоты сгорания и расчет низшей теплоты сгорания.* (In Russ).

D.V., et al. Technology for Obtaining and Using Granulated Absorbents Based on Chitosan // *Chemical and Petroleum Engineering*. 2016. 52(5-6). pp. 357-361.

17. Абрютин А.А. и др. *Тепловой расчет котлов. Нормативный метод. ГОСТ 147–2013 Топливо твердое минеральное. Определение высшей теплоты сгорания и расчет низшей теплоты сгорания.*

Authors of the publication

Evgeny L. Shaburov – Peter the Great St. Petersburg Polytechnic University, St. Petersburg, Russia

Oleg V. Derevianko – Peter the Great St. Petersburg Polytechnic University, St. Petersburg, Russia

Alexander V. Fedyukhin – National Research University Moscow Energy Institute, Moscow, Russia

Yulia A. Smyatskaya – Peter the Great St. Petersburg Polytechnic University, St. Petersburg, Russia

Natalia A. Politaeva – Peter the Great St. Petersburg Polytechnic University, St. Petersburg, Russia

Поступила в редакцию

February, 14 2019

ELECTRICAL ENGINEERING



UDC 621.313

DOI:10.30724/1998-9903-2019-21-3-4-107-115

STUDY OF THE REASONS AND PARAMETERS OF COMMON-MODE POWER OSCILLATIONS IN AUTONOMOUS ELECTRICAL COMPLEXES

A.E. Savenko, S.E. Savenko, P.S. Savenko

Kerch State Maritime Technological University, Kerch, Republic of Crimea, Russia
Savenko-70@mail.ru

Abstract: *The problem of the existence of common-mode and exchange power oscillations at the parallel operation of synchronous generators in autonomous electrical systems is considered. The methods of mathematical modeling were used to obtain the amplitude and period of common-mode oscillations in the whole possible range of settings of the object under study. A method has been developed for mapping the relationships between amplitude and period of common-mode power oscillations and transfer coefficients and rotation frequency setpoints of speed controllers of diesel generators. The use of such maps allows one to apply the method of eliminating exchange power oscillations, taking into account the possible occurrence of common-mode oscillations. Mapping the amplitude settings and the period of common-mode power oscillations makes it possible to understand the trends of amplitude and period of the common-mode power oscillations. It also helps to carry out an in-depth analysis of operation of an autonomous electrotechnical complex.*

Keywords: *exchange power oscillations, common-mode power oscillations, parallel operation, autonomous electric power equipment, generating unit, experimental research.*

For citation: Savenko A.E., Savenko S.E., Savenko P.S. Study of the reasons and parameters of common-mode fluctuations of power in autonomous electrical complexes. *Proceedings of the higher educational institutions. ENERGY SECTOR PROBLEMS*. 2019; 21(3-4):107-115. (In Russ). doi:10.30724/1998-9903-2019-21-3-4-107-115.

Introduction

The parallel operation of diesel generator units based on synchronous generators is the most commonly used mode of generating electrical energy in autonomous electrical engineering complexes [1, 2]. The advantages of such a layout are well known, which include the rational use of the generated electricity; ensuring the reliability of the power plant; operation of units with the highest efficiency; the ability to repair individual units, economy of fuel and the unit service life [3, 4]. To study the exchange power oscillations during parallel operation of diesel generator units, experimental studies were carried out at the ship-ferry Yeisk of the Kerch ferry [5, 6]. At the same time, common mode power oscillations were detected.

Figs. 1–4 show oscillograms of the generator currents for the running rowing engines, which receive power through the thyristor converters. These oscillograms show self-oscillatory processes of various amplitudes and periods. The form of these oscillations also has a different character. The oscillation amplitude reaches 100 %, and the period is 150–800 ms [6].

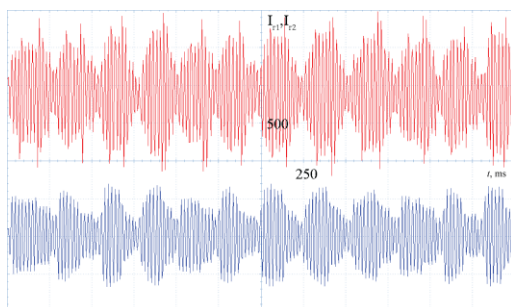


Fig. 1. Currents of parallel-running generators with rowing engines running (mode 1)

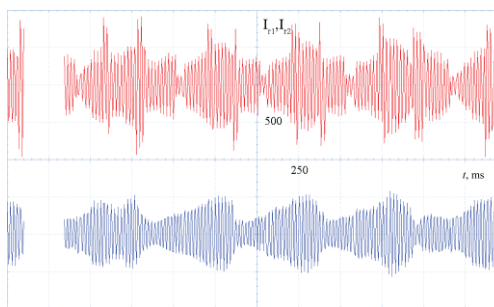


Fig. 2. Currents of parallel-running generators with rowing engines running (mode 2)

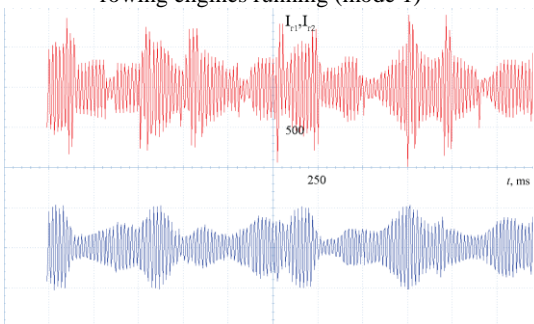


Fig. 3. Currents of parallel-running generators with rowing engines running (mode 3)

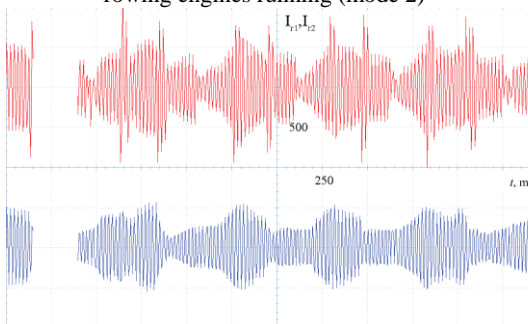


Fig. 4. Currents of parallel-running generators with rowing engines running (mode 4)

The results of the research revealed that the amplitude of the exchange power oscillations of the parallel-running diesel generator depends on the backlash clearances in the rotational speed control loops [6, 7]. A method has been developed for constructing maps of relationship between amplitude of exchange power oscillations and the backlash clearance [8]. It is necessary to carry out similar work with respect to common-mode oscillations.

Methods

To study the causes and nature of common-mode power oscillations during operation of a power plant of an autonomous electrotechnical complex, a mathematical model is used [9, 10], which allows one to construct graphs of instantaneous values of the main parameters of the parallel-running diesel generators.

The mathematical model uses the equation of a diesel engine, which is the driving engine of a generating unit, in a simplified form:

$$J_m \frac{d\omega_r}{dt} = M_d - M_g;$$

$$M_d = K_m h; M_g = \Psi_{sq} i_{sd} - \Psi_{sd} i_{sq},$$

where J_m is the reduced moment of inertia of the diesel engine shaft and the generator rotor; M_d is mechanical torque of a diesel engine; M_g is electromagnetic moment of resistance gained by the generator; h is the position of the fuel rail; K_m is diesel engine amplification frequency.

A separate equation describes the diesel engine speed controller, which is represented by an aperiodic link of the first order:

$$T_\omega \frac{dh}{dt} = K_\omega U_\varepsilon - h,$$

where T_ω is the time constant of the actuator; K_ω is transmission coefficient (gain) of the controller; U_ε is the error signal between the set ω_{r0} and the actual ω_r rotation frequencies of the diesel engine.

For mathematical description of the backlash with a gap in the control circuit of rotation frequency of a diesel engine, we use the following expression:

$$U_\varepsilon = \begin{cases} U_\varepsilon = \text{const for } |U_\varepsilon - k\varepsilon| \leq D_n \\ k\left(\varepsilon - D_n \text{sign}\left(\frac{dU_\varepsilon}{dt}\right)\right) \text{ for } \frac{dU_\varepsilon}{dt} \neq 0 \end{cases},$$

where k is transmission coefficient; D_n is backlash gap; ε is mismatch between the set ω_{r0} and the actual ω_r rotation speeds of the diesel engine.

Thus, each diesel generator unit involved in parallel operation has an automatic rotation speed controller with two main variable parameters: transmission coefficient K_ω and rotation speed setpoint [11] ω_{r0} , as well as backlash with a gap D_n .

The main objective of the study is to find an answer to the question: is there a connection between the setpoints and parameters of the rotational speed control loops of diesel generator units and common-mode power oscillations during parallel operation. It is also important to understand that the amplitude and period of common-mode oscillations depend on and to systematize the obtained results since the results of field experiments prove their variability.

The mathematical model makes it possible to analyze the common-mode power oscillations that occur when two synchronous generators of an autonomous electrotechnical complex are operating in parallel in quasi-steady-state modes.

When conducting research, we will take the range of change for the controller transmission coefficient K_ω from 10 to 200, for the setpoints for the controllers rotation frequency ω_{r0} from 0,9 to 1,1, which correspond to a stable parallel operation of the generating units. It is necessary to take into account the backlash, as, during experimental studies on the ferry Yeisk, the connection between exchange and common-mode power fluctuations became clear, and this is important when implementing measures and means to eliminate the exchange fluctuations to ensure high-quality stable parallel operation of generators. We introduce into the mathematical model the gaps of backlashes of the rotation speed controlling contours of diesel generators, respectively $D_{n1} = 0,002$ and $D_{n2} = 0,01$. To eliminate the influence of transients on the results, we choose a time range from 12 to 15 seconds, which obviously corresponds to a quasi-established mode of operation.

The simulation results confirm the existence of common-mode power oscillations and allow us to determine their amplitude and period. For this purpose, we will use the currents $IA1$, $IA2$ of parallel-running generators.

Results

Mathematical modeling of parallel operation of diesel generator units, the transmission coefficients of which are not equal, confirmed the assumption on occurrence of common-mode oscillations for this operation mode (Fig. 5).

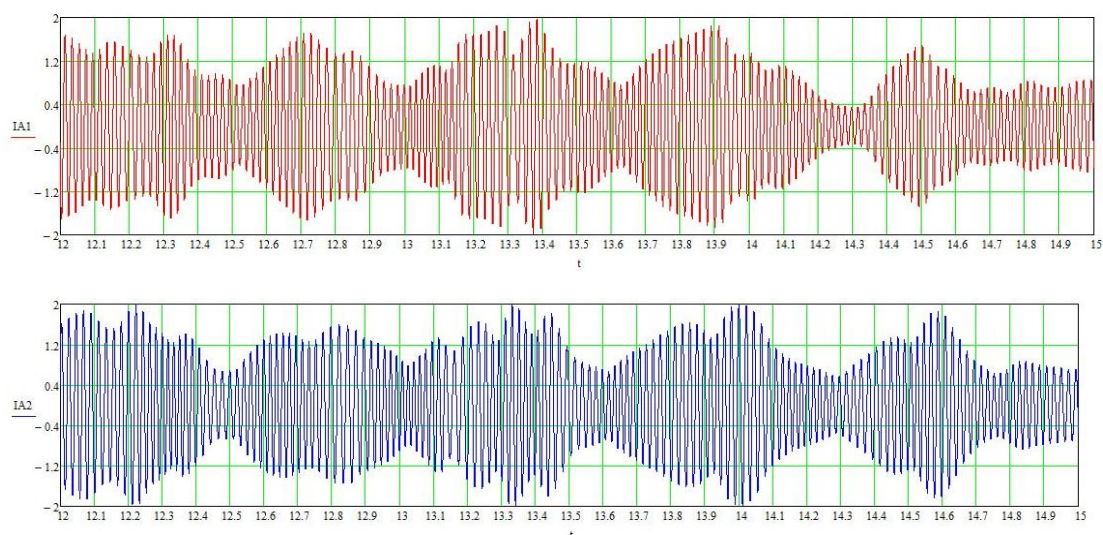


Fig. 5. Modeling results $D_{n1}=0,002$; $D_{n2}=0,01$; $K_{\omega1}=40$; $K_{\omega2}=80$; $\omega_{r01}=1$; $\omega_{r02}=1$.

$IA1, IA2$ are currents of parallel-running generators

Moreover, the selective modeling made it possible to think that the amplitude of oscillations increases with the increase in the difference between controllers transmission coefficients of the parallel-running diesel generator units. The clarity of nature of the relationship between common-mode oscillations and the ratio of transmission coefficients of frequency controllers appeared after modeling the entire field of possible setpoint ratios (Tables 1, 2) and construction of graphical visualization of the obtained results in the form of a setpoint map (Fig. 6, 7). It should be noted that for equal gain factors, there are no common-mode oscillations, and the results obtained in the tables correspond to the amplitudes of the exchange power oscillations. This is the main diagonal of the tables from left to right from top to bottom.

Also, during mathematical modeling, we detected the impact of difference in rotation frequency setpoints of the rotation frequency controllers of parallel-running generating units on the occurrence of common-mode power oscillations (Fig. 8).

Table 1

The relationship between amplitude of common-mode power oscillations of the first diesel generator and the frequency controller gain

$K_{\omega1}/K_{\omega2}$	10	20	40	60	80	100	120	140	160	180	200
10	0,01	1,1	1	0,9	0,75	1,1	0,3	0,25	0,25	0,25	0,25
20	0,95	0,01	1,1	1	1,1	0,85	1,1	1,1	0,8	0,85	0,85
40	0,9	0,85	0,05	0,9	1,05	1,5	1,1	1,25	1,05	1,1	1,05
60	1,1	0,85	1,1	0,05	0,3	0,9	0,7	0,95	1	0,95	1,05
80	0,95	1	0,8	0,2	0,05	0,2	0,9	1,2	0,9	1,2	1,1
100	0,7	0,9	1,2	1	0,25	0,05	0,16	0,8	1,05	0,8	1,25
120	0,55	0,75	1,1	0,9	0,9	0,15	0,06	0,13	1,25	0,8	1,3
140	0,75	1,2	1,1	0,9	0,9	0,22	0,15	0,06	0,13	0,7	1,1
160	1,1	1,2	1,2	0,9	0,9	0,75	0,3	0,12	0,06	0,11	0,65
180	1,1	1,2	1,2	1,05	1,05	0,75	0,7	0,23	0,14	0,06	0,1
200	1,1	1	0,9	1,05	1,1	0,75	0,7	0,6	0,2	0,13	0,07

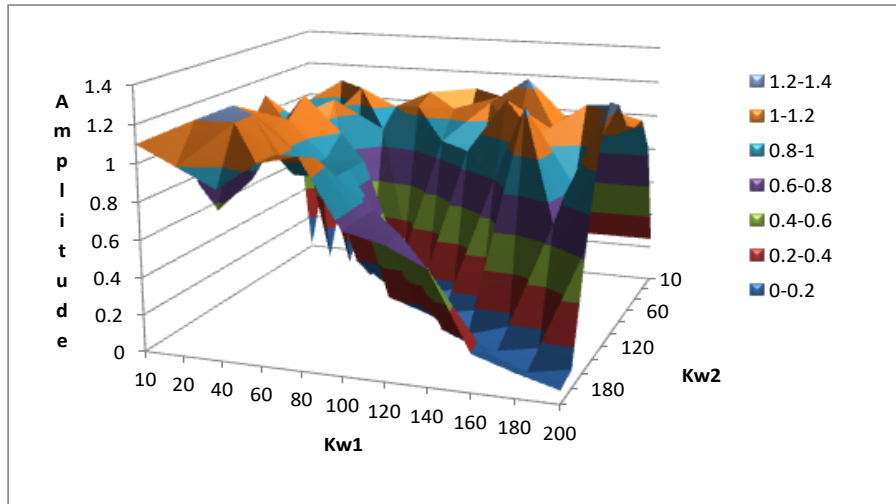


Fig. 6. Map of relationship between the amplitude of common-mode oscillations of the first diesel generator and gain coefficients of frequency controller, $K_{\omega 1}$ and $K_{\omega 2}$ are controller gain coefficients of the first and the second parallel-running diesel generators, respectively

Table 2

Relationship between amplitude of the common-mode power oscillations of the second diesel generator and frequency controller gain

$K_{\omega 1} / K_{\omega 2}$	10	20	40	60	80	100	120	140	160	180	200
10	0,01	1,2	1	0,9	0,9	1,2	0,5	0,45	0,4	0,3	0,3
20	1	0,01	0,9	1	1	1	1,1	0,95	0,8	0,75	0,9
40	0,8	0,65	0,05	1	1,1	0,9	1,2	1,2	1,35	1	1,2
60	1,1	0,95	0,95	0,05	0,3	0,9	0,7	0,95	0,95	1,05	1,1
80	1	1	0,8	0,25	0,05	0,25	0,7	1,1	0,9	1	1,3
100	0,6	0,7	1,1	1,1	0,2	0,05	0,22	0,8	0,8	0,6	1,1
120	0,4	1	1,2	1	1,1	0,1	0,06	0,17	1,1	0,8	1,2
140	0,6	1,1	1,2	0,9	0,95	0,22	0,08	0,06	0,17	0,7	1,05
160	1,2	1	1,2	0,7	0,8	0,6	0,25	0,09	0,06	0,17	0,6
180	1,1	1,2	1,05	1,1	1,2	0,75	0,7	0,2	0,07	0,06	0,14
200	1	1,05	0,95	1,05	1,05	0,75	0,7	0,6	0,15	0,06	0,07

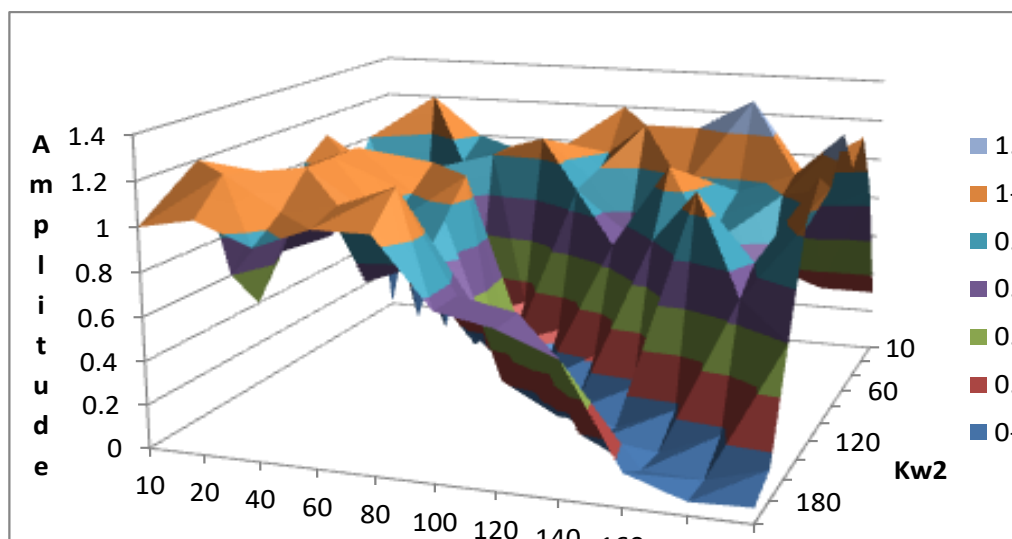


Fig. 7. Map of relationship between the amplitude of common-mode oscillations of the second diesel generator and the gain coefficients of frequency controller, K_{ω_1} and K_{ω_2} are controller gain coefficients of the first and the second parallel-running diesel generators, respectively



Fig. 8. Results of modeling: $D_{n1}=0,002$; $D_{n2}=0,01$; $K_{\omega_1}=50$; $K_{\omega_2}=50$; $\omega_{r01}=1,04$; $\omega_{r02}=0,94$. IA1, IA2 are currents of the parallel-running generators

Moreover, the selective modeling gave reason to think that the period of common-mode oscillations decreases with an increase in the difference in speed settings. Clarity of the nature of dependence of common-mode oscillation parameters on the ratio of setpoints for the frequency of rotation of frequency controllers appeared after modeling the entire field of possible setpoints ratios (table 3) and construction of graphical visualization of the results in the form of a setpoint map (Fig. 9). It should be noted that at equal rotation frequency setpoints there are no common-mode oscillations, and the results in the table correspond to the period of exchange power

oscillations. This is also the main diagonal of the table from left to right from top to bottom. According to the modeling results, the common-mode power oscillations periods can be considered identical for both generating sets.

Table 3

Relationship between period of common-mode power oscillations and setpoint of frequency controller speed

$\omega_{r01}/\omega_{r02}$	0,9	0,92	0,94	0,96	0,98	1	1,02	1,04	1,06	1,08	1,1
0,9	0,55	0,4	0,5	0,4	0,5	0,4	0,15	0,1	0,1	0,1	0,1
0,92	0,4	0,55	0,4	0,5	0,4	0,5	0,4	0,15	0,15	0,15	0,1
0,94	0,45	0,4	0,55	0,4	0,5	0,4	0,5	0,4	0,15	0,15	0,15
0,96	0,4	0,5	0,4	0,55	0,4	0,5	0,4	0,5	0,4	0,15	0,15
0,98	0,5	0,4	0,5	0,45	0,55	0,4	0,5	0,4	0,5	0,4	0,15
1	0,45	0,5	0,4	0,5	0,4	0,55	0,4	0,5	0,4	0,5	0,4
1,02	0,15	0,4	0,5	0,4	0,5	0,4	0,55	0,4	0,5	0,4	0,5
1,04	0,1	0,15	0,4	0,5	0,4	0,5	0,4	0,55	0,45	0,5	0,4
1,06	0,1	0,15	0,15	0,4	0,5	0,4	0,5	0,45	0,55	0,4	0,5
1,08	0,1	0,15	0,15	0,15	0,4	0,5	0,4	0,5	0,4	0,55	0,4
1,1	0,1	0,1	0,15	0,15	0,15	0,4	0,5	0,4	0,5	0,4	0,55

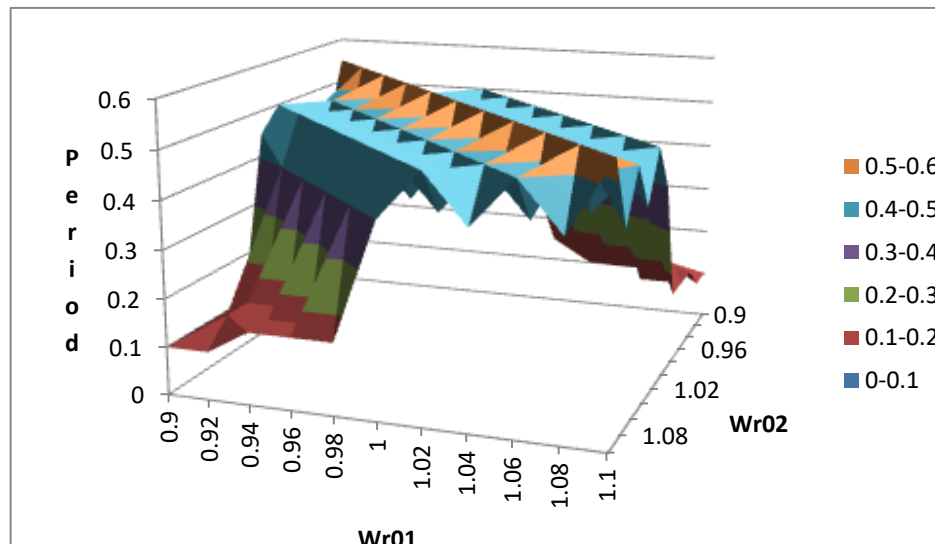


Fig. 9. Map of relationship between common-mode power oscillations period of diesel-generators and setpoints of frequency controller speed. ω_{r01} and ω_{r02} are setpoints of controller frequency of the first and second parallel-running diesel generators, respectively

Discussion

The research showed that common-mode power oscillations at parallel operation of diesel generator units can appear as a result of unequal settings of transmission coefficients and setpoints of controller rotation frequency. At the beginning of deviation of the transfer coefficients from equal values, an increase in the amplitude of common-mode oscillations is observed. When certain limit values are reached, the amplitude begins to oscillate around these values (see Fig. 6, 7). The amplitude of common-mode oscillations significantly exceeds the amplitude of the exchange power oscillations with the same backlash gaps. It should be noted that the amplitude of common-mode oscillations of the parallel-running generator, for which the controller transmission coefficient is more, is also greater. This is due to the fact that this

generator will take on more load. However, the difference in load cannot be significant in terms of parallel operation of generating units of equal power, and, consequently, the amplitudes of common-mode oscillations do not differ much, usually the difference is no more than 10–15%.

When the frequency setpoints deviate from equal values, common-mode oscillations are observed, whose amplitude does not change, and the period decreases slightly in some limits, and then there is a rapid decrease and stabilization at values several times smaller (see Fig. 9).

The obtained maps, in addition to general information, describe in detail the common-mode power oscillations for 6VD26/20-AL-2 diesel generators with S450MG 800 kVA generators and can be useful to specialists who operate and set up such units. Similar studies aimed at construction of maps of dependence of the common-mode power oscillations parameters on the transmission coefficient settings and the setpoints for the controllers rotation frequency can be performed for any diesel generator units.

Conclusions

The obtained results are the evolution of work [6], aimed at the study of power oscillations during the parallel-running of diesel generator units as part of autonomous electrical systems. The developed method for construction maps of dependence of amplitude and period of common-mode power oscillations on transfer coefficients and setpoints for the controller rotation frequency can significantly improve the quality of parallel operation of diesel generator units. The algorithm for eliminating the exchange power oscillations is based on the change of the transfer coefficients and setpoints for the controller rotation frequency. Taking into account the obtained results, in order to preserve the stable operation of the autonomous electrotechnical complex, the change in settings of the frequency controllers for parallel operating units must be performed synchronously. The time for changing the settings of the driven units must be an order of magnitude shorter than that for the driving diesel generator [12]. Mapping the amplitude and period of common-mode power oscillations together with the amplitude settings of the exchange power oscillations depending on the backlash clearances allows obtaining an in-depth analysis of the operation of the autonomous electrical complex.

References

1. Lezhnyuk PD, Nikitorovich OV, Netrebskiy VV. Optimization of partition of load between the dispersed energy sources in the in-plant electric system. *Tekhnichna elektrodinamika*. 2012; 2:38-39. (In Ukraine).
2. Gracheva EI, Sadykov RR. The study of probabilistic characteristics of power supply systems. *Proceedings of the higher educational institutions. Energy sector problems*. 2014; 3–4:109-114. (In Russ).
3. Gracheva EI, Ilyasov II, Alimova AN. The comparative analysis and research of methods of calculation of losses of the electric power in the systems of electrical power supply of the industrial enterprises. *Power engineering: research, equipment, technology*. 2018; 20(3-4):62-71. DOI: doi.org/10.30724/1998-9903-2018-20-3-4-62-71. (In Russ.)
4. Nizamiev M.F., Ivshin I.V., Vladimirov O.V., et al. Izmeritel'no-diagnosticheskiy kompleks dlya diagnostiki energeticheskikh ustanovok. *Proceedings of the higher educational institutions. Energy sector problems*. 2014; 3-4:109-114. (In Russ).
5. Khvatov OS, Dar'Enkov AB. Power plant based on variable-speed diesel generator. *Russian Electrical*

Литература

1. Лежнюк П.Д., Никиторович А.В., Нетребский В.В. Оптимизация распределения нагрузки между рассредоточенными источниками энергии в локальной электрической системе // *Технічна електродинаміка*. 2012. № 2. С. 38-39.
2. Грачева Е.И., Садыков Р.Р. Исследование вероятностных характеристик систем электроснабжения // *Известия высших учебных заведений. Проблемы энергетики*. 2017. Т.19, № 1-2. С. 95-101.
3. Грачева Е.И., Ильясов И.И., Алимова А.Н. Сравнительный анализ и исследование методов расчета потерь электроэнергии в системах электроснабжения промышленных предприятий // *Известия высших учебных заведений. Проблемы энергетики*. 2018. Т.20, № 3-4. С. 62-71.
4. Низамиев М.Ф., Ившин И.В., Владимиров О.В., и др. Измерительно-диагностический комплекс для диагностики энергетических установок // *Известия высших учебных заведений. Проблемы энергетики*. 2014. № 3–4. С. 109-114.
5. Хватов О.С., Дарьенков А.Б. Электростанция на

Engineering. 2014; 85(3):145-149.

6. Savenko AE, Golubev AN. *Obmennyye kolebaniya moshchnosti v sudovykh elektrotekhnicheskikh kompleksakh*. Ivanovo: Ivanovskiy gosudarstvennyy energeticheskiy universitet imeni V.I. Lenina, 2016. (In Russ).

7. Pyrhonen J, Jokinen T, Hrabovcov'a V. *Design of Rotating Electrical Machines*. John Wiley & Sons, Inc., Wiltshire; 2008.

8. Savenko A.E., Savenko P.S. Influence of backlash on amplitude of exchange power fluctuations in autonomous electric power equipment. *Power engineering: research, equipment, technology*. 2018; 20(5-6):46-54. DOI: doi.org/10.30724/1998-9903-2018-20-5-6-46-54. (In Russ.)

9. Savenko A.E. Matematicheskaya model' sudovogo elektrotekhnicheskogo kompleksa. *Vestnik IGEU*. 2015; 5:54-59. (In Russ.)

10. Golubev AN, Martynov VA, Alejnikov AV. Matematicheskaya model' dlya rascheta elektromagnitnykh sil v sinkhronnom elektroprivoде s postoyannymi magnitami. *Vestnik IGEU*. 2015; 1:10-13. (In Russ.)

11. Reimert D. *Protective relaying for power generation systems*. Taylor and Francis Group, LLC. 2006.

12. Voronin AI, Tyutikov VV. Procedure for the synthesis of controllers for independent formation of static and dynamic parameters of nonlinear objects. *Izvestiya sfedu. Engineering sciences*. 2015; 3(164):154-164. (In Russ).

базе дизель-генератора переменной частоты вращения // Электротехника. 2014. № 3. С. 28-32.

6. Савенко А.Е., Голубев А.Н. Обменные колебания мощности в судовых электротехнических комплексах. Иваново: Ивановский государственный энергетический университет имени В.И. Ленина, 2016. 172 с.

7. Pyrhonen J., Jokinen T., Hrabovcov'a V. *Design of Rotating Electrical Machines*. John Wiley & Sons, Inc., Wiltshire; 2008. 531 p.

8. Савенко А.Е., Савенко П.С. Влияние люфта на амплитуду обменных колебаний мощности в автономных электротехнических комплексах // Известия высших учебных заведений. Проблемы энергетики. 2018. Т. 20, № 5-6. С. 46-54.

9. Савенко А.Е. Математическая модель судового электротехнического комплекса // Вестник ИГЭУ. 2015. № 5. С. 54-59.

10. Голубев А.Н., Мартынов В.А., Алейников А.В. Математическая модель для расчета электромагнитных сил в синхронном электроприводе с постоянными магнитами // Вестник ИГЭУ. 2015. № 1. С. 10-13.

11. Reimert D. *Protective relaying for power generation systems*. Taylor and Francis Group, LLC. 2006. 545 p.

12. Воронин А.И., Тютиков В.В. Методика синтеза регуляторов для независимого формирования статических и динамических показателей нелинейных объектов // Известия ЮФУ. Технические науки. 2015. № 3(164). С. 154-164.

Authors of the publication

Alexandr E. Savenko – PhD in Engineering sciences, Associate Professor, Department «Electrical Equipment of Ships and Industrial Automation». E-mail: Savenko-70@mail.ru.

Stanislav E. Savenko – Master's Degree student in «Electrical power engineering and electrical engineering», Kerch State Maritime Technological University.

Pavel S. Savenko – marine faculty cadet, Kerch State Maritime Technological University.

Received

February, 19 2019



THE STOCHASTIC FORMULATION OF THE STEPHAN ROBLEM IN HYPERBOLIC REPRESENTATION

E.M. Kartashov¹, I.A. Soloviev²

¹ Moscow State University of thin chemical technologies of M.V. Lomonosov,
Moscow, Russia

e-mail: kartashov@mihht.ru

²State University of Land Use Planning, Moscow, Russia

e-mail: igorsoloviev@inbox.ru

Abstract: *The presented work offers the stochastic description of the Stephan problem on the basis of a deterministic model in hyperbolic representation. This description is based on the generalized Fokker-Planck-Kolmogorov equation. The basic thesis of this work is that the determined equalizations and their solutions are the average values of the stochastic Stephan problem model. This work considers the problem of phase transition front deformation. The research is performed using the introduced position of stability on solutions dispersion for average values. The conclusion of this study is that Markov diffusion coefficient results in a significant distortion of the originally flat front of the phase boundary.*

Keywords: *Stefan problem, hyperbolic equation of heat conduction, generalized Fokker-Planck-Kolmogorov equation, stability of solutions of differential equations, deformation of phase transition front.*

For citation: Kartashov E.M., Soloviev I.A. The stochastic formulation of the Stephan's roblem in hyperbolic representation. *Proceedings of the higher educational institutions. ENERGY SECTOR PROBLEMS*. 2019; 21(3-4):116-126. (In Russ). doi:10.30724/1998-9903-2019-21-3-4-116-126.

Introduction

We list the problems related to deterministic description of thermal conductivity during phase transformations. The first problem concerning deterministic Fourier model and the classical Stefan problem [1] is in infinity of propagation velocity of initial temperature perturbations, as well as in infinity of initial velocity of the phase boundary movement. The second problem is that the deterministic model did not describe the time dependent deformation of the originally flat form of the phase transition.

The study of effects in fast-flowing manifestations of heat conduction goes back to the works of Maxwell–Cattaneo–Lykov described in [2, 3]. These papers describe the generalized Fourier law:

$$\partial \bar{q}(x, y, z, t) / \partial x = -\lambda \text{grad} T(x, y, z, t) - \tau_r \partial q(x, y, z, t) / \partial t, \quad (1)$$

which takes into account the final rate of heat propagation. Here (x, y, z) are the spatial

coordinates; t is time coordinate; \bar{q} is heat flow density; T is temperature; λ is coefficient of thermal conductivity; a is coefficient of thermal diffusivity; τ_r is heat flow relaxation time, which is connected with the rate of heat propagation v_T by the ratio $v_T = \sqrt{a/\tau_r}$. Expression (1) has a simple physical meaning: when a temperature gradient occurs, it takes some time to establish the heat flow, when $\text{grad}T = 0$ the heat flow does not disappear instantaneously, but decays with the relaxation time. After analyzing the generalized problem of heat conduction for a half-space, the boundary temperature of which changes at the initial moment of time by a certain amount, remaining further constant, A.V. Lykov gave a substantiation of the physical meaning of the final velocity of heat propagation, which is a time derivative of the depth of heat penetration. Expression (1) is reduced to a deterministic transfer equation of the hyperbolic type:

$$\begin{aligned} \partial T(M, t) / \partial t = a \Delta T(M, t) - \tau_r \partial^2 T(M, t) / \partial t^2 + \\ + (\tau_r / (c\rho)) \left[\partial F(M, t) / \partial t + (1 / \tau_r) F(M, t) \right], \quad M \in D, \quad t > 0 \quad (2) \end{aligned}$$

and the corresponding boundary problems of heat conduction for equation (2) in *generalized form*. Generalized transfer problems are significantly different from the classical ones, being more complex when finding analytical solutions to these problems. This results in very insignificant progress in finding exact analytical solutions of boundary problems for equation (2). As it will be shown below, these analytical values are involved in dispersion formation. At the same time, it is necessary to note considerable attention to the Stefan problem from physicists studying the impact of laser radiation on matter [5–9].

In this paper, we present a description of the random behavior of highly non-stationary heat conduction using the generalized Fokker-Planck-Kolmogorov equation (hereinafter FPK) for probability density (hereinafter PD), from which the problem statements for the hyperbolic heat equation are obtained. The novelty lies in the fact that stochastic formulations of the Stefan type for hyperbolic thermal conductivity have so far been absent. The bibliography and the main ideas of such a stochastic description of heat conduction problems are presented in [2, 3]. The basic statement is as follows: the solution of a deterministic problem is the average value of its stochastic analog. The urgency of the problem lies in the fact that the deterministic task does not allow to identify the features that arise as a result of taking into account the random external influence on the described phenomena. In [3], it was shown how dispersion can significantly change the understanding of the conclusions which follow from the analysis of deterministic solutions to the problems posed. The study of the temporal behavior of dispersion made it possible to obtain the effect of dispersion decrease described in [3] at initial times. This effect makes it possible to plan experiments related to phase transitions. Here we will consider analysis of dispersion with a powerful pulsed thermal impact on the substance.

Stochastic model of the Stefan problem, which takes into account the finite rate of heat transfer

A stochastic model of the classical Stefan problem, based on the generalized FPK equation connected with the parabolic heat equation, was proposed in [3]. We give the formulation of this problem. First, we introduce the notations for the stochastic description of the Stefan problem, taking into account the finite rate of heat transfer. We denote by $P_1(x, t, \Omega)$ the probability density in the spatial domain $0 \leq x \leq M_y^{(1)}(t)$ (solid phase), and by $P_2(x, t, \Omega)$ the probability density in the spatial domain $x \geq M_y^{(1)}(t)$ (liquid phase), where $M_y^{(1)}(t)$ is average velocity of the interface; t is time; x is spatial coordinate; Ω is random characteristic of the temperature field in both areas. We also denote the average values as $M_{Ti}^{(1)}(x, t) = \int_{-\infty}^{+\infty} \Omega P_i(x, t, \Omega) d\Omega \quad (i = 1, 2)$; the

second order moment as $M_{Ti}^{(2)}(x, t) = \int_{-\infty}^{+\infty} \Omega P_i(x, t, \Omega) d\Omega$, ($i = 1, 2$); dispersion as $D_{Ti}(x, t) = \int_{-\infty}^{+\infty} \Omega^2 P_i(x, t, \Omega) d\Omega - \left(\int_{-\infty}^{+\infty} \Omega P_i(x, t, \Omega) d\Omega \right)^2$ ($i = 1, 2$). We also introduce the notation for PD, describing random processes occurring at the phase interface: $P_y(t, \Theta)$, here Θ is the random characteristic of processes which determine the behavior of phase interface. We denote the mean value of the time dependence of the phase boundary motion law by $M_y^{(1)}(t) = \int_{-\infty}^{+\infty} \Theta P_y(t, \Theta) d\Theta$, and dispersion by $D_y(t) = \int_{-\infty}^{+\infty} \Theta^2 P_y(t, \Theta) d\Theta - \left(\int_{-\infty}^{+\infty} \Theta P_y(t, \Theta) d\Theta \right)^2$. The Markov diffusion coefficient for random manifestations at the boundary is denoted as B_Θ . The FPK equation for PD describing a random thermal field in the solid state region is

$$\begin{aligned} \partial P_1(x, t, \Omega) / \partial t = -\partial(A_1(x, t, \Omega)P_1(x, t, \Omega)) / \partial \Omega + 0,5B_\Omega \partial^2 P_1(x, t, \Omega) / \partial \Omega^2, \\ 0 < x < M_y^{(1)}(t), \quad t > 0, \quad \Omega \in (-\infty < +\infty). \end{aligned} \quad (3)$$

Here

$$A_1(x, t, \Omega) = \Omega(a_1 \partial^2 M_{T1}^{(1)}(x, t) / \partial x^2 - \tau_r \partial^2 M_{T1}^{(1)}(x, t) / \partial t^2) / M_{T1}^{(1)}(x, t).$$

The drift coefficient has a similar form $A_2(x, t, C)$:

$$\begin{aligned} \partial P_2(x, t, \Omega) / \partial t = -\partial(A_2(x, t, \Omega)P_2(x, t, \Omega)) / \partial \Omega + 0,5B_\Omega \partial^2 P_2(x, t, \Omega) / \partial \Omega^2, \\ M_y^{(1)}(t) < x < +\infty, \quad t > 0, \quad \Omega \in (-\infty < +\infty), \end{aligned}$$

where B_Ω is the Markov diffusion coefficient; a_i ($i = 1, 2$) are thermal diffusivity coefficients in the regions corresponding to the normalization condition $\int_{-\infty}^{+\infty} P_i(x, t, \Omega) d\Omega = 1$, $t \geq 0$, $x \in (0, +\infty)$ and conditions at infinity $P_i(x, t, \pm\infty) = 0$.

Of course, the classical Stefan problem cannot claim to describe the fast-flowing effects. There is a difference between the slow-flowing formation of ice in natural phenomena and melting, when a substance undergoes a short-term thermal shock effect. Although, we note, even in such a stochastic formulation of the classical Stefan problem, the effect of the “strange” dispersion behavior was revealed in [5]. The essence of the effect is as follows. At the initial time moment, the regular component of dispersion is zero and up to the time moment $t = 1/e$ (time units) it decreases, reaching a minimum equal to $\min \operatorname{Re} g(1/e) = -B_\Theta/e$. This means that at this time interval there is resistance to changing the shape of the phase transition front. We called this phenomenon *the effect of striving to preserve the original form of the phase transition front*. After the time moment $t = 1/e$ (time units), this resistance weakens and stops at the time moment $t = 1$ (time units), when $\min \operatorname{Re} g(1) = 0$. After this, the phase of active distortion of phase transition front begins.

This seemingly insignificant effect, due to the smallness of the Markov diffusion coefficient B_Θ and time $t = 1/e$ (time units), may be important for thin technological processes, when it is required to preserve the initial planar shape of either the grown crystal or the planar shape of a solid body as long as possible under other thermal impacts, not necessarily having the nature of phase transformations, for example when applying nanocoatings. Knowing how the dispersion D_y changes over time, one should stepwisely conduct the technological process,

starting from time moment $t = 0$ up to $t = 1/e$ (time units). Then make a stop, then start again, and periodically repeat this procedure many times. In this case, unnecessary random effects will be neutralized, which contribute to the distortion of flat shape of a solid body exposed to external and internal random effects.

In this paper, we study one of the variants of stochastic formulation for the PD problem of the Stefan type.

We present the following problem statement for PD. We assume that a powerful thermal impulse affects a substance when its duration $1/\alpha$ is comparable with the time of thermal relaxation τ_r . We also assume that a fixed boundary is exposed to radiation with heat flow capacity equal to $q_0 \exp[-\alpha t]$, and a heat flow of capacity equal to $q_1 \exp[-\alpha t]$, where $q_1 > q_0$. acts on a moving boundary. The stochastic formulation of the problem for PD on the fast-flowing process of heat conduction with a pulsed effect of powerful radiation on a substance has the following form:

$$\begin{aligned} \partial P(x, t, \Omega) / \partial t &= -\partial(A_T(x, t, \Omega)P(t, x, \Omega)) / \partial \Omega + 0,5B_{\Theta} \partial^2 P(x, t, \Omega) / \partial \Omega^2, \\ 0 < x < M_y^{(1)}(t), t > 0, \Omega &\in (-\infty < +\infty). \end{aligned} \quad (4)$$

Here:

$$A_T(x, t, C) = \Omega P_T(x, t, \Omega)(a_1 \partial^2 M_T^{(1)}(x, t) / \partial x^2 - \tau_r \partial^2 M_T^{(1)}(x, t) / \partial t^2) / M_T^{(1)}(x, t) \quad (5)$$

$$P_T(0, t, \Omega) = \varphi_{\text{Трпн}}(t, \Omega), \Omega \in (-\infty, +\infty), 0 < t < +\infty. \quad (6)$$

$$\begin{aligned} -\lambda \partial P_T(x, t, \Omega) / \partial x \Big|_{x=M_y^{(1)}(t)} &= \\ &= -\partial(\Omega L \rho (dM_y^{(1)}(t) / dt + \tau_r d^2 M_y^{(1)}(t) / dt^2 + \end{aligned} \quad (7)$$

$$\begin{aligned} + q_1 \exp[-\alpha t]) P_T(M_y^{(1)}(t), t, \Omega) / M_T^{(1)}(M_y^{(1)}(t), t) / \partial \Omega + \\ + 0,5B_{\Theta} \partial^2 P_T(M_y^{(1)}(t), t, \Omega) / \partial \Omega^2, x = M_y^{(1)}(t), t > 0, \Omega \in (-\infty; +\infty). \end{aligned}$$

$$P_T(x, 0, \Omega) = \varphi_{\text{Тини}}(x, \Omega), 0 \leq x \leq M_y^{(1)}(0), \Omega \in (-\infty, +\infty). \quad (8)$$

$$\partial P_T(x, t, \Omega) / \partial t \Big|_{t=0} = 0, t \geq 0, \Omega \in (-\infty, +\infty). \quad (9)$$

$$M_y(0) = M_{y0} = \text{const}. \quad (10)$$

$$dM_y(t) / dt \Big|_{t=0} = \tilde{M}_{y0} = \text{const}. \quad (11)$$

Comparative analysis of the mathematical expectations of the hyperbolic and parabolic models of the Stefan problem

The task for the mathematical expectation corresponding to the problem (4) - (11) has the following form [8]:

$$\tau_r \partial^2 M_T^{(1)}(x, t) / \partial t^2 + \partial M_T^{(1)}(x, t) / \partial x = a \partial^2 M_T^{(1)}(x, t) / \partial x^2, \quad (12)$$

$$0 < x < M_y^{(1)}(t), t > 0.$$

$$M_T^{(1)}(0, t) = M_{T0}^{(1)}(0, t), t > 0. \quad (13)$$

$$\lambda \partial M_T^{(1)}(0, t) / \partial x = q_0 \exp[-\alpha t], t > 0. \quad (14)$$

$$-\lambda \partial M_T^{(1)}(M_y^{(1)}(t), t) / \partial x = \tau_r L \rho d^2 M_y^{(1)} / dt^2 + L \rho d M_y^{(1)} / dt + q_1 \exp[-\alpha t], t > 0. \quad (15)$$

$$M_y^{(1)}(0) = M_{y0}^{(1)} = \text{const}. \quad (16)$$

$$dM_y^{(1)}(t) / dt|_{t=0} = 0. \quad (17)$$

The following functions satisfy equations (12)–(17)

$$M_T^{(1)}(x, t) = M_{T0}^{(1)}(0, t) + q_0 \exp[-t / \tau_r] \sin(x \sqrt{\alpha(1 - \tau_r \alpha) / a}) / (\lambda \sqrt{\alpha(1 - \tau_r \alpha) / a}). \quad (18)$$

At $\alpha = 1 / \tau_r$, expression (18) is transformed to the form:

$$M_T^{(1)}(x, t) = M_{T0}^{(1)}(0, t) + q_0 \exp[-t / \tau_r] x / \lambda. \quad (19)$$

By substituting (19) into (20), we obtain the expression

$$\begin{aligned} -\lambda \partial M_T^{(1)}(M_y^{(1)}, t) / \partial x &= d^2 M_y^{(1)} / dt^2 + dM_y^{(1)} / dt = \\ &= -(1 / (\tau_r L \rho))(q_1 - q_0) \exp[-t / \tau_r], \quad t > 0. \end{aligned} \quad (20)$$

The solution for equation (20) is:

$$M_y^{(1)}(t) = M_{y0}^{(1)} - (q_1 - q_0)[1 - \exp[-t / \tau_r]](t / \tau_r + 1) / (L \rho \tau_r). \quad (21)$$

These solutions were obtained and described in [8]. Direct substitution ensures that the solutions of the corresponding problems for mathematical expectations $M_{TT}^{(1)}(t, x)$ and $M_{yy}^{(1)}(t)$ based on the parabolic heat equation and the classical Fourier law have the following form:

$$M_{TT}^{(1)} = M_{TT0}^{(1)}(0, t) + q_0 \sqrt{a / \alpha} \exp[-\alpha t] \sin(x \sqrt{\alpha / a}) / \lambda. \quad (22)$$

$$\begin{aligned} M_{yy}^{(1)}(t) &= M_{yy0}^{(1)} - 2\sqrt{a / \alpha} \operatorname{arctg}\{(\sqrt{q_1^2 - q_0^2} / (q_1 + q_0)) \times \\ &\times \operatorname{tg}[\sqrt{q_1^2 - q_0^2} / (2L\rho)(\sqrt{a\alpha}^{-1}(1 - \exp(-\alpha t)))]\}. \end{aligned} \quad (23)$$

For a comparative analysis of solutions with hyperbolic and parabolic representations of the studied Stefan problem, it is necessary to transform solutions (22) - (23) at $\alpha = 1 / \tau_r$. We obtain:

$$M_{TT}^{(1)} = M_{TT0}^{(1)}(0, t) + q_0 \sqrt{a \tau_r} \exp[-t / \tau_r] \sin(x / \sqrt{a \tau_r}) / \lambda. \quad (24)$$

$$\begin{aligned} M_{yy}^{(1)}(t) &= M_{yy0}^{(1)} - 2\sqrt{a \tau_r} \operatorname{arctg}\{(\sqrt{q_1^2 - q_0^2} / (q_1 + q_0)) \times \\ &\times \operatorname{tg}[\sqrt{q_1^2 - q_0^2} / (2L\rho)(\sqrt{\tau_r / a}(1 - \exp(-t / \tau_r)))]\}. \end{aligned} \quad (25)$$

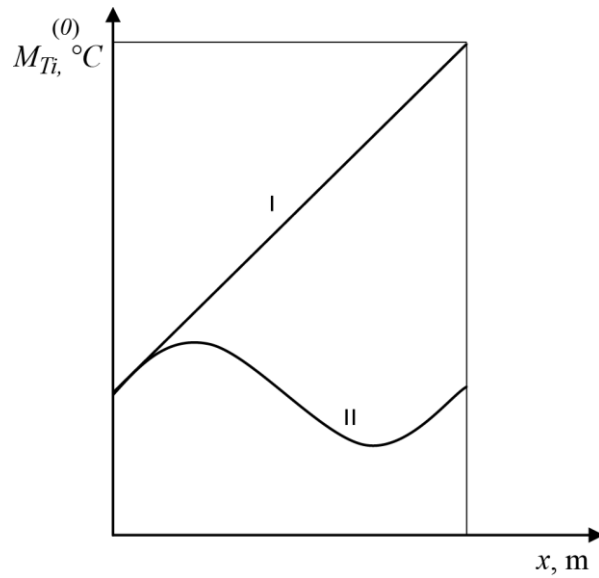


Fig.1. Relationship between temperature and the spatial coordinate:
 $i=1$ is for parabolic model; $i=2$ is for hyperbolic model

The curves for temperature dependences of $M_T^{(1)}(x,t)$ and $M_{TT}^{(1)}(x,t)$ are presented in Figs. 1 and 2. They show that solutions of problems for the hyperbolic and parabolic equations are not always of the same qualitative nature. If the function $M_{TT}^{(1)}(x,t)$ oscillates with a change in x , then the function $M_T^{(1)}(x,t)$ is strictly monotonic. For x values for which the sine in expression (24) is equal to 0, $M_{TT}^{(1)}(x,t)$ is constant in time, and $M_T^{(1)}(x,t)$ changes exponentially .

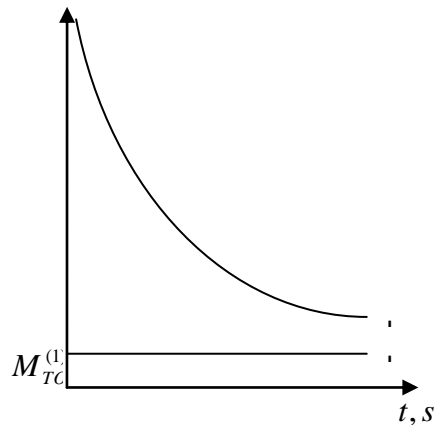


Fig.2. Relationship between temperature and time:
 $i=1$ is for parabolic model; $i=2$ is for hyperbolic model

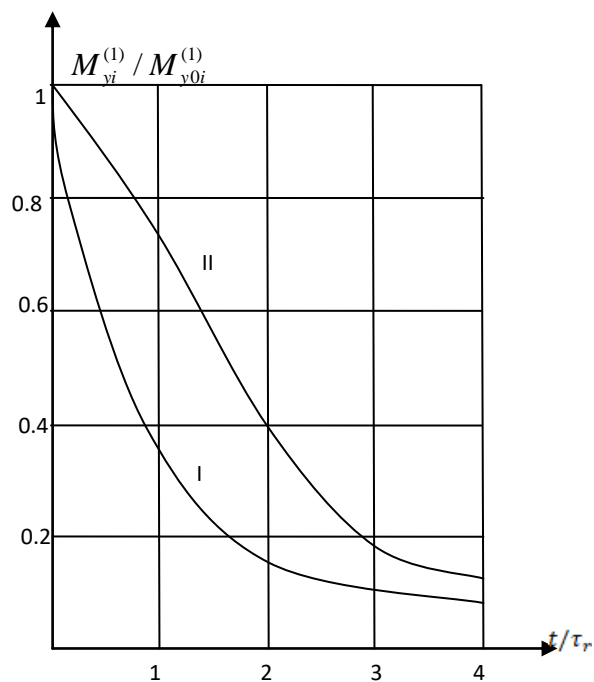


Fig. 3. Relationship between phase interface and time:
i=1 is for parabolic model; *i*= 2 is for hyperbolic model
 $\tau_r = 10^{-9} s; q_0 = 10^{-2} q_1; a = 10^{-5} m^2 / s$

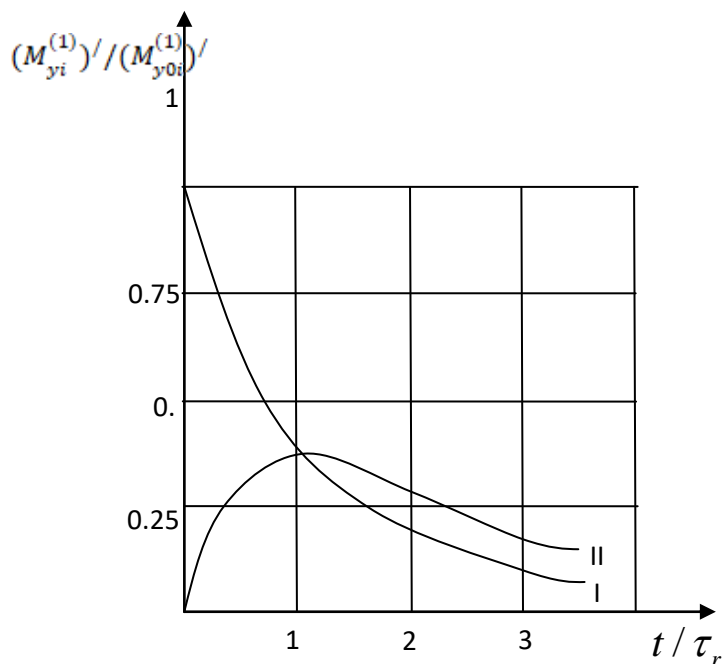


Fig. 4. Relationship between phase interface movement rate and time:
i=1 is for parabolic model; *i*= 2 is for hyperbolic model

Figures 3 and 4 show behavior of motion laws for the phase transition front $M_y^{(1)}(t)$ and $M_{yy}^{(1)}(t)$. Figures 5 and 6 show behavior of motion laws for speeds $dM_y^{(1)}(t)/dt$ and $dM_{yy}^{(1)}(t)/dt$. A model with a parabolic equation predicts that the phase transition process begins at a maximum speed, which, we note, can be arbitrarily large, depending on the ratio between q_0 and q_1 . According to the hyperbolic model, the phase transition front accelerates from zero speed to the maximum one not instantaneously, but during some time, determined by τ_r . The maximum value of $dM_y^{(1)}(t)/dt$ is limited above by the constant $\sqrt{a/\tau_r}$. Using relations (27)-(29), we can establish a relationship between the temperature at the front $M_T^{(1)}(M_y^{(1)}(t), t)$ and the kinematic characteristics of the front $dM_y^{(1)}(t)/dt$ and $d^2M_y^{(1)}(t)/dt^2$. For hyperbolic model we obtain

$$M_T^{(1)}(M_y^{(1)}(t), t) = M_{T0}^{(1)} + [(q_0 L \rho) / (\lambda (q_1 - q_0))] [\tau_r L \rho d^2 M_y / dt^2 + dM_y / dt] M_y. \quad (26)$$

In a model with a parabolic equation, we get the following relation:

$$M_{yy}^{(1)}(t), t) = (M_{T0}^{(1)} - (L \rho a) / \lambda) - a \tau_r L \rho d(\ln(M_y^{(1)})) / dt / \lambda. \quad (27)$$

Comparative analysis of dispersions of parabolic and hyperbolic models of the Stefan problem

The derivation of equations for PD and dispersion corresponding to the Stefan problems is not different from those proposed in [9]. Here we present the formulation of the problem for dispersion corresponding to the hyperbolic model of the investigated Stefan problem (20)–(25). This solution has the following form:

$$\begin{aligned} \partial D_T(x, t) / \partial t &= [(2a \partial^2 M_T^{(1)}(x, t) / \partial x^2 - 2\tau_r \partial^2 M_T^{(1)}(x, t)) / M_T^{(1)}(x, t)] D_T(x, t) + B_\Omega, \\ t > 0, x &\in (0, M_y^{(1)}(t)). \end{aligned} \quad (28)$$

$$D_T(x, 0) = D_{Tini}(x) = \delta_0^2(x) (M_{Tini}^{(1)})^2, x \in [0, M_y^{(1)}(0)].$$

Dispersion of the phase transition front is described by the following equations:

$$\partial D_y(x, t) / \partial t = [(2a \partial^2 M_{T2}^{(1)}(x, t) / \partial x^2) / M_{T2}^{(1)}(x, t)] D_{T2}(x, t) + B_\Theta, t > 0, x \in (M_y^{(1)}(t), +\infty). \quad (29)$$

$$D_T(x, 0) = D_{Tini}(x) = \delta_0^2(x) (M_{Tini}^{(1)})^2, x \in [M_y^{(1)}(0), +\infty). \quad (30)$$

Taking into account the fact that equations (12) - (17) are valid, equations (20) - (22) can be rewritten by replacing the right-hand side with the left-hand side:

$$\partial D_T(x, t) / \partial t = [\partial \ln(M_T^{(1)}(x, t))^2 / \partial t] D_T(x, t) + B_\Omega, t > 0, x \in (0, M_y^{(1)}(t)).$$

From here we get solutions for dispersions in the form:

$$D_T(x, t) = [\int_0^t B_\Omega d\xi / (M_T^{(1)}(x, \xi))^2 + \delta_0^2(x)] (M_T^{(1)}(x, t))^2, x \in (0, M_y^{(1)}(t)), t \geq 0. \quad (31)$$

$$D_y(t) = [\int_0^t B_\Theta dx / (M_y^{(1)}(x))^2 + \delta_0^2] (M_y^{(1)}(t))^2, t \in [0, 10] \quad (32)$$

For parabolic model we have:

$$D_{yy}(t) = [\int_0^t B_\Theta dx / (M_{yy}^{(1)}(x))^2 + \delta_0^2] (M_{yy}^{(1)}(t))^2, t \in [0, 10], \text{ where}$$

$$M_{yy}^{(1)}(t) = M_{yy0}^{(1)} - 2\sqrt{a\tau_r} \arctg\left\{ \left(\sqrt{q_1^2 - q_0^2} / (q_1 + q_0) \right) \times \right. \\ \left. \times \operatorname{tg}\left[\sqrt{\tau_r / a} \cdot \sqrt{q_1^2 - q_0^2} \cdot (1 - \exp(-t) / (2L\rho)) \right] \right\}. \quad (33)$$

Since the temperature mode during random impacts on a substance is unstable, to investigate the distortion of the phase transition front is of interest. This is also important because the initial moments of the motion velocities of this front differ greatly in the models under consideration.

So it turns out that the integrals $\int_0^t B_{\Theta} dx / (M_y^{(1)}(x))^2$ and $\int_0^t B_{\Omega} dx / (M_{yy}^{(1)}(x))^2$ cannot be resolved in quadratures, therefore it is proposed to find them numerically using the fourth-order Runge-Kutta method as a solution to the following Cauchy problem:

$$dz / dt = 1 / (M_y^{(1)}(t))^2, \quad M_y^{(1)}(0) = 0. \quad (34)$$

Further we present data for calculation of some material. The density is $\rho = 2,7 \cdot 10^3 \text{ kg/m}^3$. The heat of phase transition is $L = 1,0449 \cdot 10^7 \text{ J/kg}$. Heat conductivity coefficient is $\lambda = 62 \text{ W/(m} \cdot \text{deg)}$. The thermal diffusivity is $a = 25,8 \cdot 10^{-6} \text{ m}^2/\text{s}$. Thermal relaxation time is $\tau_r = 10^{-9} \text{ c}$. The initial (maximum) density of the incident flow on the moving boundary is $q_1 = 10^{11} \text{ W/m}^2$. The initial (maximum) density of the incident flow on a fixed boundary $q_0 = 10^9 \text{ W/m}^2$. The initial position of the phase transition front for the hyperbolic model is $M_{y0}^{(1)}(0) = 1 \text{ m}$. The initial position of the phase transition front for the parabolic model is $M_{yy0}^{(1)}(0) = 1 \text{ m}$. The initial temperature for the hyperbolic model is $M_{T0}^{(1)}(x, 0) = 20^\circ\text{C}$. Initial temperature for the parabolic model $M_{TT0}^{(1)}(x, 0) = 20^\circ\text{C}$. Pulse time is $1/\alpha = \tau_r, \text{ s}$. As for the Markov diffusion coefficients, their values are not presented in any reference book. In the present work, it is proposed to consider them of the same order with the thermal diffusivity coefficient $B_{\Theta} = 10^{-4}, B_{\Omega} = 10^{-4}$.

The calculation results are shown in Figs. 5 and 6.

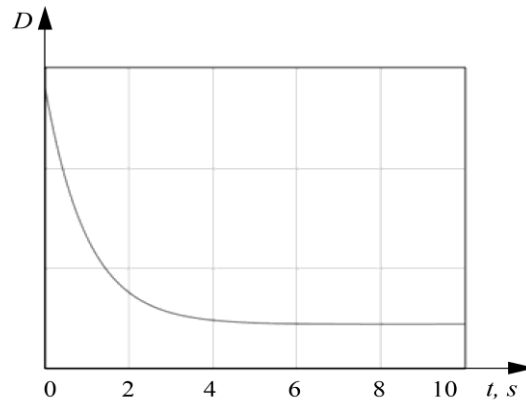


Fig. 5. The temporal behavior of the phase transition front dispersion for parabolic model

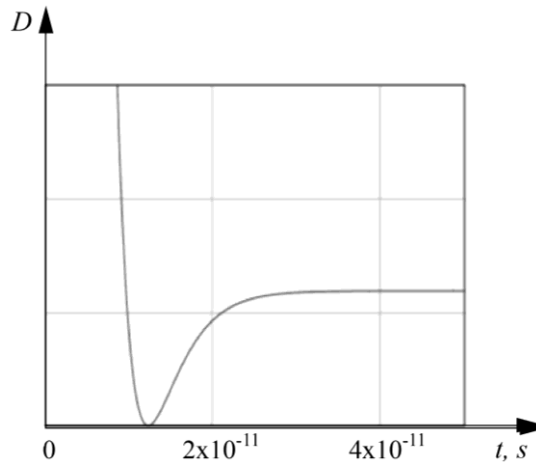


Fig. 6. The temporal behavior of the phase transition front dispersion for hyperbolic model

Further we discuss the results of the temporal behavior of the dispersion at the phase transition front. As in the case of the stochastic consideration of the Stefan problem, carried out in [5], the *effect of striving to preserve the original form of the phase transition front* is also observed here. How can we interpret the practical application of this phenomenon for the fast process of heat conduction? The relaxation time is very short, is it possible to benefit from identifying the time of occurrence of the smallest dispersion when distortion of the phase transition front shape is minimal? We try to answer this question. Despite the fact that the problem is considered here in a flat formulation, it is possible to carry out a similar quantitative and qualitative analysis for the spherical initial shape of the particle. Basing on fixing the moment of smallest dispersion, it is possible to calculate the pulse action time at which the smallest distortion of the phase transition front shape is observed, and as a result of planning the experiment, to obtain the desired configuration of the melted particle, possibly close to the initial one.

Conclusions

At present, a large mathematical apparatus has been accumulated, which describes many phenomena of a physical nature in a deterministic way. This apparatus requires its translation, figuratively speaking, into “stochastic language”. In particular, in [2] one of the authors of this article (E.M. Kartashov) obtained numerous analytical solutions for original deterministic problems in thermal physics, thermo elasticity, etc., which have already been successfully used in practice. In recent papers of authors of this article, the possibilities of combining classical deterministic concepts of physical phenomena with stochastic ones are demonstrated. New effects can be discovered, in addition to the dispersion stability conditions described above and dispersion extreme properties. The practical application of the results of stochastic studies of motion laws for phase transition front to technological processes are of particular importance. This primarily concerns the determination of the time of melting and evaporation of microparticles at a powerful impact of pulsed laser radiation on matter.

References

1. Stefan J. Under probleme derteorie der warmeleitung. *Sitz. Kais. Akad. Wiss. Mat.-Nat. Classe Wien*. 1889. Bd. 98. 11a. pp. 616-634.
2. Kartashov E.M. *Analiticheskie metody v teorii teploprovodnosti tverdyh tel*. Moscow: Vysshaya shkola; 2001. (In Russ).
3. Kartashov E.M, Kudinov V.A. *Analytical theory*

Литература

1. Stefan J. Under probleme derteorie der warmeleitung // *Sitz. Kais. Akad. Wiss. Mat.-Nat. Classe Wien* 1889. Bd. 98. 11a. pp. 616-634.
2. Карташов Э.М. Аналитические методы в теории теплопроводности твердых тел. М.: Высшая школа, 2001. 540 с.
3. Карташов Э.М., Кудинов В.А. Аналитическая

of heat conduction and thermoelasticity. Moscow: Librokom; 2018. (In Russ).

4. Kartashov EM, Soloviev IA. Stokhasticheskiy podhod k probleme Stefana. *Proceedings of the Russian Academy of Sciences. Power Engineering*. 2017; 5:134-143. (In Russ).

5. Soloviev IA, Dolicanin-Dekic HD. Stokhasticheskie modeli. Moscow: [b. i.]; 2016. (In Russ).

6. Zhirnov I, Kotoban D, Gusarov AV. Evaporation-induced gas-phase flows at selective laser melting. *Applied Physics A*. 2018; 124(2):157 DOI: 10.1007/s00339-017-1532-y.

7. Huaxia YAO. Long-Term Study of Lake Evaporation and Evaluation of Seven Estimation Methods: Results from Dickie Lake, South-Central Ontario, Canada. *Earth & Environmental Sciences*. 2009; 1(2):59-77. DOI: 10.4236/jwarp.2009.12010.

8. Meier C, Penny RW, Zou Y., et al. Thermophysical phenomena in metal additive manufacturing by selective laser melting: Fundamentals, modeling, simulation and experimentation. *Annual Review of Heat Transfer*. 2017; 20:241-316. DOI: 10.1615/AnnualRevHeatTransfer.2018019042.

9. Matthews MJ, Guss G, Khairallah S.A., et al. Denudation of metal powder layers in laser powder bed fusion processes. *Acta Mater*. 2016; 114:33-42.

10. Roscani S, Marcus E.S. Two equivalent Stefan's problems for the time fractional diffusion equation. *Fractional Calculus and Applied Analysis*. 2013; 16(4):802-815.

теория теплопроводности и прикладной термоупругости. М.: Libroком, 2018. 656 с.

4. Карташов Э.М., Соловьев И.А. Стохастический подход к проблеме Стефана // Известия РАН. Энергетика. 2017. №5. С. 134-143.

5. Соловьев И.А, Доличанин-Декич Д.Ч. Стохастические модели. Москва: [б. и.], 2016. 131 с.

6. Zhirnov I, Kotoban D, Gusarov A.V. Evaporation-induced gas-phase flows at selective laser melting // *Applied Physics A*. 2018. Vol. 124, No.2. 157 p.

7. Huaxia YAO. Long-Term Study of Lake Evaporation and Evaluation of Seven Estimation Methods: Results from Dickie Lake, South-Central Ontario, Canada // *Earth & Environmental Sciences*. 2009. Vol.1, No.2. pp. 59-77.

8. Meier C., Penny R.W., Zou Y., et al. Thermophysical phenomena in metal additive manufacturing by selective laser melting: Fundamentals, modeling, simulation and experimentation // *Annual Review of Heat Transfer*. 2017. Vol. 20. pp. 241-316.

9. Matthews M.J., Guss G., Khairallah S.A., et al. Denudation of metal powder layers in laser powder bed fusion processes // *Acta Mater*. 2016. Vol.114. pp. 33-42.

10. Roscani S., Marcus E.S. Two equivalent Stefan's problems for the time fractional diffusion equation // *Fractional Calculus and Applied Analysis*. 2013. T. 16. № 4. С. 802-815.

Authors of the publication

Eduard M. Kartashov – Professor of the Department of higher and applied mathematics Moscow University of technology. E-mail: kartashov@mitht.ru.

Igor A. Soloviev – Professor of the Department of higher mathematics and physics of the state University of Land Use Planning. E-mail: igorsoloviev@inbox.ru.

Received

November, 23 2018